Study of Optical Properties of Noninteger Dimensional Nonlinear Medium

Adil Qayyum Bhatti

Department of Electronics

Quaid-i-Azam University, Islamabad, Pakistan.

A Thesis Submitted in Partial Fulfillment of the Requirements for the Degree of

Doctor of Philosophy

in

Electronics

Feb. 2023

QUAID-I-AZAM UNIVERSITY

Department of Electronics

Author's Declaration

I, **Mr. Adil Qayyum Bhatti** hereby state that my PhD thesis titled **"Study of Optical Properties of Noninteger Dimensional Nonlinear Medium"** is my own work and has not been submitted previously by me for taking degree from **Department of Electronics, Quaid-i-Azam University** Or anywhere else in the country/world.

At any time if my statement is found to be incorrect even after my graduation, the university has the right to withdraw my PhD degree.

Adil Qayyum Bhatti

Date: 20|10|2023

QUAID-I-AZAM UNIVERSITY
Department of Electronics

Plagiarism Undertaking

I solemnly declare that research work presented in the thesis titled, "Study of Optical Properties of Noninteger Dimensional Nonlinear Medium" is solely my research work with no significant contribution from any other person. Small contribution/help wherever taken has been duly acknowledged and that complete thesis has been written by me.

I understand the zero-tolerance policy of the HEC and Quaid-i-Azam University towards plagiarism. Therefore, I as an Author of the above titled thesis, declare that no portion of my thesis has been plagiarized and any material used as reference is properly referred/cited.

I undertake that if I am found guilty of any formal plagiarism in the above titled thesis even after award of PhD degree, the University reserves the rights to withdraw/revoke my PhD degree and that HEC and the University has the right to publish my name on the HEC/University Website on which names of students are placed who submitted plagiarized thesis.

Student/Author Signature: _____

Name: **Adil Qayyum Bhatti**

Certificate

This is to certify that <u>Mr. Adil Qayyum Bhatti,</u> Ph.D. scholar has incorporated all typographical corrections and suggestions as required by externals in the thesis.

The title of the thesis is as under: -

<u>"Study of Optical Properties of Noninteger Dimensional Nonlinear Medium"</u>

<u>Prof. Dr. Manzoor Ikram</u>

(External Examiner-1)

Director

National Institute of Lasers and Optronics (NILOP)

Nilore, 45650, Islamabad.

<u>Prof. Dr. Muhammad Junaid Mughal</u>

(External Examiner-2)

Director CUI, COMSATS University

Attock.

<u>Dr. Musarat Abbas</u>

(Supervisor)

<u>Prof. Dr. Qaisar A. Naqvi</u>

(Chairman)

<u>Controller of Examination</u>

QUAID-I-AZAM UNIVERSITY
Department of Electronics
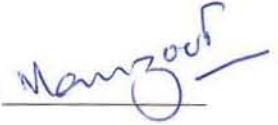
Certificate of Approval

This is to certify that the research work presented in this thesis, entitled **"Study of Optical Properties of Noninteger Dimensional Nonlinear Medium"** was conducted by **Mr. Adil Qayyum Bhatti** under the supervision of **Dr. Musarat Abbas**. No part of this thesis has been submitted anywhere else for any other degree. This thesis is submitted to the **Department of Electronics, Quaid-i-Azam University** in partial fulfilment of the requirements for the degree of Doctor of Philosophy in Field of **Electronics,** Department of Electronics, Quaid-i-Azam University.

Student Name: **Mr. Adil Qayyum Bhatti**   Signature: _____

Examination Committee:

A. Prof. Dr. Manzoor Ikram   Signature: _____
   Director
   National Institute of Lasers and Optronics (NILOP)
   Nilore, 45650, Islamabad.

B. Prof. Dr. Muhammad Junaid Mughal   Signature: _____
   Director CUI, COMSATS University
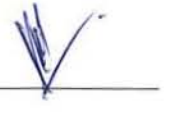   Attock.

C. Dr. Musarat Abbas   Signature: _____
   Associate Professor
   Department of Electronics
   Quaid-i-Azam University, Islamabad

D. Prof. Dr. Qaisar A. Naqvi   Signature: _____
   Chairman
   Department of Electronics
   Quaid-i-Azam University, Islamabad

Supervisor Name: **Dr. Musarat Abbas**   Signature: _____

Name of Chairman: **Prof. Dr. Qaisar A. Naqvi**   Signature: _____

Quaid-I-Azam University

Department of Electronics

Name of Candidate: **Mr. Adil Qayyum Bhatti**

Title of Thesis: **"Study of Optical Properties of Noninteger Dimensional Nonlinear Medium"**

Name of Supervisor: **Dr. Musarat Abbas**

Date of Via-voce Examination: **October 20, 2023**

The candidate has successfully defended his/her thesis. The candidate is recommended for the award of Ph.D. Degree.

External Examiners

1. Prof. Dr. Manzoor Ikram   Signature: _____
   Director
   National Institute of Lasers and Optronics (NILOP)
   Nilore, 45650, Islamabad

2. Prof. Dr. Muhammad Junaid Mughal   Signature: _____
   Director CUI,
   COMSATS University
   Attock.

Supervisor

3. Dr. Musarat Abbas   Signature: _____
   Associate Professor
   Department of Electronics
   Quaid-i-Azam University, Islamabad

(Prof. Dr. Qaisar A. Naqvi)
Chairman

Controller of Examination

بِسْمِ اللَّهِ الرَّحْمَٰنِ الرَّحِيمِ

إِنَّ فِي خَلْقِ السَّمَاوَاتِ وَالأَرْضِ وَاخْتِلاَفِ اللَّيْلِ وَالنَّهَارِ وَالْفُلْكِ الَّتِي تَجْرِي فِي الْبَحْرِ بِمَا يَنفَعُ النَّاسَ وَمَا أَنزَلَ اللَّهُ مِنَ السَّمَاءِ مِن مَّاءٍ فَأَحْيَا بِهِ الأَرْضَ بَعْدَ مَوْتِهَا وَبَثَّ فِيهَا مِن كُلِّ دَآبَّةٍ وَتَصْرِيفِ الرِّيَاحِ وَالسَّحَابِ الْمُسَخِّرِ بَيْنَ السَّمَاءِ وَالأَرْضِ لآيَاتٍ لِّقَوْمٍ يَعْقِلُونَ ○ (الْبَقَرَةِ : 164)

Verily, in the creation of the heavens and the earth, and in the alternation of the night and the day, and in the ships (and vessels) which sail through the ocean carrying cargo profitable for the people, and in the (rain) water which Allah pours down from the sky, reviving therewith the earth to life after its death, and (the earth) in which He has scattered animals of all kinds, and in the changing wind directions, and in the clouds (that trail) between the sky and the earth, duty-bound certainly, (in these) are (many) signs for those who put their reason to work.

(Al-Baqarah : 164)

Acknowledgements

Praise be to Allah Almighty who is the lord of the worlds, Most Gracious, Most Merciful. All praise and glory to Almighty Allah, Who gave me courage and patience to carry out this work. Endless blessings be showered upon His most beloved Prophet Muhammad (SallaAllahu Ta'ala 'Alaihi wa Sallam).
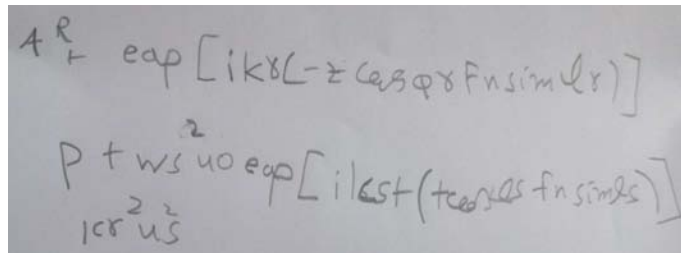
This thesis is indebted to the help, support and encouragement of several people. First of all I am indebted to my adviser, Dr. Musarat abbas for his support and advice. He is not only my mentor rather he is my motivation for my difficult times. I am also thankful to Prof. Dr. QA Naqvi for giving his time for the results discussion. Contributions of Dr. Arshad fayyaz are also highly appreciated. He taught me the basics of the research methodology. I am also thankful to higher education commission of Pakistan, for providing me the IRSIP scholarship. Although I can't utilize this scholarship completely due to sever covid conditions at that time, but this scholarship give me a chance to work under the supervision of Prof. Dr. Andrea (Department of Physics and Astronomy, University of St. Andrews, Scotland, Uk). I am pleased because he taught me how to think in a different dimension and how to align the research problems for realistic results. It is him who taught me the transition between theoretical and practical electromagnetic.

Its my pleasure to acknowledge all my family especially my parents. I concede their endeavors which they are still doing for me. Without their love and support I would not be able to imagine where I am today. I could not have completed this long but fulfilling journey without their unconditional love, strength and guidance. I am grateful to my parents, for striving hard, to provide me

good education and very friendly environment. I offer my deepest gratitude to them for their affectionate behavior. I always fall short of words and felt impossible to describe their greatness in words. Whenever I was stuck badly, they listened to my research problems wholeheartedly, (even though they didn't known the basics but still they listen to me) and encourage me with stories of various historical or scientific achievements.

I am eternally grateful for the patience, understanding, and encouragement to my amigos: my sisters; Hina, Sana, Sabahat, Aiman and my wife Aniqa, for their love, thoughtfulness and care. I admire their support and encouragement.

I would also like to thanks my little angle Abisha and nephews Saim and Azan, for their cute gestures, jokes and their attempts to copy my work on their notebooks. Because of them, I always feel fresh even in my difficult times.

List of Publications

- **Adil Qayyum** and Musarat Abbas. Study of reflection/transmission behavior of a planar nonlinear dielectric–NID interface. Results in optics. 5: 100119; 2021.

- **Adil Qayyum** and Musarat Abbas. Impact of non–linearity and noninteger dimension on the reflection and transmission coefficients. Journal of electromagnetic waves and applications. 2022.

- **Adil Qayyum** and Musarat Abbas. Study of reflection and transmission coefficients of a linear dielectric–nonlinear NID planar interface. Physica B: physics of condensed matter. 644: 414217; 2022.

- **Adil Qayyum** and Musarat Abbas. Quasi phase matched second order reflection and transmission coefficients. Physica B: physics of condensed matter. 650: 414506; 2023.

Abbreviation

Acronym	Description
NL	Nonlinear
NLO	Nonlinear optical
NID	Noninteger dimensional
SHG	Second harmonic generation
$\chi^{(1)}$	First order susceptibility (Linear susceptibility)
$\chi^{(2)}$	Second order susceptibility (Nonlinear susceptibility)
EN	Epsilon negative
MN	Mu negative
D	Dimension of the NID medium
SVA	Slowly varying amplitude
MSV	method of separation of variables
DM	Dielectric magnetic
$\mathbf{P}^{(2)}$	Second order induced polarization
α	Angle formed between induced nonlinear polarization and the wave vector
$A_\perp^R$	S-polarized reflection coefficient for second order nonlinear dielectric–linear dielectric NID planar interface
$A_\perp^T$	S-polarized transmission coefficient for second order nonlinear dielectric–linear dielectric NID planar interface

$A_{\parallel}^{R}$	P-polarized reflection coefficient for second order nonlinear dielectric–linear dielectric NID planar interface
$A_{\parallel}^{T}$	P-polarized transmission coefficient for second order nonlinear dielectric–linear dielectric NID planar interface
$B_{\perp}^{R}$	S-polarized reflection coefficient for linear dielectric–second order nonlinear dielectric NID planar interface
$B_{\perp}^{T}$	S-polarized transmission coefficient for linear dielectric–second order nonlinear dielectric NID planar interface
$B_{\parallel}^{R}$	P-polarized reflection coefficient for linear dielectric–second order nonlinear dielectric NID planar interface
$B_{\parallel}^{T}$	P-polarized transmission coefficient for linear dielectric–second order nonlinear dielectric NID planar interface
$C_{\perp}^{R}$	S-polarized reflection coefficient for linear dielectric NID–second order nonlinear dielectric NID planar interface
$C_{\perp}^{T}$	S-polarized transmission coefficient for linear dielectric NID–second order nonlinear dielectric NID planar interface
$C_{\parallel}^{R}$	P-polarized reflection coefficient for linear dielectric NID–second order nonlinear dielectric NID planar interface
$C_{\parallel}^{T}$	P-polarized transmission coefficient for linear dielectric NID–second order nonlinear dielectric NID planar interface
θ_i	Incident angle
ϵ_i	Fundamental permittivity (linear permittivity)
ϵ_s	Nonlinear permittivity
μ_r	Nonlinear permeability

ω_i	Fundamental excitation frequency
ω_s	Second harmonic frequency
ς	Nonlinear conversion efficiency
I^a	Nonlinear dielectric magnetic–linear dielectric magnetic NID planar interface
I^b	Linear dielectric magnetic–nonlinear dielectric magnetic NID planar interface
I^c	Linear dielectric magnetic NID–nonlinear dielectric magnetic NID planar interface

Appendix

$$A_r = \left(k_r^c q \cos\theta_r\right)^{o_1} H_{o_1}^{(1)}\left(k_r^c q \cos\theta_r\right), \qquad A_t = \left(k_t^c q \cos\theta_t\right)^{o_2} H_{o_2}^{(2)}\left(k_t^c q \cos\theta_t\right),$$

$$A_s = \left(k_s q \cos\theta_s\right)^{o_2} H_{o_2}^{(2)}\left(k_s q \cos\theta_s\right), \qquad B_r = \left(k_r^c q \cos\theta_r\right)^{oh_1} H_{oh_1}^{(1)}\left(k_r^c q \cos\theta_r\right),$$

$$B_t = \left(k_t^c q \cos\theta_t\right)^{oh_2} H_{oh_2}^{(2)}\left(k_t^c q \cos\theta_t\right), \qquad B_s = \left(k_s q \cos\theta_s\right)^{oh_2} H_{oh_2}^{(2)}\left(k_s q \cos\theta_s\right),$$

$$\omega = E_i^2 \eta_t^c \epsilon_o \mu_o \chi \omega_s^2, \qquad \vartheta = A_s B_r \eta_s \cos\theta_r + A_r B_s \eta_r \cos\theta_s,$$

$$\eta_{v_1}^{a'} = \sqrt{\mu_{v_1}^{a'}/\epsilon_{v_1}^{a'}} : \quad v_1 = \{r,t,s\}, \qquad k_{v_2} = (\omega_s/c)\sqrt{\epsilon_{v_2}^{a'}} : \quad v_2 = \{r,t,i\},$$

$$\psi_1 = A_r B_t \eta_r^c \cos\theta_r, \qquad \psi_2 = A_t B_r \eta_t^c \cos\theta_t,$$

$$\psi_3 = A_s B_t \eta_s \cos\theta_s, \qquad \psi_4 = A_t B_s \eta_t^c \cos\theta_t,$$

$$\psi_5 = A_s B_t \eta_s \cos\alpha \sin\theta_s, \qquad \psi_6 = A_r B_s \eta_r^c \cos\theta_r \sin\alpha$$

$$A = \left(k_t^a q \cos\theta_t\right)^{o} H_o^{(2)}\left(k_t^a q \cos\theta_t\right), \qquad \lambda_1 = e^{-jk_r^a q \cos\theta_r},$$

$$B = \left(k_t^a q \cos\theta_t\right)^{oh} H_{oh}^{(2)}\left(k_t^a q \cos\theta_t\right), \qquad \lambda_2 = e^{-jk_s q \cos\theta_s},$$

$$\delta_{rt} = \eta_r^a \cos\theta_t, \qquad \delta_{rs} = \eta_r^a \cos\theta_s,$$

$$\delta_{sr} = \eta_s \cos\theta_r, \qquad \delta_{tr} = \eta_t^a \cos\theta_r,$$

$$\delta_{ts} = \eta_t^a \cos\theta_s, \qquad \delta_{st} = \eta_s \cos\theta_t,$$

$$\delta_{cc}^r = E_o^2 \epsilon_o \eta_r^a \mu_o \chi \omega_s^2 \qquad a' = \{a,b,c\}$$

$$\delta_{cc}^t = E_o^2 \epsilon_o \eta_t b, c \mu_o \chi \omega_s^2, \qquad exp_{kr} = e^{-jk_r^b q \cos\theta_r}$$

$$\omega_i = 1 \times 10^{16}, \quad \omega_s = 2\omega_i, \quad \mu_o = 1/(\epsilon_o c^2), \quad k_s = 2k_r^a,$$

$$o_1 = |\tfrac{3-D_1}{2}|, \quad oh_1 = \left|\tfrac{D_1-1}{2}\right|, \quad o_2 = |\tfrac{3-D_2}{2}|, \quad oh_2 = \left|\tfrac{D_2-1}{2}\right|.$$

$$\delta_{tt} = \eta_t^b \cos\theta_t, \quad \delta_{rr}^b = \eta_r \cos\theta_r, \quad \eta_s^e = exp_{kr}\eta_s \quad \delta_t^e = exp_{kr}\delta_{tt}$$

Abstract

Study of the optical characteristics of materials, objects and geometries has wider role and applications in science and engineering. Reflection and transmission coefficients are used to study the optical properties of planar geometries and usually S and P-polarized electromagnetic waves are used. Primary aim of the presented work is to study the reflection and transmission of second harmonic generation in non-integer dimensional environment. Three types of planar interface geometries are considered one by one in order of increasing complexity. First is nonlinear dielectric magnetic–linear dielectric magnetic noninteger dimensional (NID) planar interface. The second one, linear dielectric magnetic–nonlinear dielectric magnetic NID planar interface and the last is linear dielectric magnetic NID–nonlinear dielectric magnetic NID planar interface. Special cases are also produced taking negative values of the permittivity and/or permeability. Nonlinear materials considered in the study are of second harmonic generation type, hence only second order reflection and transmission characteristics are noted and analyzed. Slowly varying amplitude approximation is used to obtain the solution of the nonlinear wave equation. Furthermore, all the NID materials taken in this study have noninteger dimension in only one direction which is normal to the planar interface.

Impact of the presence and absence of non-linearity and/or NID on the behavior of the coefficients is noted. It is noticed that impact of non-linearity on the coefficients is dependent on how the NID environment is used in a particular geometry. For instance, in case of a linear ordinary–nonlinear NID interface, S-polarized coefficients increases with increase of the non-linearity. Whereas,

anti-reflection property is achieved for S-polarization excitation for linear NID–nonlinear NID medium interface. On the other hand, for linear ordinary–nonlinear NID interface, amplitude of the P-polarized transmission (reflection) coefficient increases (decreases) as the value of nonlinear permittivity increases. For both excitation polarizations, amplitude of the coefficients increases by taking smaller values of the noninteger dimension in all cases. It is also studied that dimension of the NID medium, nonlinear permittivity and nonlinear permeability are used to control the behavior of the coefficients.

Contents

List of Figures

Chapter 1

Introduction

1.1 Linear optics

Primary aim of the presented thesis is to investigate the impact of the non-linearity and noninteger dimensions on the behavior of the second order reflection and transmission for a dielectric magnetic–dielectric magnetic (DM–DM) interface. Non-linearity and noninterger dimensions are considered in one and/or both half spaces in this regard. To develop the foundation for the nonlinear optics, initially wave equation and the poynting vector for a linear medium are discussed. This initial discussion helps the reader to understand the linkage between the linear and nonlinear optics. Moreover, the poynting vector discussion also elaborate how the electromagnetic energy is related in linear and nonlinear materials.

The Maxwell's equation to derive the solutions of the wave equation for a linear medium are,

$$\nabla \cdot \mathbf{D} = \rho \tag{1.1a}$$

$$\nabla \cdot \mathbf{B} = 0 \tag{1.1b}$$

$$\nabla \times \mathbf{E} = -\frac{\partial \mathbf{B}}{\partial t} \tag{1.1c}$$

$$\nabla \times \mathbf{H} = \mathbf{J} + \frac{\partial \mathbf{D}}{\partial t} \tag{1.1d}$$

In the above equations, the four vector quantities which are also known as electromagnetic fields, are: the electric flux density $\mathbf{D}$ (C/m^2); the electric field strength $\mathbf{E}$ (V/m); the magnetic flux density $\mathbf{B}$ (Wb/m^2) and the magnetic field strength $\mathbf{H}$ (A/m). Where, $\mathbf{J}$ (A/m^2) and ρ (C/m^3) are the current density and the electric charge density, respectively. Both these quantities represent the sources of the electromagnetic fields. The Maxwell's equation Eq.(1.1a) corresponds to the differential Gauss's law. Integral of this equation,

$$\oint_s \mathbf{D}.d\mathbf{S} = \oint_v \rho.dV,$$

states that the net electric flux over a volume S bounded by a surface S is equal to the total charges enclosed by that surface. The Eq.(1.1b), is the magnetic analogue of Eq.(1.1a). Integral of this equation,

$$\oint_S \mathbf{B}.d\mathbf{S} = 0,$$

states that magnetic monopoles do not exist.
The Eq.(1.1c), is "Faraday's law of induction". Integral of this equation,

$$\int_s (\nabla \times \mathbf{E}).d\mathbf{S} = \oint_C \mathbf{E}.dl = - \int_S \frac{\partial B}{\partial t}.d\mathbf{S},$$

states that the electromotive force ($\oint_C \mathbf{E}.dl$) induced in a loop is equal to the time rate of change of the magnetic flux passing through the area of the loop. The negative sign on the right hand side is due to the Lenz's law which stats that the induced emf always opposes the magnetic field's variation.
Eq.(1.1d), is the Ampere's law. Integral of this equation,

$$\oint_c \mathbf{H}.dl = \int_S \frac{\partial D}{\partial t}.d\mathbf{S} + \int_S \mathbf{J}.d\mathbf{S}, \tag{1.2}$$

states that the line integral of the magnetic field around a closed loop is equal to the net current passing through the surface of the loop.
Constitutive relations of a material define how the flux and fields are related to each other. For an isotropic and homogeneous medium, the constitutive

relations are defined as,

$$\mathbf{D} = \epsilon \mathbf{E} + \mathbf{P_o} \qquad (1.3\text{a})$$

$$\mathbf{B} = \mu \mathbf{H}, \qquad (1.3\text{b})$$

where ϵ, μ and $\mathbf{P_o}$ are the relative permittivity, permeability and polarization of the medium, respectively. Permittivity (also known as dielectric constant) determines the ability of a medium to store the electric energy. Similarly, permeability defines the formation of the magnetic field lines (magnetization) in a material. Materials permittivity is related to capacitance while permeability relates to the inductance. It is important to note that mathematical modeling discussed in later chapters, contain two parts of the permittivity: linear and nonlinear. Linear part corresponds to the permittivity observed at fundamental frequency whereas, nonlinear part corresponds to the permittivity observed at second harmonic frequency. Hence, all the wave vectors related to the incident electromagnetic waves contain the linear part whereas, the wave vectors of the second harmonic reflected and transmitted fields contain nonlinear part of the permittivity.

Polarization of the medium determine its optical properties. Generally, polarization is expressed in the form of power series,

$$\mathbf{P_o} = \mathbf{P}^{(1)} + \mathbf{P}^{(2)} + \mathbf{P}^{(3)} \ldots \qquad (1.4)$$

This series is expressed for time harmonic polarization of the form $e^{-j\omega t}$, which is suppressed throughout this thesis for simplicity. In Eq.(1.4), superscripts (.) represent the order of the polarization, written below as [1],

$$\mathbf{P}^{(1)}(t) = \epsilon_o \chi^{(1)} \mathbf{E(t)}$$
$$\mathbf{P}^{(i)}(t) = \epsilon_o \chi^{(i)} \mathbf{E^i}(t), \quad i = 2, 3, \cdots \qquad (1.5)$$

It is worth mentioning that first order susceptibility $(\chi^{(1)})$ is related to the linear optics whereas the higher order susceptibilities are related to the NL optical effects. First order susceptibility is also known as linear susceptibility, which

is of the order of unity. In the presented study NL mediums with only second order susceptibility ($\chi^{(2)}$), are taken into account. Therefor in mathematical modeling, only second order polarization ($\mathbf{P^{(2)}}$) is used and is written as '$\mathbf{P}$' for simplicity. It is important to note that if transmitted wave is propagating in a nonlinear medium then $\mathbf{P^{(2)}} = \epsilon_o \chi^{(2)} T^2 E_o^2$, where, E_o and is the amplitude of the excitation electromagnetic wave and T is used to represent the transmission coefficient. This expression shows that induced nonlinear polarization will behave as a source for electromagnetic waves.

1.1.1   Linear wave equation

This section is devoted for the general solution of the wave equation for the linear medium. Curl of Eq.(1.1c) is given as,

$$\nabla \times \nabla \times \mathbf{E} = -\nabla \times \frac{\partial \mathbf{B}}{\partial t} = -\mu \frac{\partial}{\partial t}(\nabla \times \mathbf{H}) \qquad (1.6)$$

Using Eq.(1.1d) and applying the vector identity,

$$\nabla \times \nabla \times \mathbf{A} = \nabla(\nabla.\mathbf{A}) - \nabla^2 \mathbf{A}, \qquad (1.7)$$

Eq.(1.6) becomes,

$$\nabla^2 \mathbf{E} = -\mu\epsilon \frac{\partial^2 \mathbf{E}}{\partial t^2} \qquad (1.8)$$

Eq.(1.8), is the general wave equation of electric field for linear medium. Similarly wave equation for the magnetic field is,

$$\nabla^2 \mathbf{H} = \mu\epsilon \frac{\partial^2 \mathbf{H}}{\partial t^2} \qquad (1.9)$$

1.1.2   Poynting's theorem

It is well established that electromagnetic wave propagation is transverse in nature, i.e; electric and magnetic both fields are transverse to the direction of propagation. To calculate the net power, the general form of the electric and

the magnetic fields associated with a wave propagating in the z direction is,

$$\mathbf{E} = \mathbf{E_x} + \mathbf{E_y} + \mathbf{E_z}$$
$$\mathbf{H} = \mathbf{H_z} + \mathbf{H_z} + \mathbf{H_z}$$

Substituting above equations in Eq.(1.1a), and using the definitions of the constitutive relations for a linear source free medium ($\mathbf{J} = \rho = 0$), one can find that, $\mathbf{E_z} = \mathbf{H_z} = 0$, i.e; there is no component of electric and the magnetic field parallel to the direction of propagation. Moreover, it is interesting to note that $\mathbf{E} \times \mathbf{H}$ has a units of W/m^2, i.e; power per unit area. This product is known as poynting vector. The average incident ($\mathbf{S_i}$), reflected ($\mathbf{S_r}$) and transmitted ($\mathbf{S_t}$) powers for an electromagnetic wave propagating in the z-direction, derived by Balanis [2] are written below as,

$$\mathbf{S_i} = \frac{\hat{a}_z |E_o|^2}{2\eta_1} \tag{1.11a}$$

$$\mathbf{S_r} = -\hat{a}_z |R|^2 S_i \tag{1.11b}$$

$$\mathbf{S_t} = \frac{\hat{a}_z |T|^2 E_o^2}{2\eta_2} \tag{1.11c}$$

Fluck and Günter [3] originally developed the theory of nonlinear cascade crystals. This theory is applicable under the assumption that fundamental beam's depletion is negligible. This means that the phase and magnitude of the fundamental beam do not change due to the nonlinear interactions. It is also established that the power of the second harmonic wave (P_{ω_s}) is related to the power of the fundamental wave (P_{ω_i}) by the following relation [4],

$$P_{\omega_s} = P_{\omega_i} \tan h^2 \sqrt{\varsigma P_{\omega_i}}, \tag{1.12}$$

It is important to note that this relation is not valid for strictly focused beams. Moreover, this relation does not take into account the thermal effects. The

expression of nonlinear conversion efficiency '(ς)' has been derived in [5],

$$\varsigma = \frac{P_{\omega_s}}{P_{\omega_i}} \propto \omega_i^s d^2 L^2 \frac{\sin^2(\frac{\triangle kL}{2})}{(\frac{\triangle kL}{2})^2} \frac{P_{\omega_i}}{E_o}$$

Above expression is derived for a nonlinear crystal having length "L", nonlinear coefficient "d", and the amplitude of the incident electromagnetic field is E_o. Moreover, it has also been established that the nonlinear conversion efficiency is $<< 1$ [4].

Results presented in this study converges to the simpler cases ([1, 6]) by taking integer dimension and positive values of the permittivity and permeability. Moreover, in the next chapters, sum of the reflected and transmitted powers $(P_r + P_t)$ are plotted by using, Eq.(1.11) and Eq.(1.12) for the verification of the analytical results. It is important to note the only powers carried by the second harmonic reflected and transmitted waves are plotted.

1.2   Nonlinear optics

1.2.1   Second harmonic generation

Optical frequency conversion (also known as harmonic generation) is an important topic in nonlinear (NL) optics, since past decade. This field describes how the light–matter interaction changes, when the material's polarization (Eq.(1.4)), responds non-linearly to the excitation laser beam. Nonlinear optical (NLO) theory remained unexplored until Frank et al. [7] reported an experimental study in 1961. A red light ruby laser beam (694.2 nm) and a quartz crystal, was used in this experiment to generate an UV wavelength signal (347.1 nm) [8]. This discovery was given the name "second harmonic generation" (SHG), because a twice frequency signal was generated corresponding to a fundamental frequency. After the discover of SHG, Bass et al. [9] discovered the optical rectification in 1962, by using an induced quasi static polarization. The discovery of SHG also paved the way for the discoveries of the higher harmonics, for example; in 1967, New and Ward reported the observation of

the third harmonic generation in gases [10] and in 1976, Reintjes et al. experimentally demonstrated the fifth harmonic generation [11]. After the Franken's discovery, NL materials has been studied and prepared widely due to their frequency and phase shifting properties [12, 13], as well. Among these materials organic materials were especially synthesized for different applications including: optical switching, information storage, telecommunication, signal processing and photonics [14–20], due to their fast response timing, structural flexibility and ease of manufacturing.

Now a days, there are two primary aims of the SHG generation, one is the efficient conversion of a fundamental frequency (ω_i) signal to twice harmonic (ω_s) frequency. Whereas, the other is related to the production of such wavelength sources which are difficult to achieve by using ordinary lasers [21]. However some physical constraints were reported in the experimental studies. First is related to the operating wavelength and the second is to achieving perfect phase matching across the interface. Phase matching condition is required to constructively accumulate the NL energy at the microscopic region. Traditionally, this was achieved by enhancing the source intensity and the device size. Hence different devices and theoretical approaches have been reported to achieve the target, and still the researchers are trying to overcome the phase matching requirement and improvement in the device size [22–26].

Initially, metallic meta-surface devices (having second-order non-linearity), were reported to study the SH waves behavior [27], but the higher losses of metallic structure, limited the use of such devices. This causes the emergence of III–V semiconductor materials, possessing second order non-linearity and the crystals are also of noncentrosymmetric nature, for example; GaAs, AlGaAs and GaP [28–31]. Researchers also used Mie resonance theory to study the SH effects of the above mentioned semicondusctor materials, but the narrow bnad gap of these materials limit the SH spectral range [32]. Because of these all issues, fabrication of a new NL device for SHG application is still an important topic. The study of SHG is also important in numerous other fields: biophotonics, optical sources, quantum information, hybrid plasmonic waveguide [33–39], and also in epsilon near zero meta-surfaces, electromagnetics, angular and quasi phase matching [40–46], and many other fields as well [1, 47–

49].

1.2.2   Nonlinear wave equation

In nonlinear optics, coupled nonlinear wave equation is derived under the following assumptions [5],

* The nonlinear coefficient is nonzero, this implies that medium has certain symmetry.

* Conductivity of the medium is negligible.

* A fraction of the incident power is converted to new frequency (ω_s).

Nonlinear wave equation is derived by using Eq.(1.1), Eq.(1.3) and Eq.(1.4), written as

$$\nabla \times \nabla \times \mathbf{E}(\omega_s) + \frac{1}{c^2}\frac{\partial^2 \mathbf{E}(\omega_s)}{\partial t^2} = -\frac{1}{\epsilon_o c^2}\frac{\partial^2 \mathbf{P}}{\partial t^2}, \quad\quad (1.13)$$

where c, ϵ_o and μ_o are the physical constants which defines the speed of light, permittivity and permeability of free space, respectively. It is interesting to note that the presence of last term, Eq.(1.13), shows an inhomogeneous solutions, whereas in the absence of this term, Eq.(1.13) admits the linear solutions (homogeneous). It is important to note that in linear optics $\nabla.\mathbf{E} = 0$, but, in NL optics, usually the term $\nabla.\mathbf{E}$ is not small to be ignored [50]. To eliminate this term usually different approximations has been used. A commonly used approximation is slowly varying amplitude approximation [6] as discussed in Sec.1.2.3. Under this approximation there is no contribution of $\nabla.\mathbf{E}$ term, so the vector identity Eq.(1.7) is applied. By applying the vector identity under the SVA approximation, Eq.(1.13) reduces to

$$\nabla^2 \mathbf{E}(\omega_s) - \frac{1}{c^2}\frac{\partial^2 \mathbf{E}(\omega_s)}{\partial t^2} = \frac{1}{\epsilon_o c^2}\frac{\partial^2 \mathbf{P}}{\partial t^2} \quad\quad (1.14)$$

This equation is a general form of the nonlinear wave equation.

1.2.3   Slowly varying amplitude (SVA) approximation

It is experimentally demonstrated that phase matching condition across the interface is necessary to achieve high frequency conversion efficiency [51]. In phase mismatching condition, poynting vector of the inhomogeneous wave do not move parallel to the propagation vector, and the wave walk-off earlier which imposes limitations on the NL frequency conversion and ultimately overall efficiency. This is also termed as angle tuning [52]. Phase matching conditions are often difficult to achieve because of the dispersive nature of material's permittivity which becomes negative for some NLO materials, for example, Al:ZnO and Sn:InO [53]. Hence, the waves propagating through such materials has purely imaginary wave vectors. This sign specification corresponds to the NL polarization, that results in real to complex valued wave vectors in NL medium. Paul Kinsler [54] supports the idea of positive and negative wave vectors. Nonlinear responses of KDP and DKDP, is studied experimentally by Duanliang et al [55]. Furthermore, it is also reported that the refractive index of a NL material is also dependent on crystal direction [56]. Strong practical and theoretical evidences show that the phase velocity in a NL material can be real or complex or just purely imaginary.

Phase mismatching discussed above is expressed as $\triangle k = k_s - 2k_i$, where k_s and k_i are the wave vectors of the inhomogeneous and homogenous solutions of Eq.(1.14). Hence, perfect phase matching ($\triangle k \rightarrow 0$) is achieved when k_s=$2k_i$. Varying techniques and geometries has been reported by researchers to achieve the perfect phase matching condition: e.g; epsilon near zero interfaces [40, 41], angular and quasi phase matching techniques [37, 42]. In the presented work slowly varying amplitude (SVA) approximation is used to achieve quasi-phase matching condition [1, 6, 57, 58]. This approximation requires that the fractional change in amplitude (ζ) over a distance of an optical wavelength should be very small [59, 60], as written below

$$\left| \frac{d^2\zeta}{dz^2} \right| << \left| k\frac{d\zeta}{dz} \right| ; \left| \frac{d^2\zeta}{dt^2} \right| << \left| \omega\frac{d\zeta}{dt} \right|$$

By using this approximation, higher order derivatives of the NL wave equation is neglected. The SVA approximation, can be also observed in III-V semiconductors [61]. This approximation also has importance in short-wavelength generation and parametric oscillation [62, 63]. In [64, 65] authors also used this approximation to study the electromagnetic response due to second order non-linearity.

1.3 Fractal materials

Generally, the space time dimensions are taken to be integer dimensions. Which are commonly known as Euclidean space and is used to explain the Cartesian geometries. But, some naturally occurring situations, like coastlines and crystals, are not regular/Euclidean geometries. Such geometries are treated as fractal materials/structures. Fractal structures are mathematically treated by using the non-differential Fractional calculus, which is also used for the description of the complex phenomena because classical euclidean theory become invalid [66], e.g, in classical mechanics, diffusion of water molecules were treated as continuous Brownian motion but, experimental studies revel that it follows the flick law [67] which is a fractal phenomena.

Mandelbrot initially coined the term fractal in his book [68]. He divided the materials into two broader categories, fractals and non-fractals. Fractal materials are self similar structures in miniature [69], whereas the parameter which defines the structural details of a fractal material is known as dimension (D) of the fractal material [70] which is usually in whole number powers, for example; for soil particles D ranges between 2 and 3, for Von Koch snowflake (Sierpinski triangle) scale is $D = 1.585$ ($D = 1.262$), whereas a surface and an uneven line has $D = 2.2$ and $D = 1.3$, respectively [71–73]. Menger sponge is also an example of fractal structures [74], which is a three dimensional cantor bar fractal [75]. Study of fractal materials has also been reported in soil erodibility, quantum mechanical oscillator system, antenna radiation problems, microwave, THZ resonators, high gain antennas and lasers [76–82]. In [83–85] authors studied the electromagnetic response of a fractal material, whereas, researchers also report the importance of fractal materials in optical scattering,

multilayer analysis of optical structures, transmission lines and wave scattering from rough surfaces [86–89].

1.3.1   NID space and fractal materials

It was reported that fractal materials are NID metric sets (as can be seen from above examples, fractal materials has non-integer dimensionality), which can be managed in continuous model with the help of NID space [90], fractal materials are also reported as NID materials in the literature [91], because NID space is the main characteristics of the fractal material [92]. In [93] definition of the NID Laplacian operator has been proposed which was used by Palmer and Stavrinou [94] to study the equation of motion. The NID half-space geometry were also treated to study the electromagnetic scattering [95], charges distribution and material's optical properties [96, 97]. In [98] derivation of the solutions of the NID Helmholtz's equation are given. Abbas et al. [99] discussed the NID half-space geometry by using the two dimensional Green's function [100] and Jaggard et al [101] reported the NID material wave interaction, whereas side-lobe-ratio in antenna array were studied in [102–104] and multiband NID array is reported in [105]. It was also reported that NID integrals and derivatives played an important role in many applications of physics [106]. Some other important applications of NID are found in statistical mechanics [107], electromagnetic theory [108, 109], kinetic theories [110] and dynamics in complex media [111].

The proposed definition of the NID Laplacian operator is written as [112],

$$\nabla_D^2 = \frac{\partial^2}{\partial x^2} + \frac{\beta_1 - 1}{x}\frac{\partial}{\partial x} + \frac{\partial^2}{\partial y^2} + \frac{\beta_2 - 1}{y}\frac{\partial}{\partial y} + \frac{\partial^2}{\partial z^2} + \frac{\beta_3 - 1}{z}\frac{\partial}{\partial z},$$

where

$$\beta_u = 0 < \beta_u \leq 1: \quad u = \{1, 2, 3\},$$

define the coordinate (x, y, z) measurement and is also used to define the geometric dimensionality: $D = \beta_1 + \beta_2 + \beta_3$. Similarly the curl operator for NID

space is defined as [97, 112],

$$\nabla_D \times \mathbf{F} = \left[\left(\frac{\partial F_z}{\partial y} + \frac{1}{2} \frac{(\beta_2 - 1)F_z}{y} \right) - \left(\frac{\partial F_y}{\partial z} + \frac{1}{2} \frac{(\beta_3 - 1)F_y}{z} \right) \right] \hat{x}$$

$$\left[\left(\frac{\partial F_x}{\partial z} + \frac{1}{2} \frac{(\beta_3 - 1)F_x}{z} \right) - \left(\frac{\partial F_z}{\partial x} + \frac{1}{2} \frac{(\beta_1 - 1)F_z}{x} \right) \right] \hat{y}$$

$$\left[\left(\frac{\partial F_y}{\partial x} + \frac{1}{2} \frac{(\beta_1 - 1)F_y}{x} \right) - \left(\frac{\partial F_x}{\partial y} + \frac{1}{2} \frac{(\beta_2 - 1)F_x}{y} \right) \right] \hat{z}$$

Following the procedure of MSV in NID space as outlined in [97, 100, 112], electric field associated with the incident electromagnetic wave in NID medium is expressed as,

$$\mathbf{E}(\omega) = E_o e^{-jk_x x} \left(k_z z \right)^{o_1} H_{o_1}^{(2)} \left(k_z z \right) \tag{1.15}$$

In Eq.(1.15), E_o and k depict the electric field's amplitude and the wave number of the NID medium, respectively. and $H_{o_1}^{(2)}$ is the hankel function of second kind with order 'o_1'. Moreover, it is also important to note that to derive the above it has been assumed that medium has noninteger dimension in only z-axis.

1.4 Motivation and objective

As discussed in previous chapter, perfect phase matching conditions are necessary to obtain maximum frequency conversion efficiency. For this purpose NL materials specifically having uni-axial or bi-axial properties has been proposed. Later, the advancement in optical materials provided the ease of NL frequency conversion without requiring strict phase matching conditions [113]. For example, meta-surfaces and nano-particles were used to study SHG phenomena [114–119] because these new proposed devices provide better power conversion efficiencies without requiring the strict phase matching conditions [120, 121], whereas dielectric and semiconductor materials has also been used to obtain higher NLO efficiencies due to their negligible intrinsic losses [122–

124]. Due to these advantages, dielectric and semiconductor materials triggered the interest of many researchers for technological applications of harmonic generation [125–128]. Various applications like beam steering, zero-index directional emission, Huygens' metasurfaces, ultrathin waveplates, and polarization insensitive holograms has been reported in the literature [129–136] due to the advancement in nonlinear semiconductor technology. However, due to the infancy of this field, two targets must be fulfilled in this regard. First: achieving conversion efficiencies at higher frequencies, e.g, very small efficiencies of the order of 10^{-2}–10^{-3} are used for fluorescent markers in bio sensing. In [137] SHG efficiency of the order of 10^{-3} is predicted by using a nano-structure composed of AlGaAs. Secondly, the second harmonic generation pattern. This target helps to properly direct the radiations into the desired direction. For example, in [137] it is reported that despite of strong SHG efficiency, no SH signal was detected in either forward or backward directions.

As mentioned in above paragraph, maximum frequency conversion efficiency can be achieved by using, dielectric materials with second order susceptibility ($\chi^{(2)}$) and the crystals are also of non-centrosymmetric nature. This help to achieve conversion efficiencies at higher frequencies (first target) but to achieve the target of radiation pattern, it was proposed that NL materials should be embedded or used in combination with other materials [138]. To achieve these targets, I used planar interface geometries containing linear–nonlinear materials: for example; second order NL dielectric magnetic medium and linear dielectric magnetic NID material. Hence this study not only improve the understanding of NLO process and SH field enhancement, rather also highlight the opportunities of NL frequency conversion without requiring the strict phase matching conditions. Further, presented study can also be used for the study of the higher harmonics and can also be extended for complex layered geometrical device. Although presented study is largely focused on the naturally occurring nonlinear crystals, but this can also be extended for the NL metasurfaces in future. Some other potential medical applications of the presented work are also given at the end of this thesis.

1.5   Thesis outline

The primary aim of presented work is to study the optical characteristics of a dielectric magnetic–dielectric magnetic (DM–DM) interface geometry, in the presence of non-linearity and/or noninteger dimensions, for both S and P-polarized excitations. Three different scenarios are considered in this regard. In the first case, contributions of the non-linearity and noninteger dimensions are added to different half spaces, i.e; nonlinear DM–linear DM noninteger dimensional interface (I^a). The derivation and results of this study are presented in chapter 3. In the second considered case non-linearity and noninteger dimensions are incorporated in the same half space, i.e; linear DM–nonlinear DM noninteger dimensional interface (I^b). The derivation and results of this study are presented in chapter 4. In the last considered scenario, optical charactersctisc are studeid when non-linearity and noninteger dimension are added simultaneously in both half spaces, i.e; linear DM noninteger dimensional–nonlinear DM noninteger dimensional interface (I^c). Derivation and discussion of this case are given in chapter 5. All planar interface geometries are defined in such a way that first part of the planar interface geometry corresponds to the excitation side. Moreover, first part of every chapter is devoted to the S-polarized excitation results and the second part is devoted to the P-polarized excitation results. Diagrammatic description of the considered cases is given in Fig.1.1 and a tabular outline of the research work presented in this thesis is given in Table.1.1.

For simplicity, all the physical constants considered in chapter 3 (related to I^a), chapter 4 (related to I^b) and chapter 5 (related to I^c) are represented by using a superscript 'a', 'b' and 'c', respectively. Hence, ϵ_i^a, ϵ_i^b and ϵ_i^c are linear permittivities taken in respective chapters. Similarly, μ_r^a, μ_r^b and μ_r^c represent the respective nonlinear permeabilities, and μ_t^a, μ_t^b and μ_t^c are the respective permeabilities of the half spaces in which transmitted wave propagates. Plots given in this thesis are obtained by taking fundamental frequency ($= \omega_i$) $= 1 \times 10^{16}$ rad/s, nonlinear condensed material with $\chi^{(2)}(2\omega_i) \simeq 6.94 \times 10^{-12}$ and ϵ_s is taken $\epsilon_o(1 + \chi^{(2)})$ [1].

Chapter No.	Excitation Electromagnetic Wave Taken		Planar Interface Geometry		Special Cases	Unknown Coefficients Symbols
	S-Polarization	P-Polarization	Left Half Space Medium	Right Half Space Medium	Left Half Space	S-Polarized Coefficients; P-Polarized Coefficients
3	✓	✓	Nonlinear Dielectric Magnetic	Linear Dielectric Magnetic NID	Nonlinear Epsilon Negative, Nonlinear Mu Negative	$A_\perp^R, A_\perp^T$; $A_\parallel^R, A_\parallel^T$
4	✓	✓	Linear Dielectric Magnetic	Nonlinear Dielectric Magnetic NID	Linear Epsilon Negative, Linear Mu Negative	$B_\perp^R, B_\perp^T$; $B_\parallel^R, B_\parallel^T$
5	✓	✓	Linear Dielectric Magnetic NID	Nonlinear Dielectric Magnetic NID	Linear Epsilon Negative NID, Linear Mu Negative NID	$C_\perp^R, C_\perp^T$; $C_\parallel^R, C_\parallel^T$

Table 1.1: An outline of the thesis
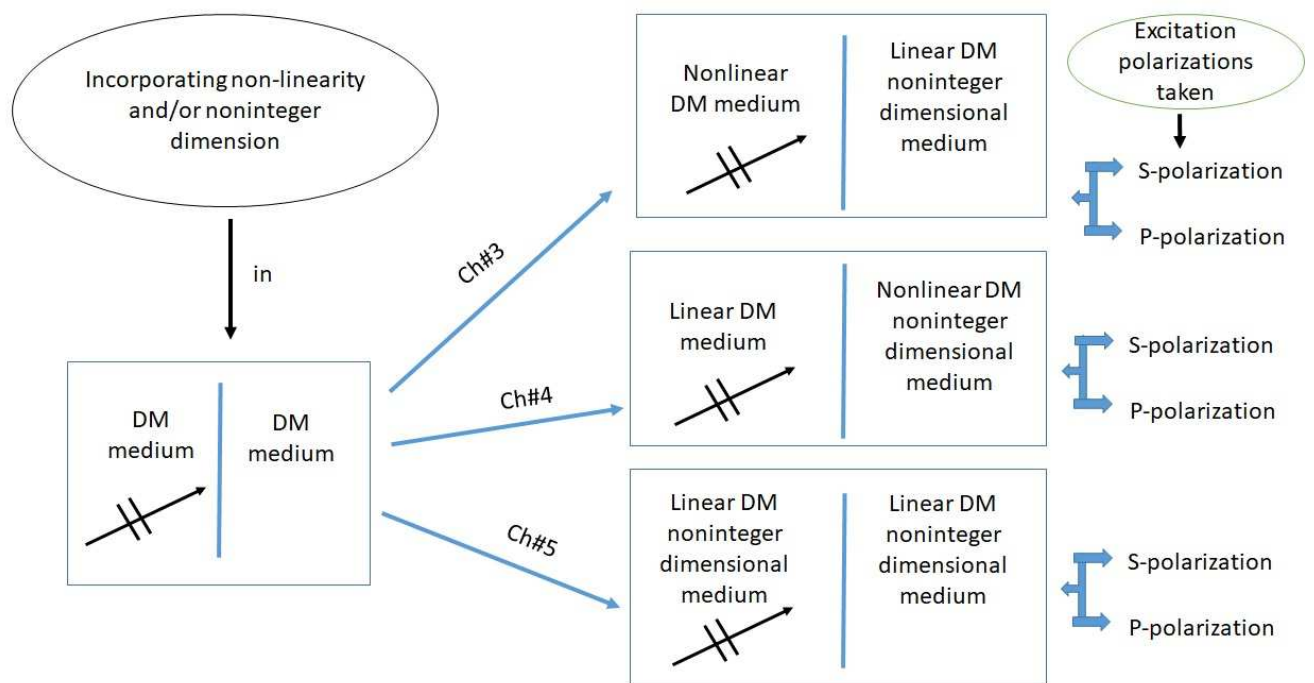
Figure 1.1: Diagrammatic representation of the work carried out in this thesis.

Chapter 2

Nonlinear dielectric magnetic and linear dielectric magnetic NID planar interface

This chapter is dedicated to the derivation and discussion of the reflection and transmission coefficients from a planar interface of second order nonlinear dielectric magnetic–linear dielectric magnetic NID medium. Nonlinear half space is represented as 'm_1' whereas linear half space is symbolized by 'm_2', for simplicity. Initially the unknown coefficients for S-polarization are calculated and discussed and in the second part derivation and discussion of the P-polarized coefficients are given. Solution of the nonlinear wave equation is obtained by using the SVA approximation, and the wave propagation in NID medium is modeled by using the MSV in NID space (discussed chapter 1). Changes in the behavior of the coefficients are also reported when NL dielectric magnetic medium is replaced with NL epsilon negative and mu negative mediums. Variations in the behavior of the coefficients are also studied when linear dielectric magnetic NID medium is replaced with the linear epsilon negative NID medium.
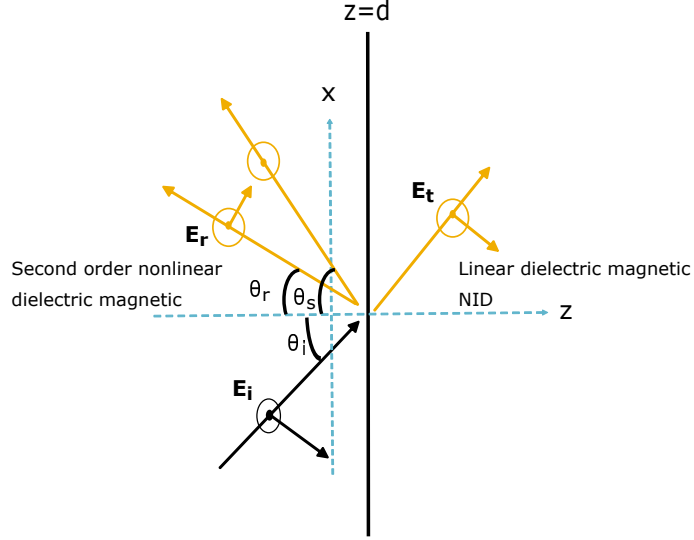
Figure 2.1: Second order NL dielectric magnetic and linear dielectric magnetic NID planar interface excited by S-polarized electromagnetic wave.

2.1 S-polarization excitation

2.1.1 Description of the geometry and mathematical formulation

Consider a planar interface placed at $z = q$, making two half space geometry as depicted in Fig.2.1. The Half space, $z < q$, contains second order NL dielectric magnetic medium which is represented by 'm_1'. Wave number of m_1 half space is $k_i^a = \sqrt{\epsilon_i^a(\omega_i)}\omega_i/c$. The other half space, $z > q$, is filled with linear dielectric magnetic NID medium, which is symbolized by 'm_2'. The wave number of medium m_2 is $k_t^a = \sqrt{\epsilon_t^a(\omega_s)}\omega_s/c$. In the expressions of the wave numbers, $\epsilon_i^a(\omega_i)$ and $\epsilon_t^a(\omega_s)$ represent the fundamental permittivity and the permittivity of the medium m_2 at second harmonic, which are hereafter written as ϵ_i^a and ϵ_t^a, for simplicity. Furthermore, D_1 ($1 < D_1 \leq 2$), is used to define the dimension of the dielectric magnetic NID medium.

S-polarized plane wave (Eq.(2.1)) making an angle θ_i with the normal to the interface is used to excite the planar interface. Electric field associated with the

incident electromagnetic wave is,

$$\mathbf{E_i}(\omega_i) = \hat{\mathbf{y}} E_o(\omega_i) e^{jk_i^a(\omega_i)(x \sin \theta_i + z \cos \theta_i)} \tag{2.1}$$

Solution of the nonlinear wave equation is obtained by using the SVA approximation as discussed in chapter 1. This solution provides the second harmonic reflected field as written below,

$$\mathbf{E_r}(\omega_s) = \hat{\mathbf{y}} \left[A_{\perp}^R e^{jk_r^a(x \sin \theta_r - z \cos \theta_r)} + \frac{P \omega_s^2 \mu_o}{(k_s^2 - k_r^{a2})} e^{jk_s(x \sin \theta_s - z \cos \theta_s)} \right] \tag{2.2}$$

It is noted that this equation is a combination of homogeneous and inhomogeneous waves. The wave vector of the inhomogeneous wave is represented by $\mathbf{k_s} = \sqrt{\epsilon_s(\omega_s)}\omega_s/c$. Transmitted field propagating in medium m_2, is obtained by using the MSV in NID space, is written as,

$$\mathbf{E_t}(\omega_s) = \hat{\mathbf{y}} A_{\perp}^T e^{jk_t^a x \sin \theta_t} \left(k_t^a \cos \theta_t z \right)^{o1} H_{o1}^{(2)}(k_t^a \cos \theta_t z) \tag{2.3}$$

Corresponding magnetic fields associated with the reflected and transmitted waves are,

$$\mathbf{H_r}(\omega_s) = \left(\hat{\mathbf{x}} \cos \theta_r + \hat{\mathbf{z}} \sin \theta_r \right) \left[\frac{A_{\perp}^R}{\eta_r^a} e^{jk_r^a(x \sin \theta_r - z \cos \theta_r)} \right.$$

$$\left. + \frac{P \omega_s^2 \mu_o}{\eta_s (k_s^2 - k_r^{a2})} e^{jk_s(x \sin \theta_s - z \cos \theta_s)} \right] \tag{2.4a}$$

$$\mathbf{H_t}(\omega_s) = \left(\hat{\mathbf{z}} \sin \theta_t - \hat{\mathbf{x}} \cos \theta_t \right) \frac{A_{\perp}^T}{\eta_t^a} e^{jk_t^a \sin \theta_t x} \left(k_t^a \cos \theta_t z \right)^{o_h} H_{o_h}^{(2)}(k_t^a \cos \theta_t z) \tag{2.4b}$$

In above equations, $H_{o_1}^2$ and $H_{o_h}^2$ are the hankel functions of second kind with order $o_1 = |\frac{3 - D_1}{2}|$ and $o_h = |\frac{D_1 - 1}{2}|$, respectively, where D_1 is the dimension of the NID medium. Continuity of the tangential components of the fields across

the interface is expressed as,

$$A_\perp^R e^{-jk_r^a q \cos\theta_r} + \frac{P\omega_s^2 \mu_o}{k_s^2 - k_r^{a2}} e^{-jk_s^a q \cos\theta_s} = A_\perp^T A \tag{2.5a}$$

$$\frac{A_\perp^R \cos\theta_r \lambda_1}{\eta_r^a} + \frac{P\cos\theta_s \omega_s^2 \mu_o \lambda_2}{\eta_s (k_s^2 - k_r^{a2})} = -\frac{A_\perp^T \cos\theta_t B}{\eta_t^a} \tag{2.5b}$$

Analytical solution of Eq.(2.5) provides the unknown reflection and transmission coefficients,

$$A_\perp^R = \frac{\eta_s (k_r^{a2} - k_s^2)(A\delta_{tr} + B\delta_{rt})e^{-\iota d(k_r^a \cos\theta_r - k_s \cos\theta_s)}}{\delta_{cc}^r (A\delta_{ts} + B\delta_{st})} \tag{2.6a}$$

$$A_\perp^T = \frac{\eta_s \eta_t (k_r^{a2} - k_s^2)(-\delta_{sr} + \delta_{rs})(A\delta_{tr} + B\delta_{rt})e^{-\iota d(2k_r^a \cos\theta_r - k_s \cos\theta_s)}}{\eta_r \delta_{cc}^r (A\delta_{ts} + B\delta_{st})^2} \tag{2.6b}$$

In above equations, $A_\perp^R$ and $A_\perp^T$ are the unknown reflection and transmission coefficients, respectively and subscripts are used to indicate the polarization of the incident electromagnetic wave. All definitions used to write Eq.(2.6) in compact form are given in appendix. Moreover, the unknown angles θ_r, θ_s and θ_t, are obtained by using the NLO generalization of Snell's law that is,

$$\sqrt{\epsilon_i}(\omega_i)\sin\theta_i = \sqrt{\epsilon_r}(\omega_s)\sin\theta_r = \sqrt{\epsilon_t}(\omega_s)\sin\theta_t = \sqrt{\epsilon_s}(\omega_s)\sin\theta_s \tag{2.7}$$

It is important to note that ϵ_i is the permittivity of the material observed at fundamental frequency, whereas $\epsilon_t, \epsilon_r, \epsilon_s$ are the permittivities observed at second harmonic frequency.

2.1.2 Results and discussions

The unknown reflection and transmission coefficients which are derived in previous section are discussed here as a function of $\epsilon_i^a, \epsilon_t^a, \mu_r^a$ (nonlinear permeability) and θ_i. Changes in the behavior of the unknown coefficients are studied when nonlinear epsilon negative (NL–EN) and nonlinear mu negative (NL–MN) mediums are taken as mediums of reflection and epsilon negative noninteger dimensional (EN–NID) medium is taken as medium of transmis-

sion. In all these cases impact of the non-linearity and the noninteger dimension are studied separately.

In the first part of analysis, to note the impact of non-linearity on the coefficients coefficients are studied for ordinary medium of transmission i.e; for $D_1 = 2$, (Fig.2.2–Fig.2.4). In Fig.2.2, behavior of the coefficients is studied as a function of ϵ_i^a for specific values of ϵ_t^a (Fig.2.2a), μ_r^a (Fig.2.2b) and θ_i (Fig.2.2c). In Fig.2.2a, it is observed that amplitude of the transmission coefficient decreases by increasing the value of ϵ_t^a, whereas amplitude of the reflection coefficient decreases for $-3 < \epsilon_i^a < 0.4$ and $\epsilon_i^a (> 2)$ and increases for $0.4 < \epsilon_i^a < 2$. In Fig.2.2b, it is noted that amplitude of the reflection coefficient increases by increasing μ_r^a. On the other hand, amplitude of the transmission coefficient increases for specific ranges of ϵ_i^a, i.e; $-3 < \epsilon_i^a < -0.4$ and $0.4 < \epsilon_i^a < 3$ and decreases for $-0.4 < \epsilon_i^a < 0.4$. In Fig.2.2c, it is studied that both coefficient's curves shift towards left by increasing the value of θ_i for only dielectric magnetic medium. Results also depict that maximum amplitude of the coefficients can be achieved by taking $\epsilon_i^a = -3$, $\epsilon_t^a = 1.9$, $\mu_r^a = 0.09$ and $\theta_i = 45°$ for epsilon negative (EN) medium, whereas for NL dielectric magnetic medium, maximum amplitude of the coefficients can be achieved for $\epsilon_i^a = 0.8$, $\epsilon_t^a = 2.4$, $\mu_r^a = 0.01$ and $\theta_i = 60°$.

In Fig.2.3, behavior of the coefficients is given as a function of ϵ_t^a. It can be noted that amplitude of the coefficients decreases by increasing ϵ_i^a for EN–NID, and increases for dielectric magnetic NID medium (except at $\epsilon_i^a = 1.8$). Furthermore, peaks of the coefficients also shift towards right by increasing ϵ_i^a (Fig.2.3a). In Fig.2.3b, it is noted that amplitude of the coefficients for EN–NID (dielectric magnetic NID) medium can be decreased (increased) by increasing μ_r^a. Results also depict that amplitude of the transmission coefficient is almost negligible for any positive value (s) of ϵ_t^a compared to negative value (-s) of ϵ_t^a, for example; $|A_\perp^T| = 1.5$ and 0.2, for $\epsilon_t^a = -3$ and $\epsilon_t^a = 3$, respectively. In Fig.2.3c, it can be noted that by taking higher values of θ_i amplitude of the coefficients decreases (increases) for EN–NID (dielectric magnetic NID) medium. Comparing the results depicted Fig.2.3, it is observed that maximum amplitude of the coefficients can be achieved by taking (i) $\epsilon_i^a = 0.8$ or 2.3, $\epsilon_t^a = 0.8$–1.2 or (ii) $\epsilon_t^a = -3$, $\epsilon_i^a = 0.8$ for $\mu_r^a = 0.01$, $\theta_i = 45°$.

In Fig.2.4, coefficients are studied as a function of μ_r^a for specific values of ϵ_i^a (Fig.2.4a), ϵ_t^a (Fig.2.4b) and θ_i (Fig.2.4c). Results depict that amplitude of the reflection coefficient increases by increasing either ϵ_i^a, ϵ_t^a and θ_i. It is also noted that amplitude of both coefficients is greater for mu near zero medium. Comparing all the results depicted in Fig.2.4, it is studied that higher amplitude of the reflection coefficient is achieved for denser NL dielectric magnetic medium with $\theta_i = 60°$. From the comparison of all subplots given in Fig.2.2–Fig.2.4, it is noted that higher transmission can be achieved by using mu near zero (MNZ) material, whereas for other positive or negative values of μ_r^a, transmission coefficient remain negligible.

Now the aim is to study the impact of the noninteger dimension on the behavior of the reflection and transmission coefficients. Plots given in Fig.2.5–Fig.2.6 are obtained for $D_1 \neq 2$. Coefficient are studied as a function of ϵ_i^a, ϵ_t^a and μ_t^a in Fig.2.5, by taking specific values of D_1. It is interesting to note that amplitude of the reflection coefficient decreases by increasing D_1 for $-3 < \epsilon_i^a < -1.4$ and $\epsilon_i^a > 0.4$ and increases for $-1.4 < \epsilon_i^a < 0.4$ (Fig.2.5a). Results also depict that for a NL–EN (NL dielectric magnetic) medium, amplitude of the transmission coefficient increases (decreases) by taking higher dimensions. It can be noted that for NL–EN (NL dielectric magnetic) medium amplitude of the reflection coefficients increases (decreases) by increasing the dimension parameter. Moreover, higher amplitude of the reflection coefficient is noted for epsilon near zero medium (Fig.2.5b), whereas maximum amplitude of both the coefficients is noted for mu near zero medium (Fig.2.5c). It is also noted that amplitude of the reflection coefficient increases by increasing the noninteger dimension for $-3 < \epsilon_t^a < -0.2$ whereas, decreases for $\epsilon_t^a > 0.4$. In Fig.2.5c, it is noted that amplitude of the coefficients increases by increasing the dimension of NL–MN and NL dielectric magnetic noninteger dimensional mediums. In Fig.2.6, coefficients are studied as a function of the dimension parameter by taking fixed values of the other parameters (ϵ_i^a, ϵ_t^a and μ_r^a). It can be noted that amplitude of the coefficients decrease as $D_1 \rightarrow 2$ except at $\theta_i = 30°$. From the comparison of all plots given in Fig.2.5–Fig.2.6, it is also noted that amplitude of the coefficients can be enhanced by using NL mu near zero medium and an epsilon near zero NID medium having dimension $1 < D_1 < 1.2$ for smaller

value of the incident angle.

(a)

(b)

(c)
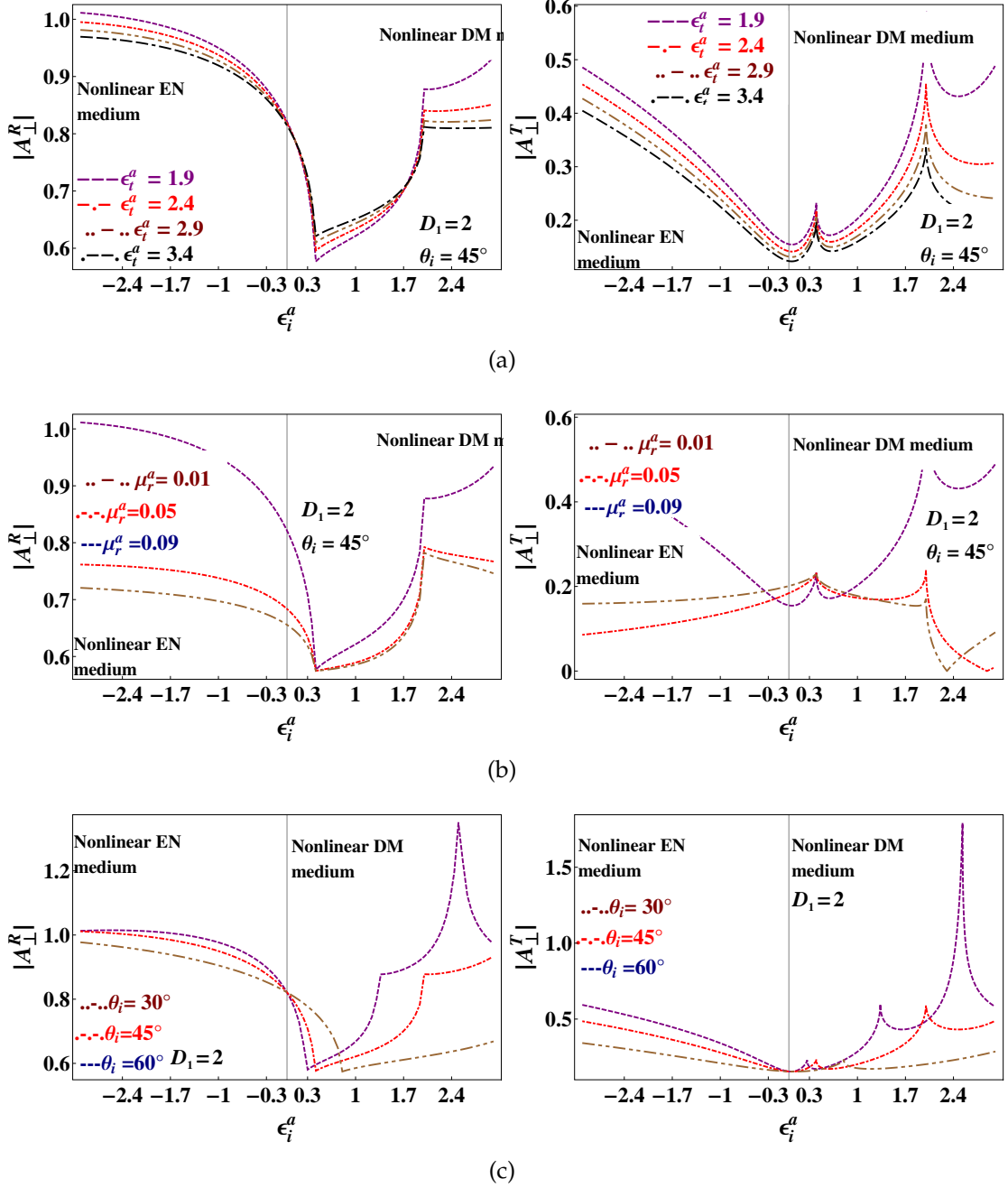
Figure 2.2: Behavior of $|A_\perp^R|$ and $|A_\perp^T|$ with respect to ϵ_i^a for $D_1 = 2$.
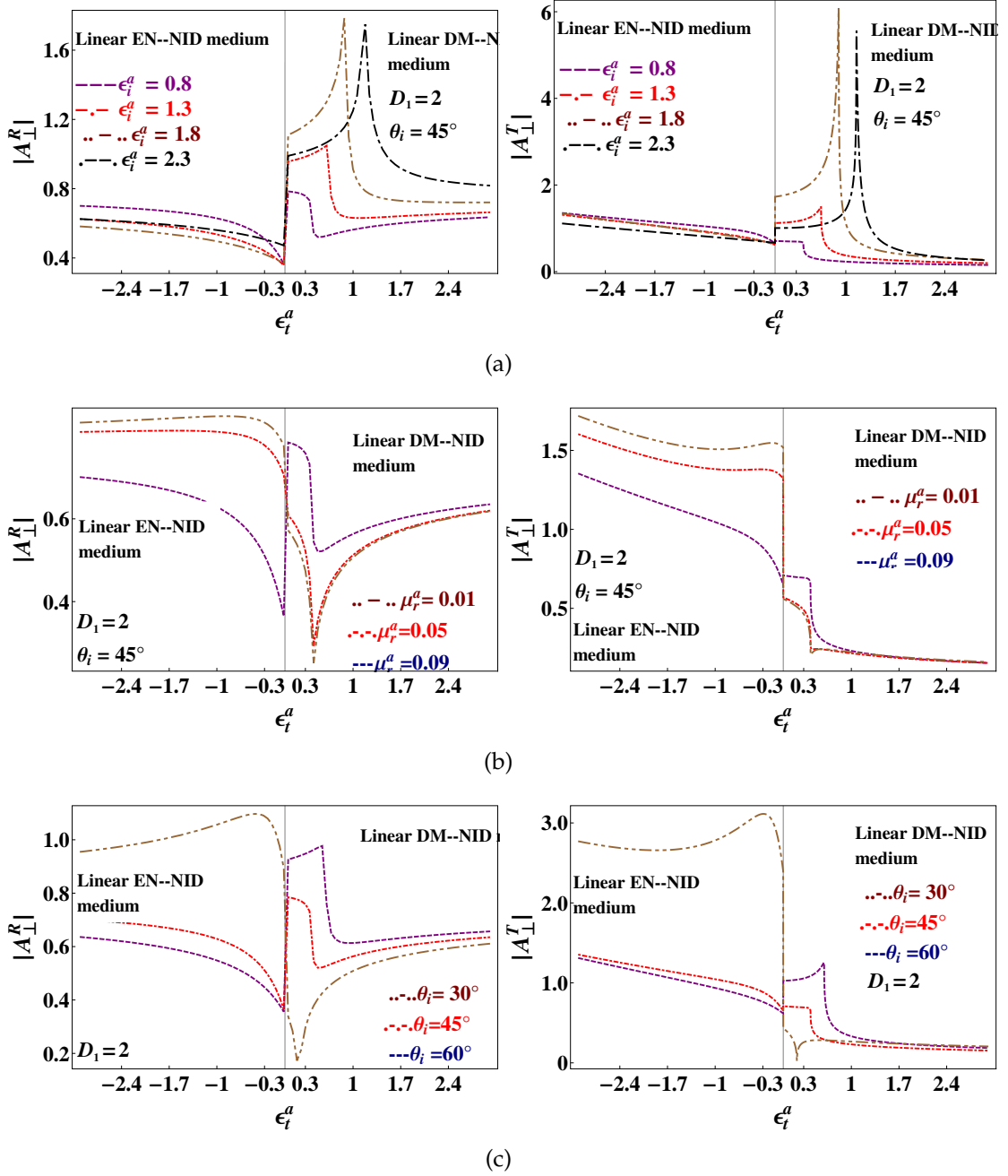
Figure 2.3: Behavior of $|A_\perp^R|$ and $|A_\perp^T|$ with respect to ϵ_t^a for $D_1 = 2$.
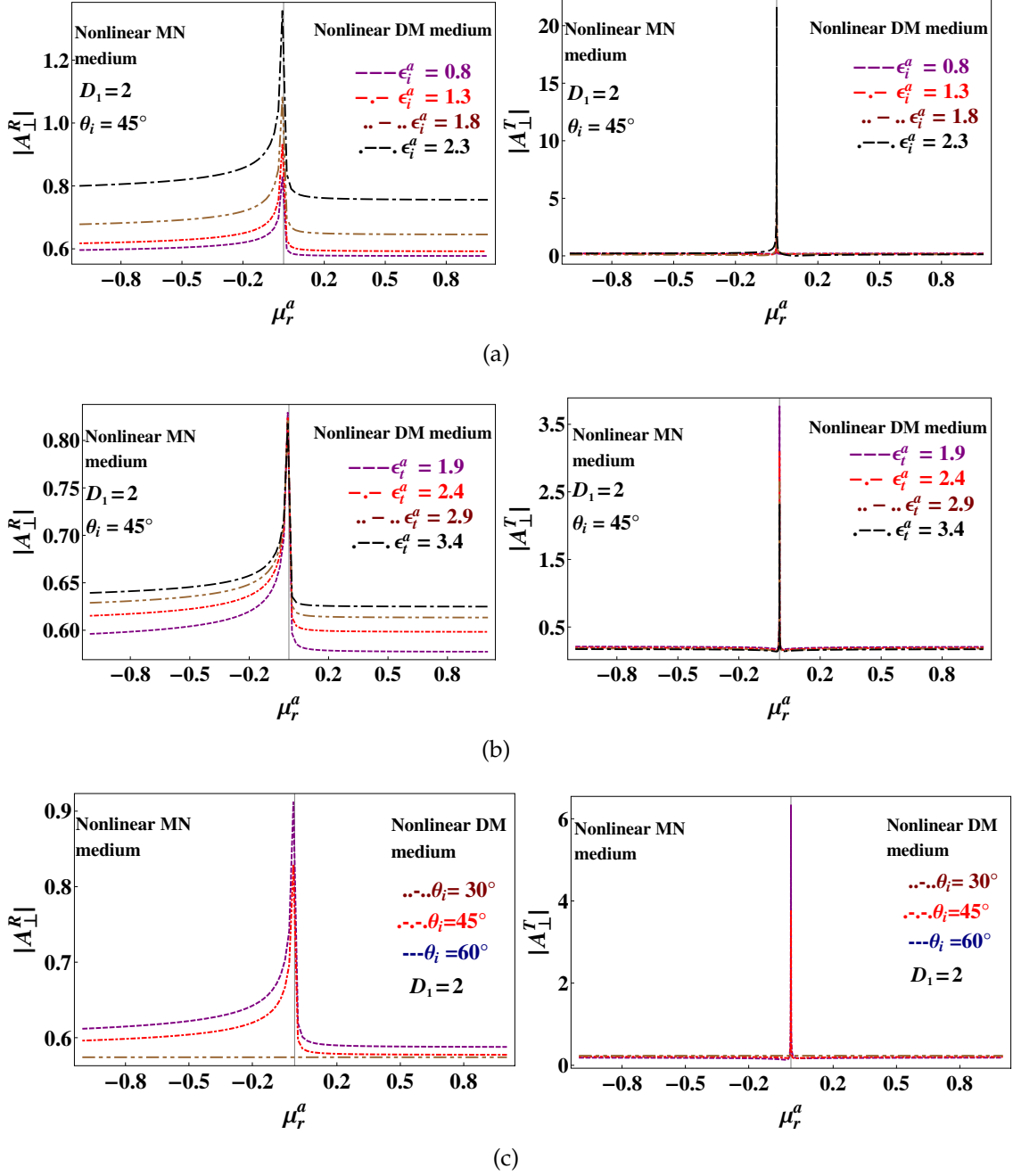
Figure 2.4: Behavior of $|A_\perp^R|$ and $|A_\perp^T|$ with respect to μ_r^a for $D_1 = 2$.

(a)

(b)

(c)
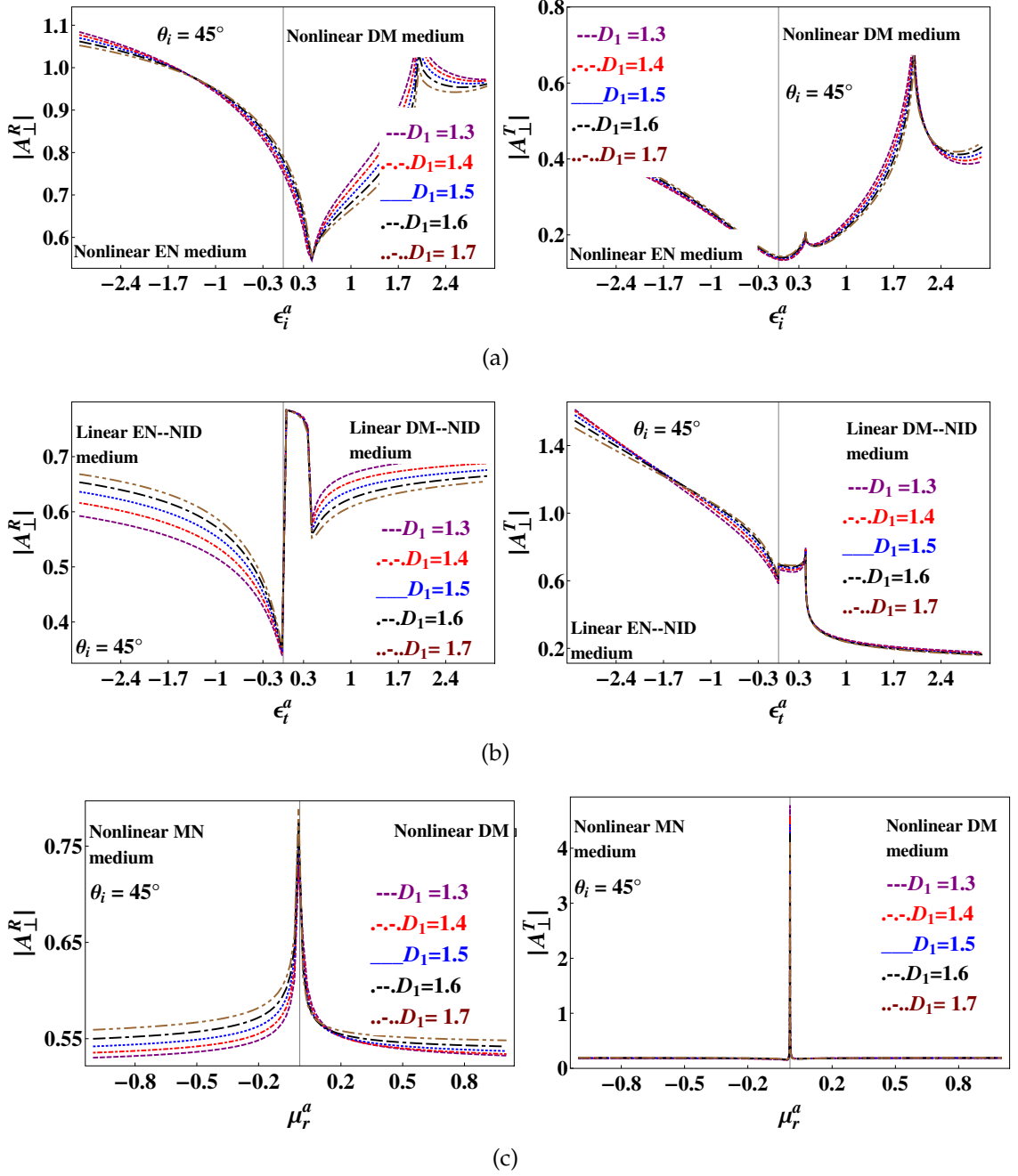
Figure 2.5: Behavior of $|A_\perp^R|$ and $|A_\perp^T|$ with respect to (a) ϵ_i^a (b) ϵ_t^a and (c) μ_r^a for the variations of the dimension parameter.

(a)

(b)

(c)

Figure 2.6: (cont.)

(d)
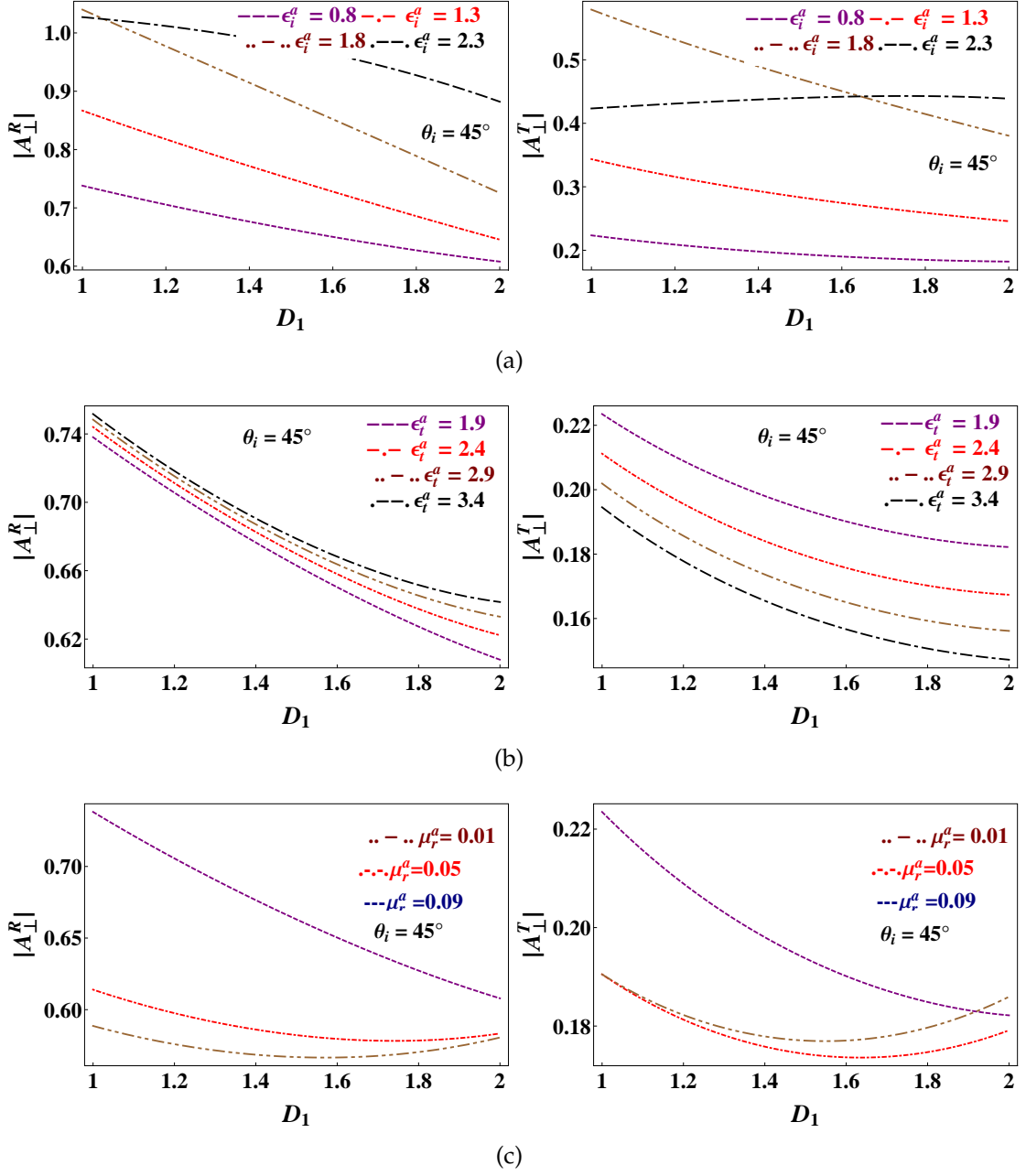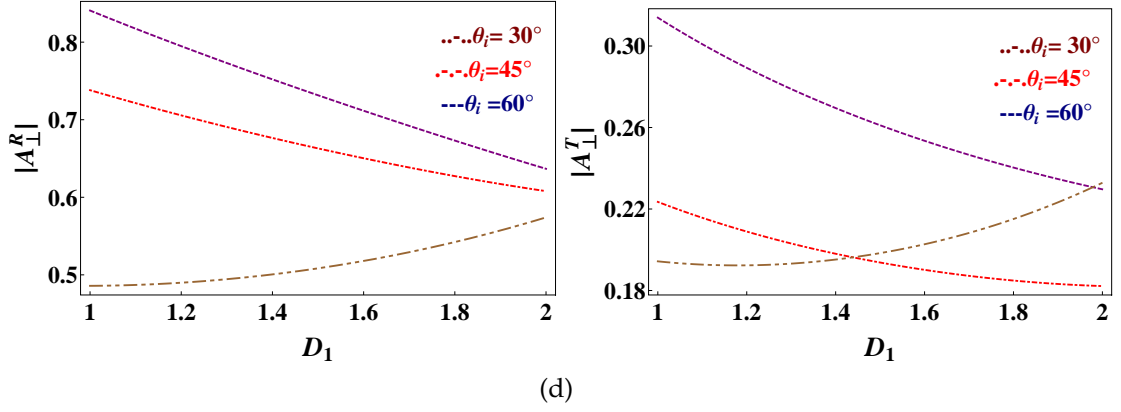
Figure 2.6: Behavior of $|A_\perp^R|$ and $|A_\perp^T|$ with respect to dimension parameter.
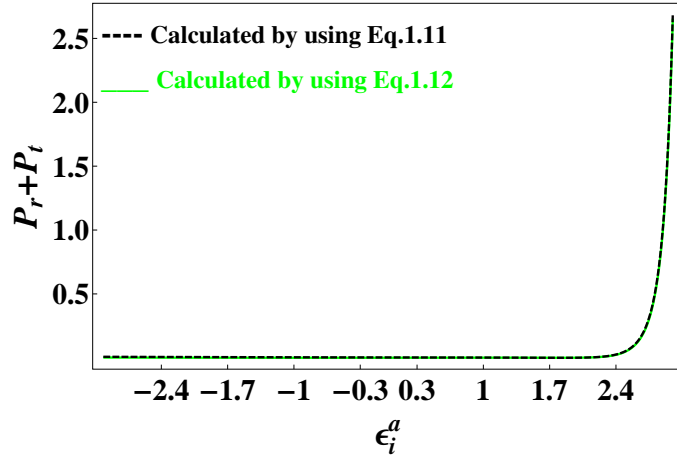
Figure 2.7: Sum of S-polarized reflected and transmitted powers for I^a .

2.1.3   Conclusions

This section is dedicated to study the S-polarized reflection and transmission characteristics of a DM–DM planar geometry, when non-linearity and non-integer dimension are considered in opposite half spaces, i.e; NL dielectric magnetic–linear dielectric magnetic NID planar interface. It is noted that considerable enhancement in the amplitude of the coefficients is achieved by using epsilon near zero NID and NL mu near zero mediums as left half spaces. Results depict that amplitude of the reflection coefficient increases by increasing the nonlinear permeability. On the other hand, amplitude of the transmission

coefficient increases for only $-3 < \epsilon_i^a < -0.4$ and $0.4 < \epsilon_i^a < 3$ range, whereas, for $-0.4 < \epsilon_i^a < 0.4$, amplitude of the transmission coefficient decreases by increasing the nonlinear permeability. It is also noticed that maximum amplitude of the coefficients is achieved by taking $\epsilon_i^a = -3$, $\epsilon_t^a = 1.9$, $\mu_r^a = 0.09$ and $\theta_i = 45°$ for NL epsilon negative medium, whereas for NL dielectric magnetic medium, higher amplitude of the coefficients is observed by taking $\epsilon_i^a = 0.8$, $\epsilon_t^a = 2.4$, $\mu_r^a = 0.01$ and $\theta_i = 60°$. It is also noted that impact of the non-linearity on the amplitude of the coefficients is of considerable importance for all considered materials, for example; NL epsilon negative, NL mu negative and NL dielectric magnetic mediums. Among these all mediums, strongest contribution of the non-linearity is noted for NL mu near zero material. Results also depict that amplitude of the coefficients is controlled by using the noninteger dimension of the material. Furthermore, it is also noted that amplitude of the reflection coefficient increases (decreases) by increasing the noninteger dimension of EN–NID (dielectric magnetic NID) medium.

2.2   P-polarization excitation

2.2.1   Description of the geometry and mathematical formulation

Consider a planar interface placed at $z = q$ and excited by a P-polarized electromagnetic wave, as depicted in Fig.2.8. Description of the geometry is given in Sec.2.1. Electric and magnetic fields associated with the incident plane wave are $\mathbf{E_i} = (E_{ix}, 0, E_{iz})^T$ and $\mathbf{H_i} = (0, H_{iy}, 0)^T$, respectively. Furthermore induced NL polarization is $\mathbf{P}$, where $\hat{p}$ depicts a unit vector in the plane of Fig.2.8.

Reflected field propagating in medium m_1, is the solution of the nonlinear wave equation,

$$\mathbf{E_r}(\omega_s) = (\hat{E}_{rx} + \hat{E}_{rz})A_\parallel^R e^{jk_r^a(x\sin\theta_r - z\cos\theta_r)} + \hat{p}\frac{\omega_s^2\mu_o P}{(k_s^2 - k_r^{a2})}e^{jk_s(x\sin\theta_s - z\cos\theta_s)} \quad (2.8)$$
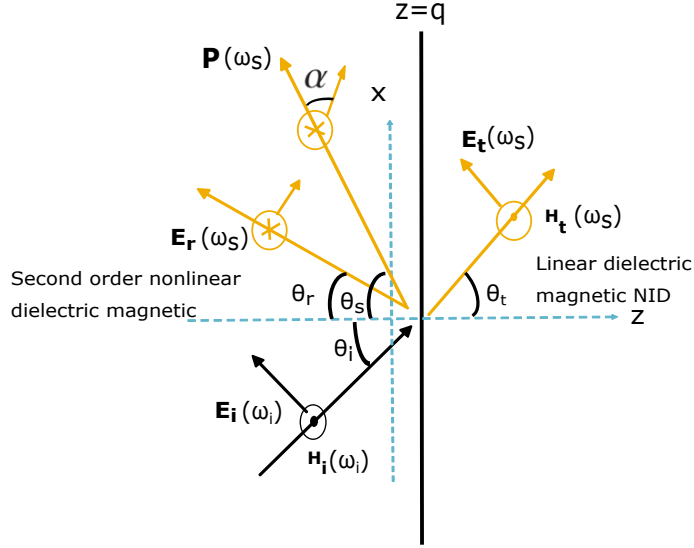
Figure 2.8: Second order NL dielectric magnetic and linear dielectric magnetic NID planar interface excited by P-polarized plan wave.

This solution is obtained by using SVA approximation (discussed in chapter 1). Following the procedure of MSV in NID space (Sec.1.3.1), transmitted field propagating in medium m_2 is obtained as written below,

$$\mathbf{E_t}(\omega_s) = (\hat{E}_{tx} + \hat{E}_{tz})A_{\parallel}^T e^{-jk_t^a \sin\theta_t x} \left(k_t^a \cos\theta_t q\right)^{o_1} H_{o_1}^{(2)}\left(k_t^a \cos\theta_t q\right) \qquad (2.9)$$

It is worth-mentioning that medium m_2 has noninteger dimension in only z-axis direction i.e; following definition of the Laplacian operator (∇_D^2) has been used [100]

$$\nabla_D^2 = \frac{\partial^2}{\partial x^2} + \frac{\partial^2}{\partial z^2} + \frac{D-2}{z}\frac{\partial}{\partial z'}$$

Equating the tangential components of the fields across the interface, following equations are obtained,

$$A_{\parallel}^T \cos\theta_t A = A_{\parallel}^R \cos\theta_r + \frac{P\omega_s^2 \mu_o \sin\alpha \cos\theta_s}{k_s^2 - k_r^{a2}} + \frac{P\omega_s^2 \mu_o \cos\alpha \sin\theta_s}{k_r^{a2}} \qquad (2.10a)$$

$$-\frac{A_{\parallel}^T B}{\eta_t^a} = \frac{A_{\parallel}^R}{\eta_r^a}e^{-jk_r q \cos\theta_r} + \frac{\omega_s^2 \mu_o P \sin\alpha}{\eta_s(k_s^2 - k_t^{a2})}e^{-jk_r^a q \cos\theta_r} \qquad (2.10b)$$

In above equations, $A_\parallel^R$ and $A_\parallel^T$ are the unknown coefficients, where superscripts (R, T) are used to differentiate between reflection and transmission coefficients and the subscript is used to indicate the polarization of the incident wave. In Eq.(2.10), α is representing the angle formed between **P** and $\mathbf{k_t^a}$, as depicted in Fig.2.8. Analytical solution of Eq.(2.10), is written below as,

$$A_\parallel^R = \frac{\tau_1}{\tau_2} \tag{2.11a}$$

$$A_\parallel^T = \frac{\tau_3}{\tau_4}, \tag{2.11b}$$

where,

$$
\begin{aligned}
\tau_1 =\ & k_r^{a2}\eta_s\left(k_r^{a2}-k_s^2\right)\left(B\delta_{rr}+A\delta_{tt}\lambda_1\right) \\
\tau_2 =\ & \delta_{cc}^r\left[k_r^{a2}\left(B\delta_{ss}+A\eta_t^a\gamma_2\lambda_2\right)\right. \\
& \left. + B\eta_s\gamma_1(k_s^2-k_r^{a2})\right] \\
\tau_3 =\ & k_r^{a2}\eta_s\eta_t^a\left(k_r^{a2}-k_s^2\right)\left(B\delta_{rr}+A\delta_{tt}\lambda_1\right)\left[k_r^{a2}\left(\delta_{rr}\lambda_2\right.\right. \\
& \left.\left. - \delta_{ss}\lambda_1\right)\sin\alpha + \lambda_1\left(k_r^{a2}-k_s^2\right)\eta_s\gamma_1\right] \\
\tau_4 =\ & \delta_{cc}^r\eta_r^a\left[k_r^{a2}\left(B\sin\alpha\delta_{ss}+A\lambda_2\eta_t^a\gamma_2\right)\right. \\
& \left. + B\left(k_s^2-k_r^{a2}\right)\eta_s\gamma_1\right]^2.
\end{aligned}
$$

Different definitions used to write the above equations in compact form are given in appendix.

2.2.2 Results and discussion

P-polarized reflection and transmission coefficients, derived in previous section are discussed in this section as a function of ϵ_i^a, ϵ_t^a and μ_r^a. Analysis is also conducted by taking nonlinear epsilon negative and nonlinear mu negative mediums as medium m_1 and epsilon negative noninteger dimensional medium as medium m_2.

Initially, analysis is conducted for ordinary dimension of medium m_2 ($D_1 = 2$),

to note the nonlinear contributions, Fig.2.9–Fig.2.11 depict these results. In Fig.2.9, coefficients are studied as a function of ϵ_i^a by taking specific values of ϵ_t^a (Fig.2.9a), μ_r^a (Fig.2.9b) and θ_i (Fig.2.9c). It is also noted that amplitude of the coefficients, decreases by increasing ϵ_t^a. It can be noted that for a NL–EN medium amplitude of the coefficients can be increased by increasing ϵ_i^a for any particular value of ϵ_t^a (Fig.2.9a). On the other hand, amplitude of the coefficients increases by increasing μ_r^a for both NL–EN and NL dielectric magnetic mediums (Fig.2.9b). It is interesting to note that amplitude of the coefficients for NL–EN medium decreases by increasing θ_i and increases for NL dielectric magnetic medium. Moreover, peaks shifting towards left is also observed by increasing θ_i for only NL dielectric magnetic medium (Fig.2.9c). It is also noted that behavior of the coefficients changes as $\epsilon_i^a \to 0$. Furthermore, the observed amplitude of the reflection coefficient for NL dielectric magnetic medium is smaller compared to amplitude observed for NL–EN medium. Comparing all the results given in Fig.2.9, it is noted that higher amplitude of the coefficients is achieved by taking $\epsilon_t^a = 1.9$ and $\mu_r^a = 0.09$.

In Fig.2.10, behavior of the coefficients are given as a function of ϵ_t^a for specific values of ϵ_i^a (Fig.2.10a), μ_r^a (Fig.2.10b) and θ_i (Fig.2.10c). Results depict that amplitude of the reflection coefficient increase by increasing ϵ_i^a, for $-3 < \epsilon_t^a < -1.7$, and decreases for $-1.7 < \epsilon_t^a < -1$ and $-0.3 < \epsilon_t^a < -0.01$. On the other hand, for dielectric magnetic NID medium amplitude of the reflection coefficient increases by increasing ϵ_i^a (Fig.2.10a). It is noted that amplitude of the reflection coefficient decreases by increasing μ_r^a for $-3 < \epsilon_t^a < -1.3$, whereas increases for $\epsilon_t^a > -1.3$ (Fig.2.10b). Whereas, for higher values of the incident angle amplitude of the reflection coefficient decreases for $-3 < \epsilon_t^a < -0.3$ (Fig.2.10c). Results also depict that, maximum amplitude of the coefficients can be achieved by taking $\epsilon_i^a = 0.8$ and $\mu_r^a = 0.09$, for epsilon near zero medium (Fig.2.10).

In Fig.2.11, behavior of the coefficients are depicted as a function of μ_r^a. It is noted that amplitude of the coefficients increases by increasing ϵ_i^a (Fig.2.11a) and ϵ_t^a (Fig.2.11b). In Fig.2.11c, it is noted that maximum amplitude of the reflection and transmission coefficient can be achieved for $\theta_i = 60°$ and $\theta_i = 30°$, respectively. Comparing all the results given in Fig.2.11, it is noted that behav-

ior of the coefficients changes when $\mu_r^a \to 0$. Results also depict that for mu near zero medium, maximum amplitude of the reflection (transmission) coefficient is achieved by taking $\epsilon_i^a = 2.3$ ($\theta_i = 30°$).

Plots given in Fig.2.12–Fig.2.14, depict the impact of the noninteger dimension on the behavior of the P-polarized coefficients. Behavior of the coefficients as a function of ϵ_i^a are given in Fig.2.12. It is noted that amplitude of the coefficients decreases by taking higher noninteger dimensions for $1 < \epsilon_i^a < 2$ and increases for $\epsilon_i^a > 2$. For NL–EN medium, amplitude of the coefficients decreases by increasing the dimension parameter (Fig.2.12b) . In Fig.2.13 and Fig.2.14, it is noted that amplitude of the coefficients decreases by increasing the noninteger dimension for all taken cases. Results also depict that amplitude of the coefficients are controlled by using the noninteger dimension.

(a)

(b)

(c)

Figure 2.9: Behavior of $|A_{\parallel}^R|$ and $|A_{\parallel}^T|$ with respect to ϵ_i^a for $D_1 = 2$.

(a)

(b)

(c)

Figure 2.10: Behavior of $|A_{\parallel}^R|$ and $|A_{\parallel}^T|$ with respect to ϵ_t^a for $D_1 = 2$.

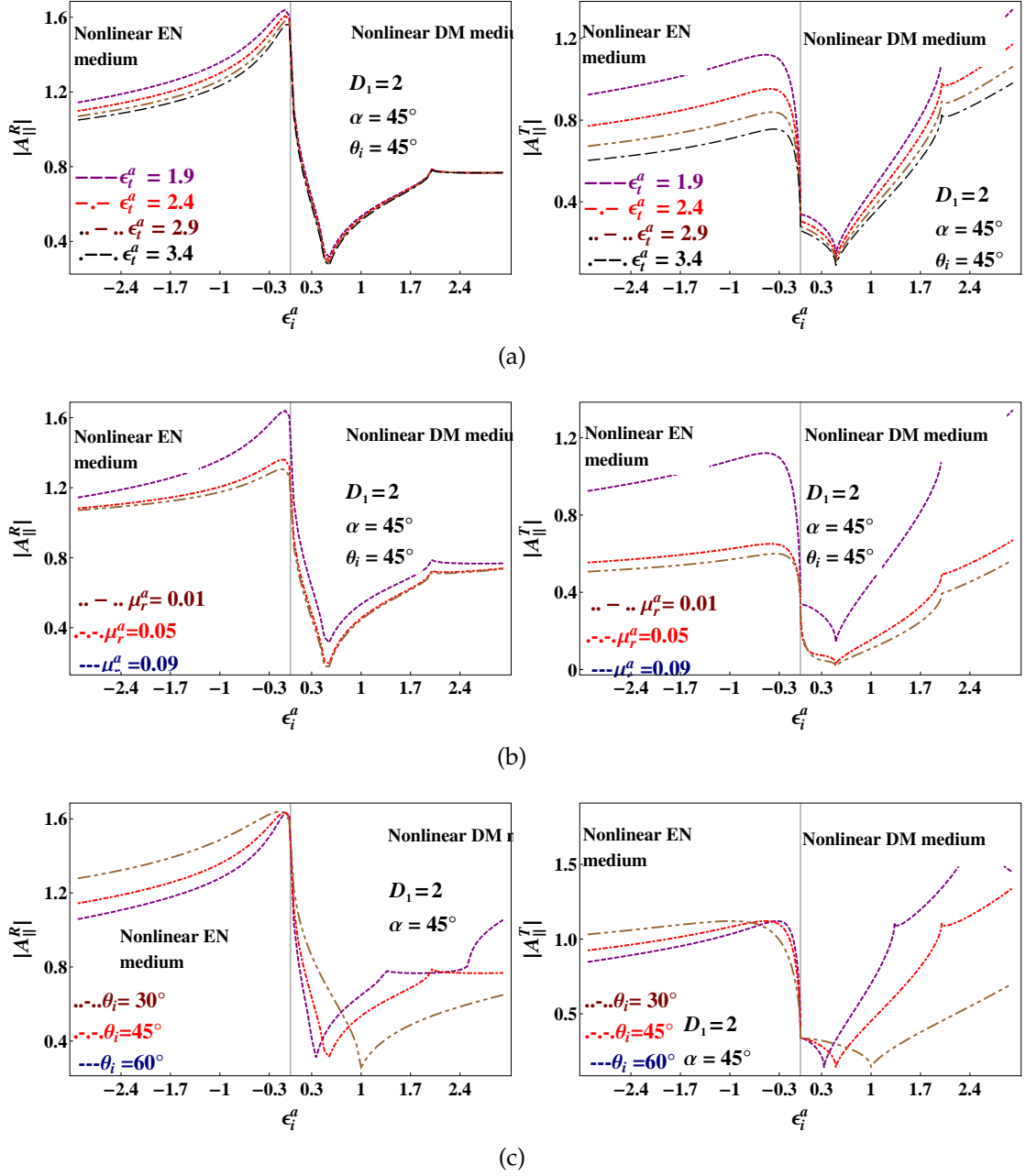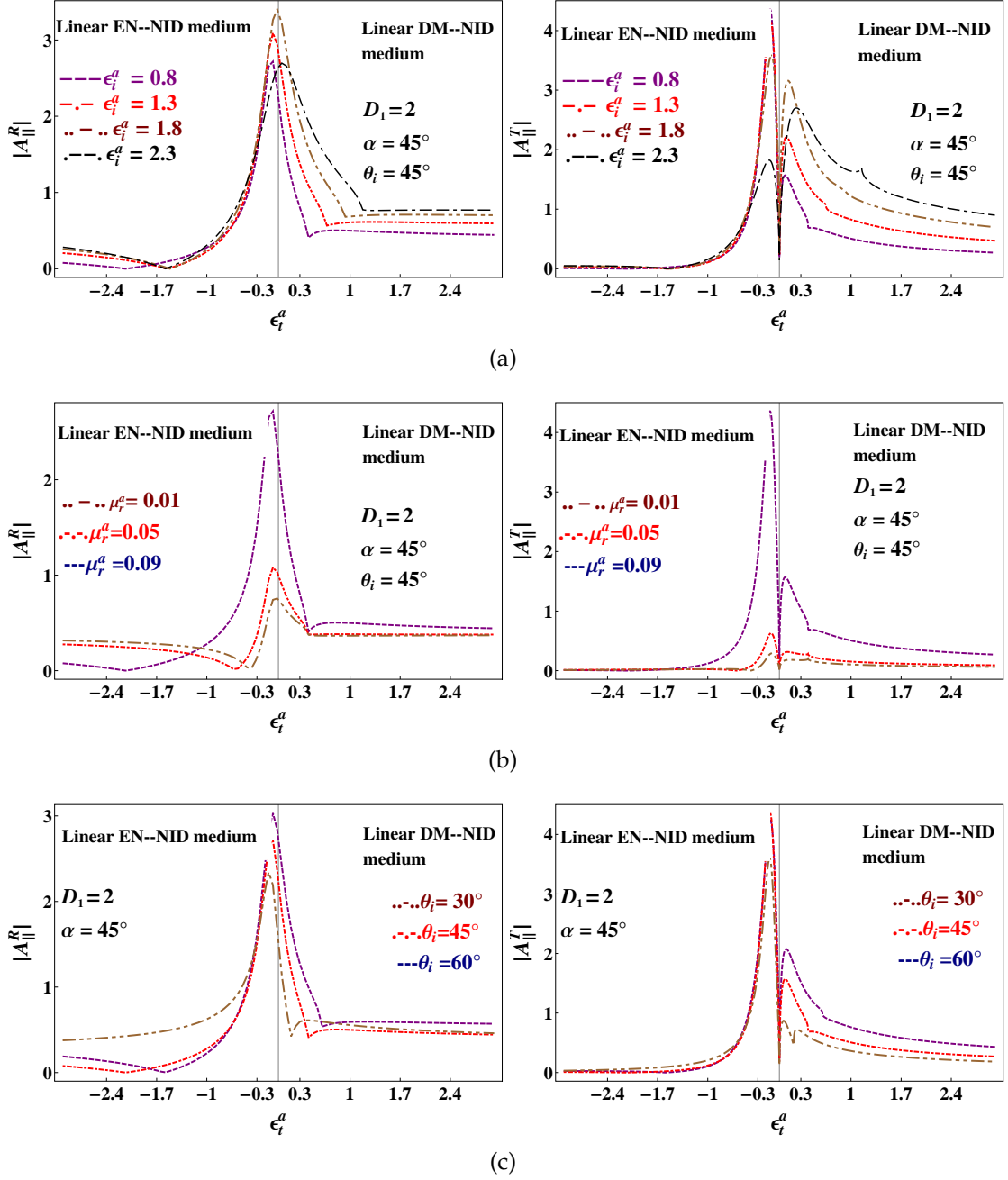(a)

(b)

(c)
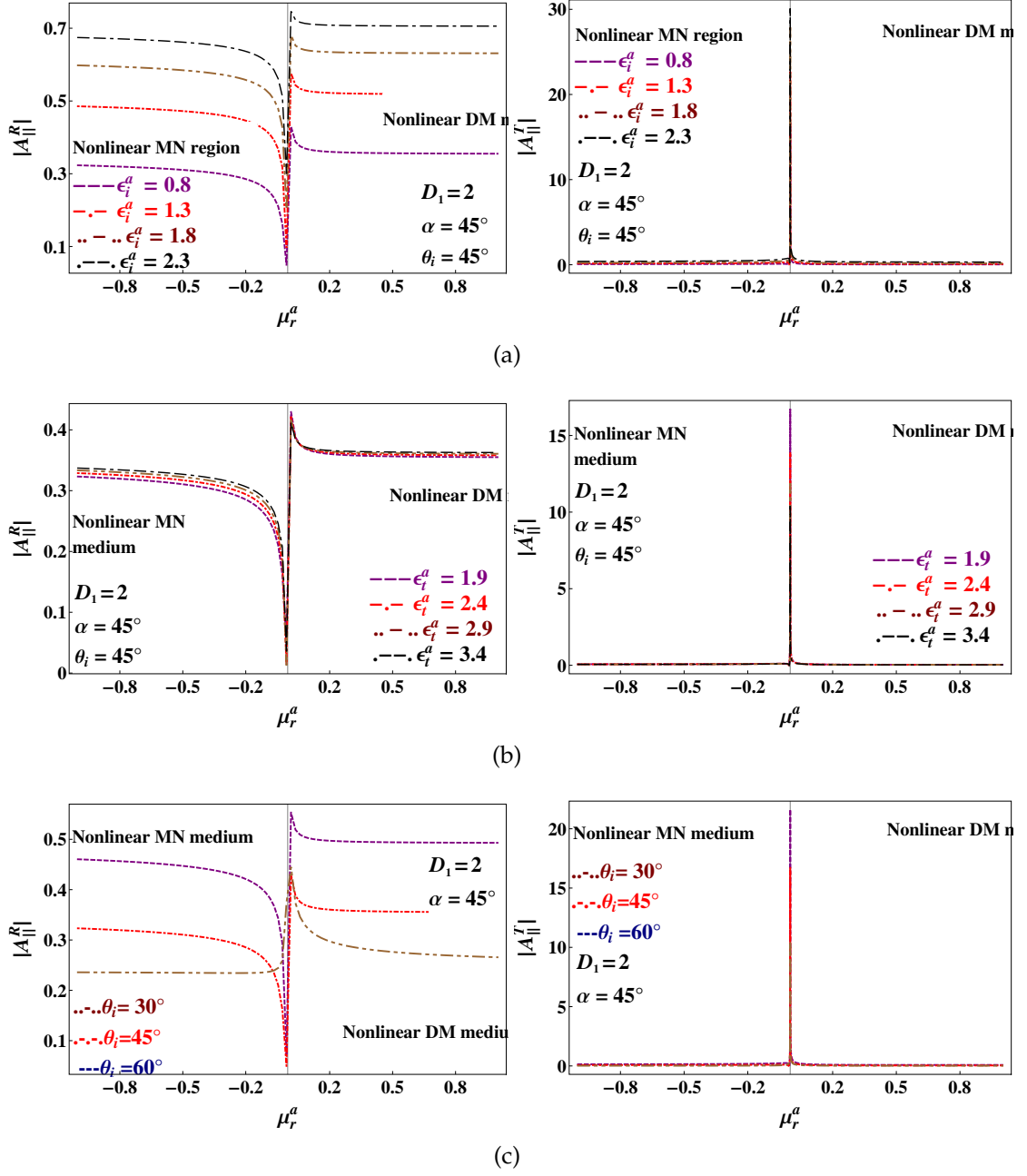
Figure 2.11: Behavior of $|A_{\parallel}^R|$ and $|A_{\parallel}^T|$ with respect to μ_r^a for $D_1 = 2$.

(a)

(b)

Figure 2.12: Behavior of $|A_{\parallel}^R|$ and $|A_{\parallel}^T|$ with respect to ϵ_i^a for the variations of the dimension parameter.
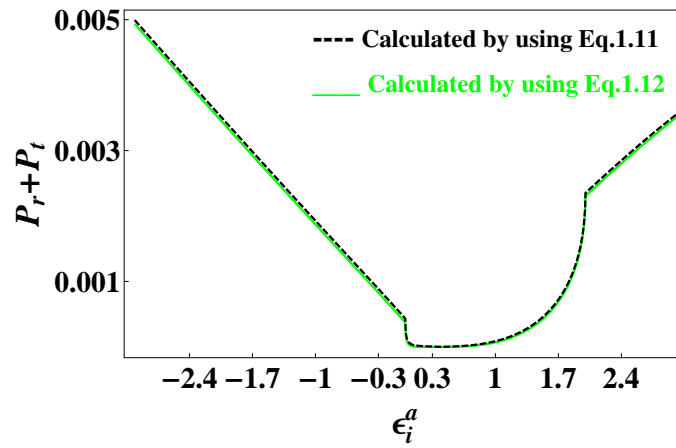
Figure 2.15: Sum of P-polarized reflected and transmitted powers for I^a .

2.2.3 Conclusion

The derivation and discussion of the P-polarized reflection and transmission characteristics is given in this section for a DM–DM interface when non-linearity and noninteger dimension are considered in opposite half spaces, i.e; NL dielectric magnetic–linear dielectric magnetic NID planar interface. Results depict that amplitude of the coefficients increases by increasing ϵ_i^a for nonlinear epsilon negative medium. Similarly, for nonlinear dielectric magnetic medium, amplitude of the coefficients increases by increasing nonlinear permeability. It is observed that amplitude of the coefficients decreases by increasing θ_i when nonlinear epsilon negative medium is taken as reflected half space. On the other hand, higher amplitude of the reflection coefficient is noticed when nonlinear dielectric magnetic medium is used as reflected half space. Results also
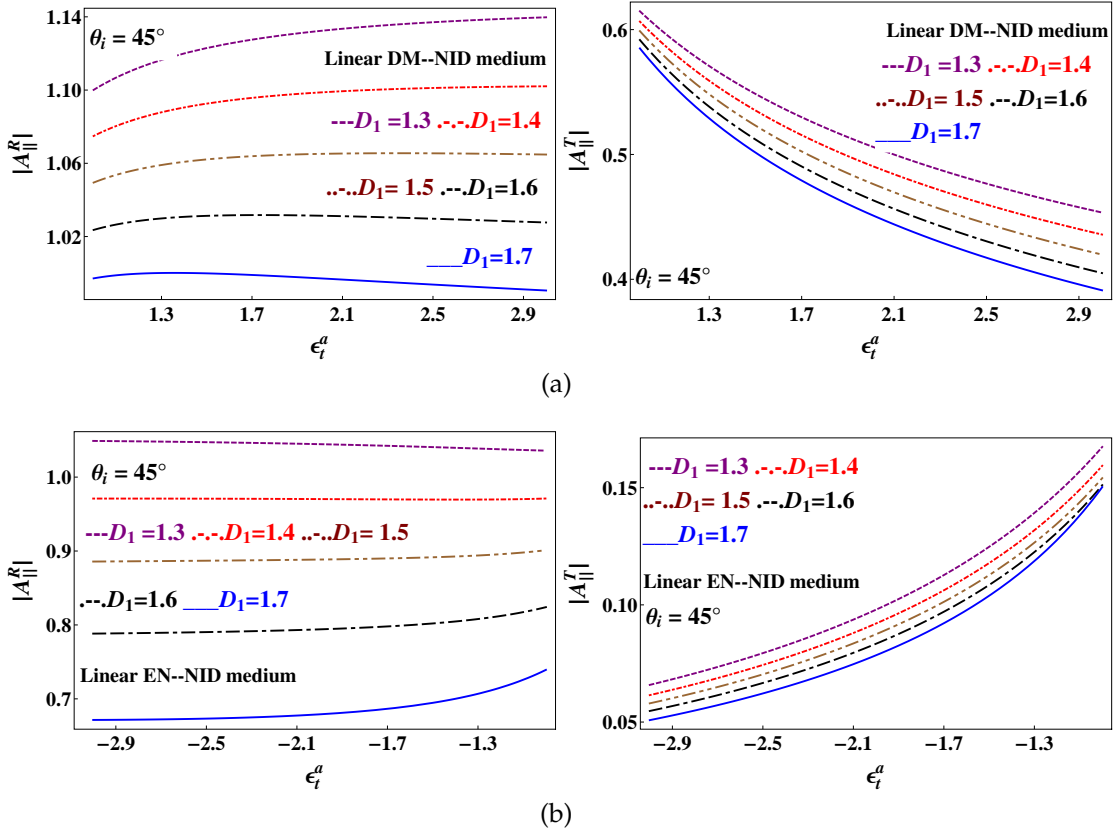
Figure 2.13: Behavior of $|A_\parallel^R|$ and $|A_\parallel^T|$ with respect to ϵ_t^a for the variations of the dimension parameter.
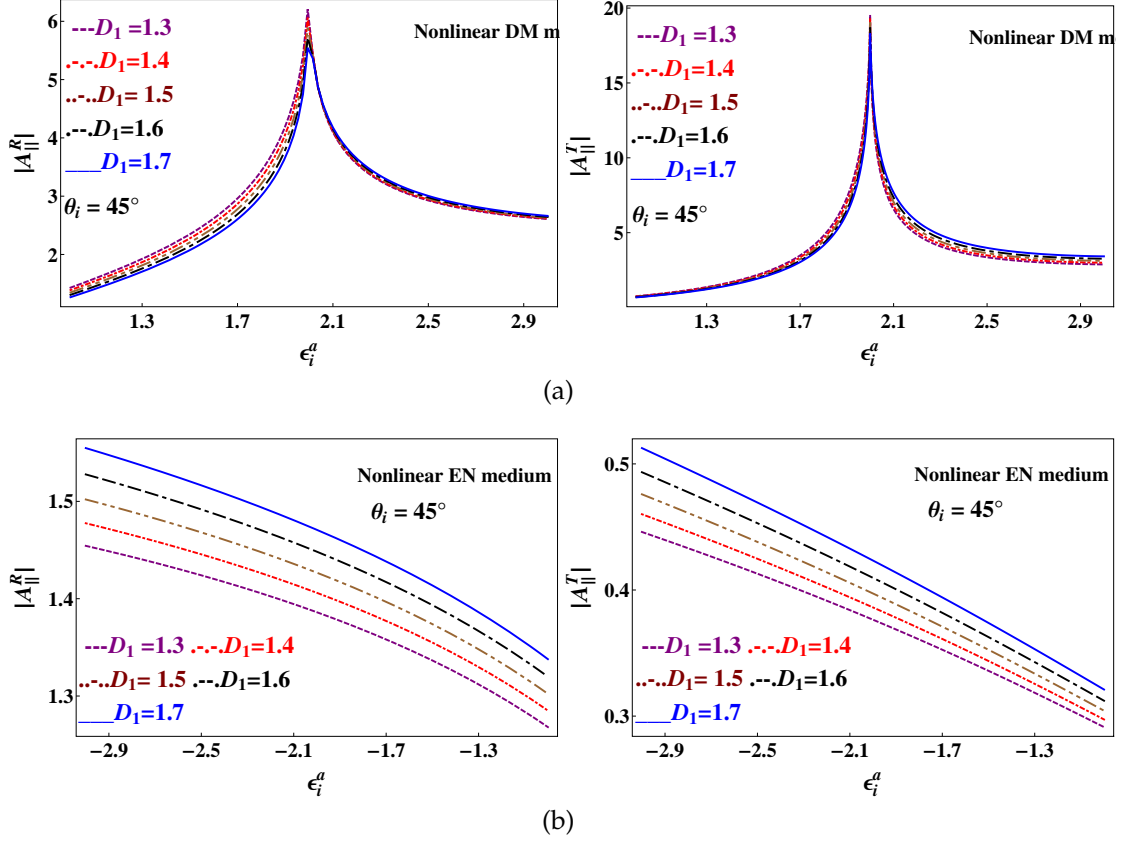
(a)

(b)
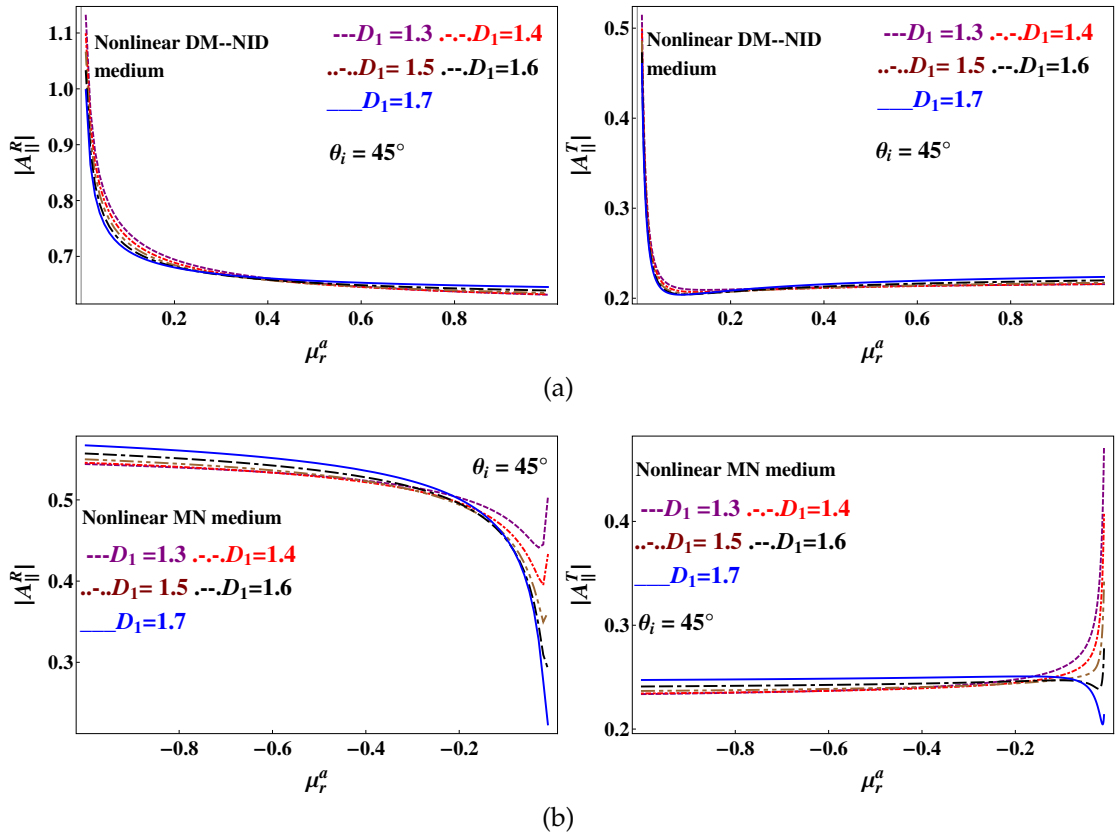
Figure 2.14: Behavior of $|A_\parallel^R|$ and $|A_\parallel^T|$ with respect to μ_r^a for the variations of the dimension parameter.

depict that maximum amplitude of both the coefficients are achieved by taking $\epsilon_t^a = 1.9$ and $\mu_r^a = 0.09$ for specific values of linear permittivity. Whereas, by taking $\epsilon_i^a = 0.8$ and $\mu_r^a = 0.09$ for specific values of ϵ_t^a only maximum amplitude of the reflection coefficient is achieved. It is also observed that for $1 < \epsilon_i^a < 2$ ($\epsilon_i^a > 2$) amplitude of the coefficients decreases (increases) by increasing the noninteger dimension. For nonlinear epsilon negative medium (reflected half space), amplitude of the coefficients decreases by increasing the noninteger dimension of NID medium used as transmitted half space. Results also depict that dimension parameter can be used to control the amplitude of the coefficients by keeping the same shape.

Chapter 3

Linear dielectric magnetic and nonlinear dielectric magnetic NID planar interface

This chapter is devoted to the derivation and study of the behavior of reflection and transmission coefficients from a linear dielectric magnetic–second order NL dielectric magnetic NID planar interface for both S and P-polarization excitation. Changes in the behavior of the coefficients are also reported when linear dielectric magnetic half space is replaced with linear epsilon negative and linear mu negative mediums. In all these cases, contributions of the non-linearity and the noninteger dimension are studied separately. From the comparison of special cases with the results of the original geometry, it is studied that for S-polarization excitation, amplitude of the reflection coefficient increases by taking higher noninteger dimensions. Oppositely, for P-polarized excitation, amplitude of the coefficients increases by taking smaller values of the noninteger dimensions.

3.1   S-polarization excitation

3.1.1   Description of the geometry and mathematical formulation

Consider a planar interface located at $z = q$ and excited by a S-polarized plane wave as depicted in Fig.3.1. Left half space is filled with linear dielectric magnetic medium and the right half space is composed of second order nonlinear dielectric magnetic NID medium. Electric field associated with the incident electromagnetic wave is expressed as,

$$\mathbf{E_i}(\omega_i) = \hat{\mathbf{y}} E_o(\omega_i) e^{jk_i^b(x \sin \theta_i + z \cos \theta_i)} \tag{3.1}$$

In the following discussion, left half space is symbolized as 'm''. Wave number of this medium is $k_i^b = \omega_i \sqrt{\epsilon_i^b(\omega_i)}/c$, where $\epsilon_i^b(\omega_i)$ (hereafter it is written as ϵ_i^b for simplicity) is the linear permittivity, whereas, right half space is termed as medium 'm''' which is characterized by the wave number $k_t^b = \omega_s \sqrt{\epsilon_t^b(\omega_s)}/c$, where $\epsilon_t^b(\omega_s)$ (hereafter written as ϵ_t^b for simplicity) is the m'' medium permittivity for second harmonic frequency To obtain the transmitted electric field propagating in nonlinear dielectric magnetic NID medium, SVA approximation is used on the solution of the electric field obtained by applying the MSV in NID space,

$$
\begin{aligned}
\mathbf{E_t}(\omega_s) = \hat{\mathbf{y}} \Bigg[& B_\perp^T e^{jk_t^b x \sin \theta_r} (k_t^b z \cos \theta_r)^{o1} H_{o1}^{(2)}(k_t^b z \cos \theta_r) \\
& + \frac{P \omega_s^2 \mu_o}{(k_s^2 - k_t^{b2})} e^{jk_s x \sin \theta_s} (k_s z \cos \theta_s)^o H_{o1}^{(2)}(k_s z \cos \theta_s) \Bigg]
\end{aligned} \tag{3.2}
$$

Similarly, magnetic field expressions are evaluated as discussed in chapter.2. Equating the tangential components of the fields across the planar interface,
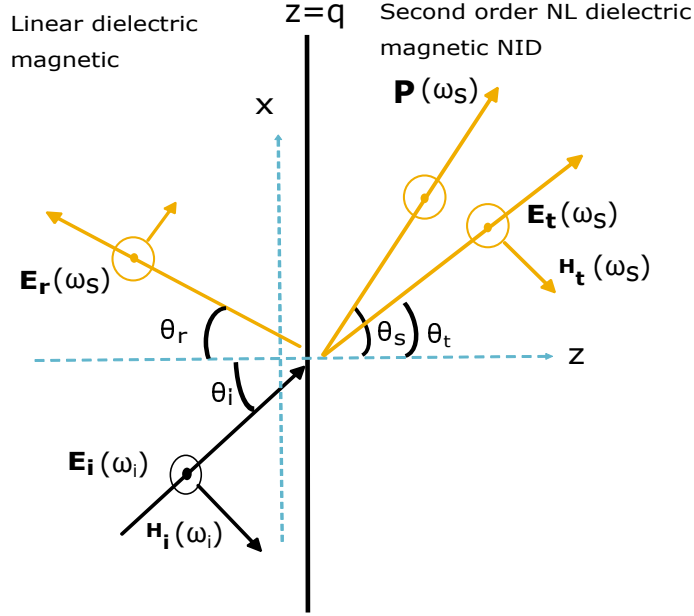
Figure 3.1: Linear dielectric magnetic and second order nonlinear dielectric magnetic NID planar interface excited by S-polarized plane wave.

following boundary conditions are obtained,

$$B_\perp^R e^{-jk_r^b q \cos \theta_r} = B_\perp^T A_1 + \frac{P \omega_s^2 \mu_o A_2}{k_s^2 - k_t^{b2}} \tag{3.3a}$$

$$\frac{B_\perp^R \cos \theta_r e^{-jk_r^b q \cos \theta_r}}{\eta_r^b} = -\frac{B_\perp^T B_1 \cos \theta_t}{\eta_t^b} - \frac{\cos \theta_s P \omega_s^2 \mu_o B_2}{\eta_s^b (k_s^2 - k_t^{b2})}, \tag{3.3b}$$

where $B_\perp^R$ and $B_\perp^T$ are the unknown reflection and transmission coefficients, respectively and the subscript is used to indicate the polarization of the incident electromagnetic wave. Analytical solution of Eq.(3.3) yields the following

unknown coefficients for S-polarization incidence

$$B_\perp^R = -\frac{\left(k_s^2 - k_t^{b2}\right)\left(A_1\delta_{tr} + B_1\delta_{rt}\right)\left(A_1B_2\delta_{ts} - A_2B_1\delta_{rt}\right)}{e^{-jk_r^b q\cos\theta_r}\delta_{cc}^t\eta_t^b\left(A_2\cos\theta_r + B_2\cos\theta_s\right)^2} \tag{3.4a}$$

$$B_\perp^T = -\frac{\left(k_s^2 - k_t^{b2}\right)\left(A_1\delta_{tr} + B_1\delta_{rt}\right)}{\delta_{cc}^t\left(A_2\cos\theta_r + B_2\cos\theta_s\right)}, \tag{3.4b}$$

Different notations used to write Eq.(3.4) in compact form are given in appendix.

3.1.2 Results and discussion

The S-polarized unknown coefficients derived in previous section are discussed in this section. Behavior of the unknown coefficients are also studied when left half space is filled with linear epsilon negative (EN) or linear mu negative (MN) medium instead of linear dielectric magnetic medium. In all these cases, impact of the non-linearity and noninteger dimensions on the unknown coefficients are studied separately.

Initially, study of the behavior of the coefficients is reported by taking ordinary m'' medium, i.e; $D_2 = 2$. Plots given in Fig.3.2–Fig.3.4 depict these all results. In Fig.3.2, behavior of the coefficients are given as a function of ϵ_i^b for specific values of ϵ_r^b (Fig.3.2a), μ_r^b (Fig.3.2b) and θ_i (Fig.3.2c). In Fig.3.2a, it is studied that amplitude of the reflection coefficient increases by increasing ϵ_r^b for $-3 < \epsilon_i^b < 0.4$, and $\epsilon_i^b > 2.3$. Whereas, amplitude of the coefficients decreases for $0.4 < \epsilon_i^b < 2.3$. It can be noted that amplitude of the transmission coefficient decrease by increasing ϵ_r^b. It is also noted that amplitude of the reflection coefficient is smaller for positive values of the permittivity compared to the negative values of the permittivity. In Fig.3.2b, results depict that for linear EN medium, amplitude of the reflection coefficient increases by increasing μ_r^b. It is also noted that amplitude of the reflection (transmission) coefficient decreases (increases) by increasing incident angle for linear EN medium and vice-versa for linear dielectric magnetic medium (Fig.3.2c). Moreover, it is also

studied that curves of the coefficients shift towards left by increasing the incident angle. Results depict that higher amplitude of the reflection (transmission) coefficient is obtained by taking $\mu_r^b = 0.01$, $\theta_i = 30°$ and $1.7 < \epsilon_i^b < 2.4$ ($\epsilon_i^b > 2.4$).

In Fig.3.3, coefficients are studied as a function of ϵ_r^b by taking specific values of ϵ_i^b (Fig.3.3a), μ_r^b (Fig.3.3b) and θ_i (Fig.3.3c). In Fig.3.3a, it is noted that amplitude of the coefficients decrease (increases) by increasing ϵ_i^b for linear EN (DM) medium, whereas peaks of the curves also shift towards right by increasing the value of the linear permittivity. In Fig.3.3b, it is noted that amplitude of the coefficients decreases (increases) by taking the higher values of μ_r^b for linear EN (DM) medium. It is also observed that amplitude of the coefficients decreases by increasing the value of the incident angle (Fig.3.3c). Results depict that higher amplitude of both the coefficients is achieved by taking $\mu_r^b = 0.01$, $\epsilon_r^b = 0.4$ and $\theta_i = 45°$.

In Fig.3.4, coefficients are studied as a function of μ_r^b for specific values of ϵ_i^b (Fig.3.4a), ϵ_r^b (Fig.3.4b) and θ_i (Fig.3.4c). In Fig.3.4, it is noted that amplitude of the coefficients increases by increasing the value of either permittivities (ϵ_i^b and ϵ_r^b) and incident angle (θ_i) for both linear MN and linear DM mediums. Whereas, for mu near zero medium, higher amplitude of the coefficients is noted for $\theta_i = 30°$. It is also noted that coefficients curves shift towards right by increasing the values of the permittivities. From the comparison of all plots given in Fig.3.2–Fig.3.4, it is noted that higher amplitude of the coefficients is achieved for epsilon near zero mediums.

(a)

(b)

(c)

Figure 3.2: Behavior of $|B_\perp^R|$ and $|B_\perp^T|$ with respect to ϵ_i^b for $D_2 = 2$.

Figure 3.3: Behavior of $|B_\perp^R|$ and $|B_\perp^T|$ with respect to ϵ_r^b for $D_2 = 2$.
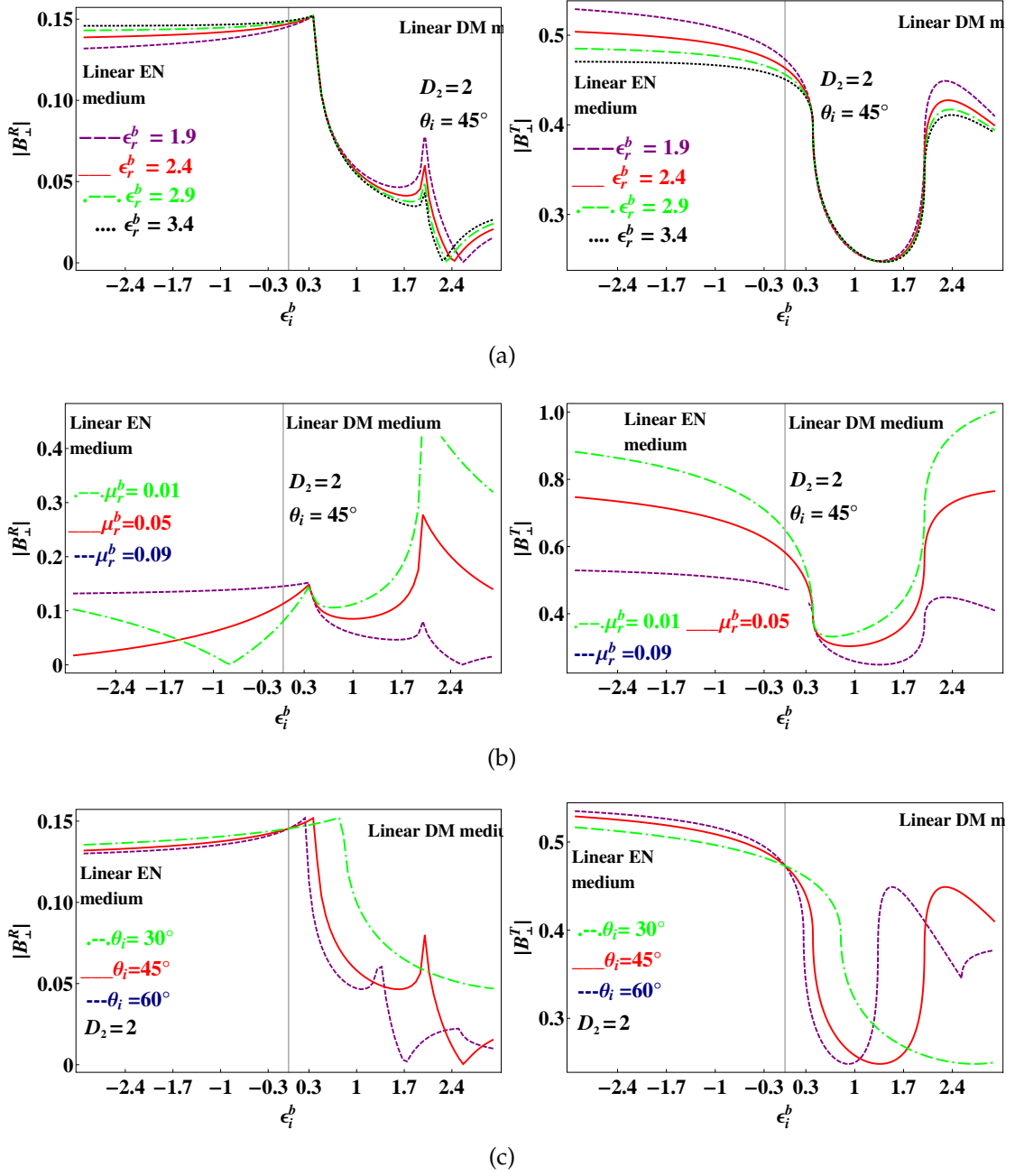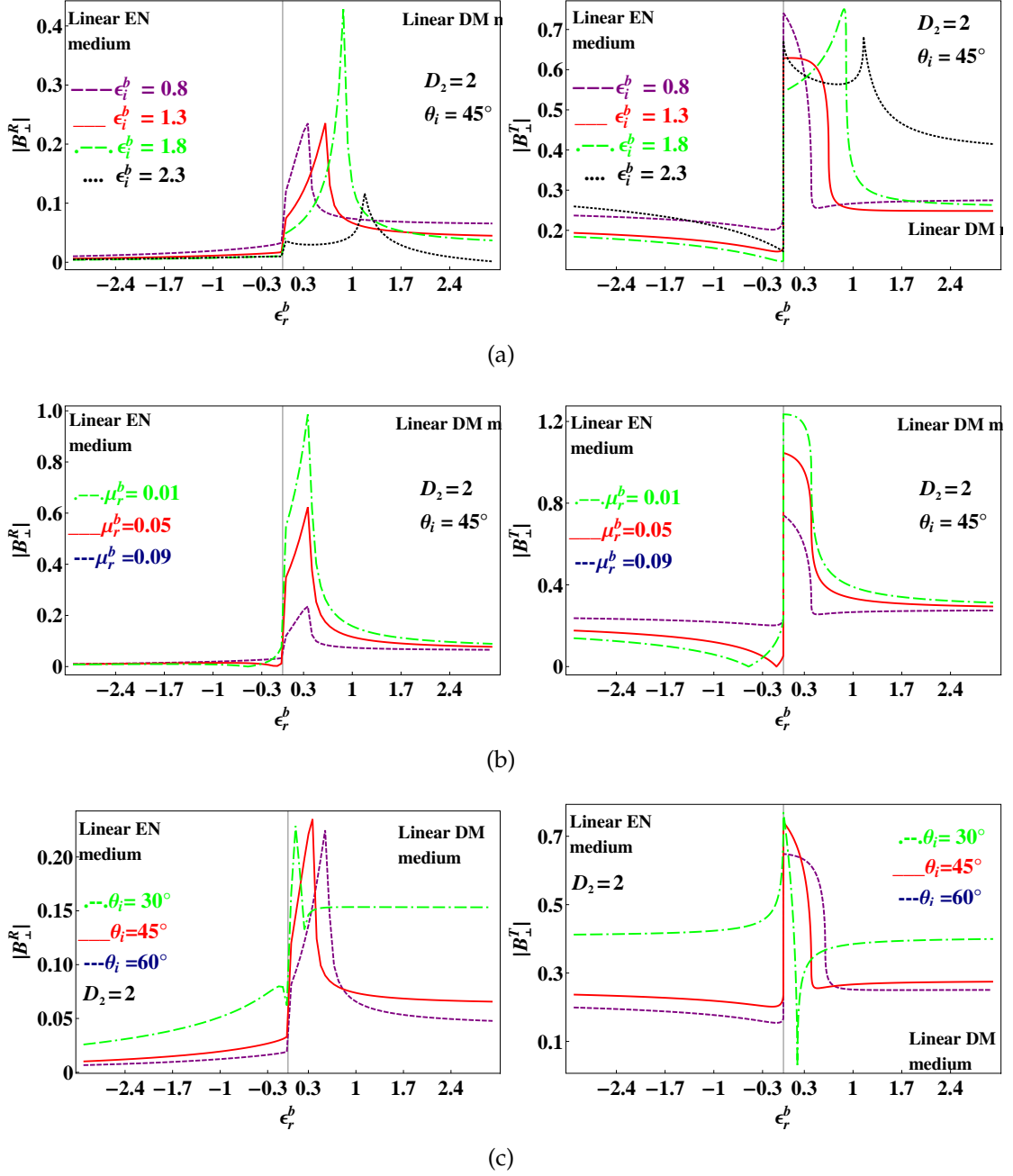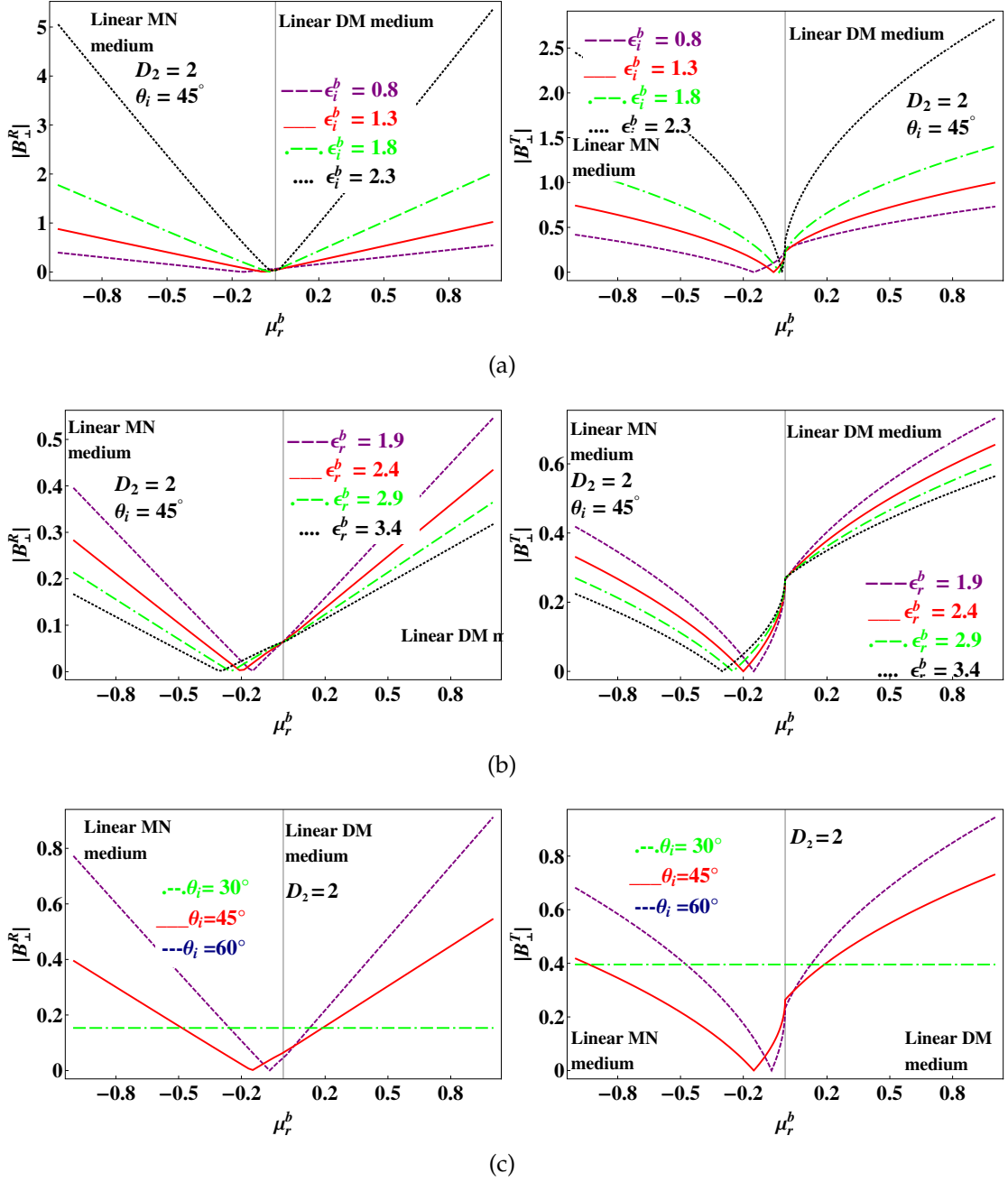
(a)

(b)

(c)

Figure 3.4: Behavior of $|B_\perp^R|$ and $|B_\perp^T|$ with respect to μ_r^b for $D_2 = 2$.
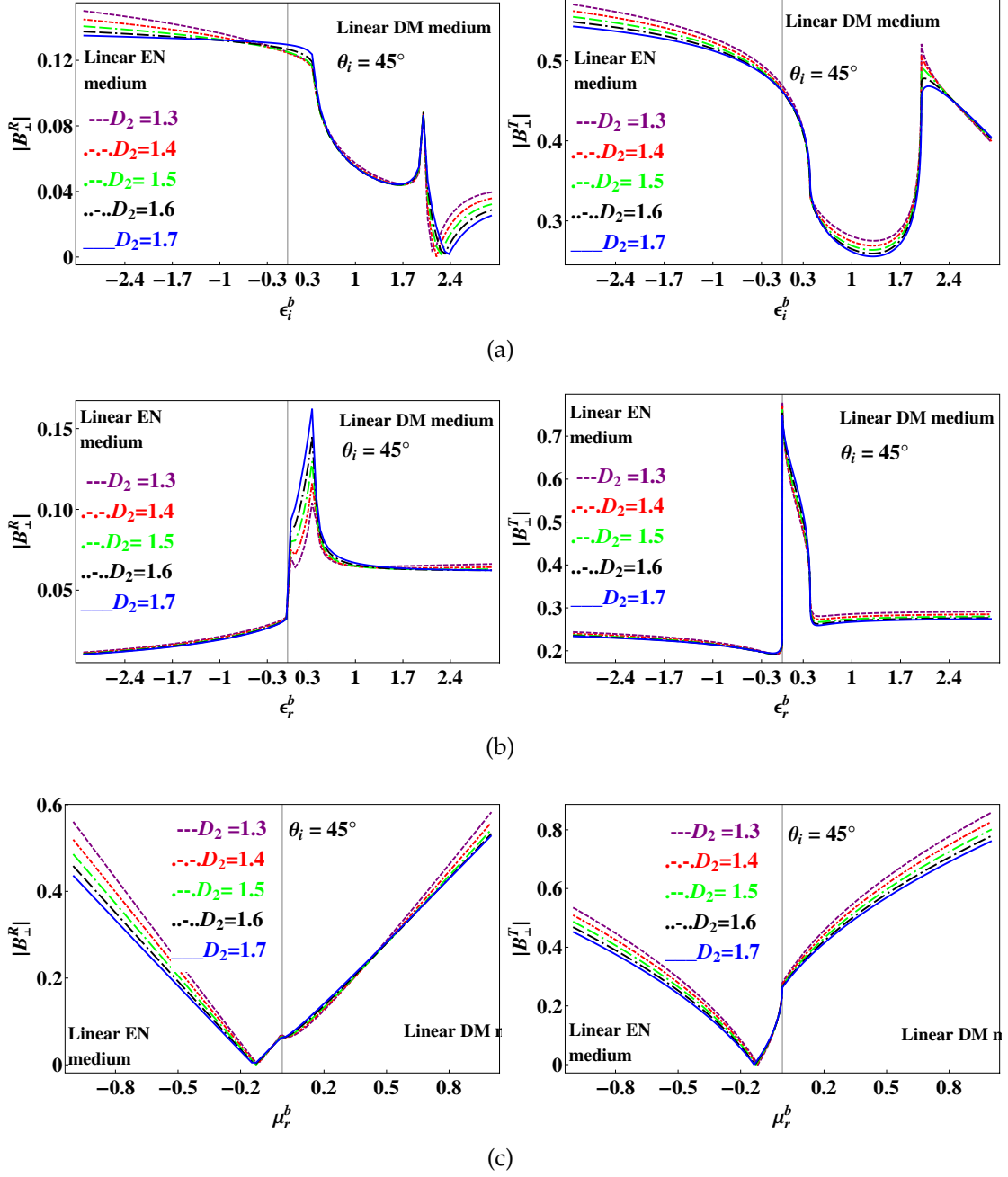
Figure 3.5: Behavior of $|B_\perp^R|$ and $|B_\perp^T|$ with respect to (a) ϵ_i^b (b) ϵ_r^b and (c) μ_r^b for the variations of the dimension parameter.

(a)

(b)

(c)

Figure 3.6: (cont.)

(d)
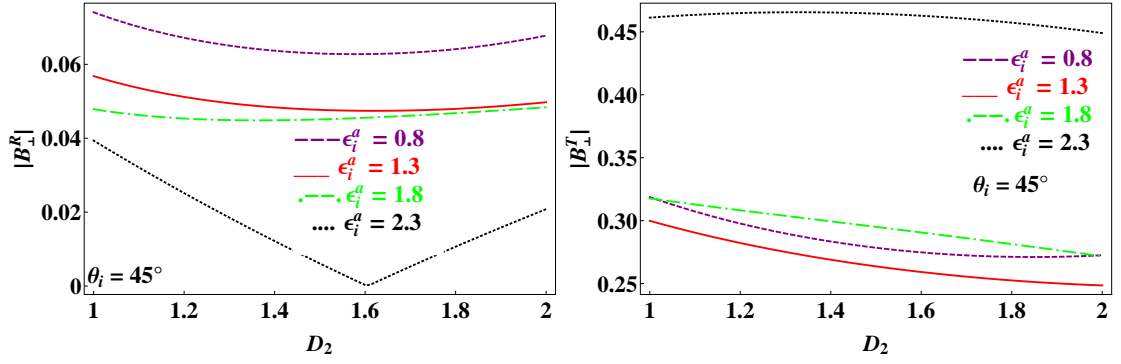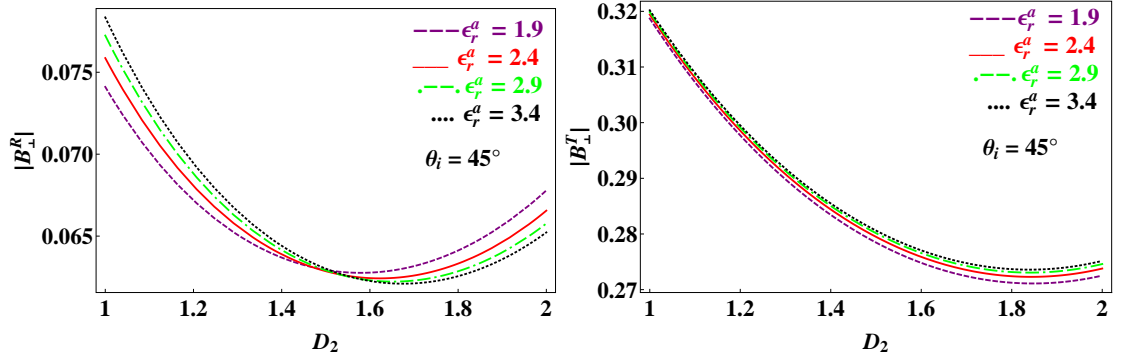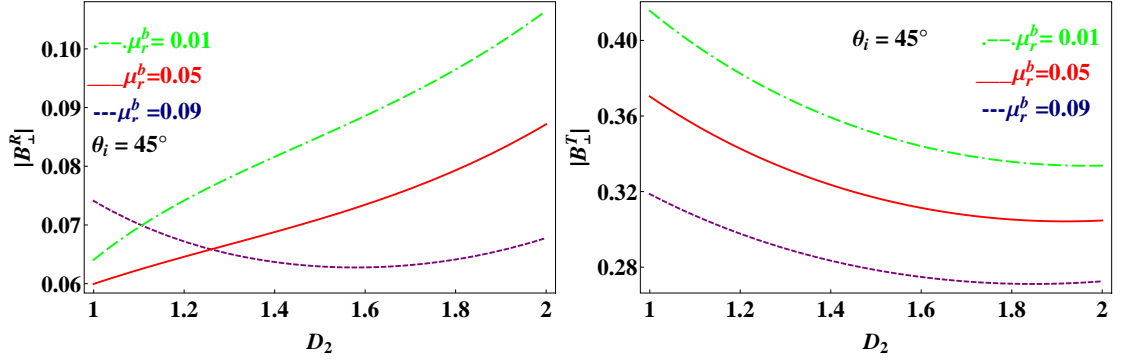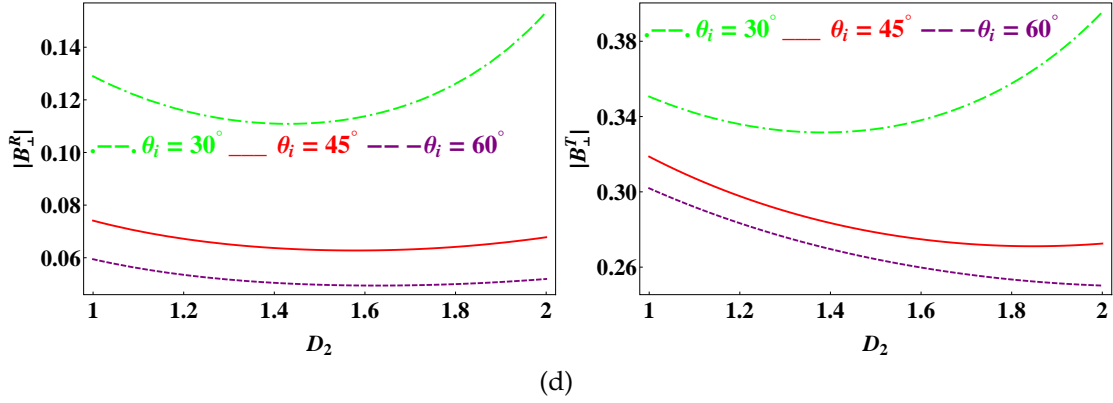
Figure 3.6: Behavior of $|B_\perp^R|$ and $|B_\perp^T|$ with respect to dimension parameter.
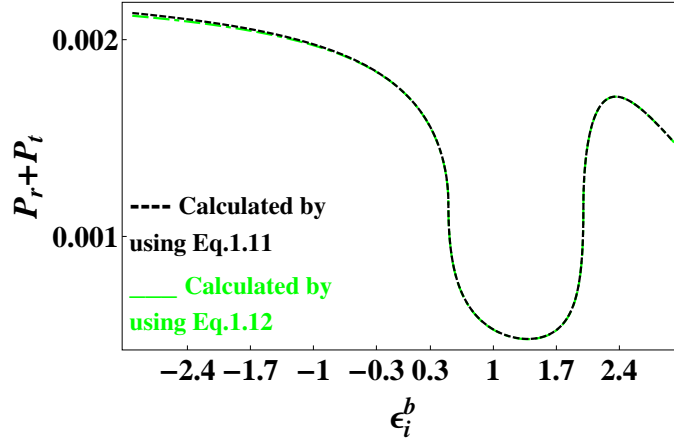
Figure 3.7: Sum of S-polarized reflected and transmitted powers for I^b .

Impact of the noninteger dimension of medium m'' is given in Fig.3.5–Fig.3.6. In Fig.3.5, behavior of the reflection and transmission coefficients is given as a function of ϵ_i^b (Fig.3.5a), ϵ_r^b (Fig.3.5b) and μ_r^b (Fig.3.5c) by taking specific values of the noninteger dimension parameter. Results depict that amplitude of the reflection coefficient decreases by taking higher values of the noninteger dimension for $-3 < \epsilon_i^b < -0.4$ and $2.4 < \epsilon_i^b < 3$, but increases for $-0.4 < \epsilon_i^b < 0.4$ and $2 < \epsilon_i^b < 2.4$. On the other hand, amplitude of the transmission coefficient, decreases by increasing the values of D_2 for the complete taken range of ϵ_i^b i.e; $-3 < \epsilon_i^b < 3$. In Fig.3.5b, it is studied that amplitude of the reflection coefficient decreases by taking higher values of noninteger dimension for $-3 < \epsilon_r^b < -0.01$ and $\epsilon_r^b > 1.4$ but, increases for $-0.01 < \epsilon_r^b < 1.4$. Whereas, amplitude of the transmission coef-

ficient decreases for $-3 < \epsilon_r^b < -0.01$ and $0.4 < \epsilon_r^b < 3$ and increases for $-0.01 < \epsilon_i^b < 0.4$. In Fig.3.5c, it is noted that amplitude of the reflection coefficient decreases by increasing the value of D_2 for $-1 < \mu_r^b < -0.1$ and $\mu_r^b > 0.5$ but, increases for $0.1 < \mu_r^b < 0.5$. In Fig.3.6, it is noted that amplitude of the coefficients decreases as $D_2 \to 2$ when coefficients are studied for fixed value of μ_r^b and varying values of the permittivities (Fig.3.6a–Fig.3.6b), and increases by taking smaller value of $\mu_r^b (= 0.01)$ as depicted in Fig.3.6c.

3.1.3   Conclusion

Derivation and study of the behavior of the second order S-polarized reflection and transmission coefficients is given in this section for linear dielectric magnetic–second order nonlinear dielectric magnetic NID planar interface. Smaller amplitude of the reflection coefficient is observed for positive values of permittivity (linear dielectric magnetic medium) compared to the negative values (linear epsilon negative medium). It is also noted that amplitude of the reflection coefficient increases (decreases) by taking higher values of the nonlinear permeability when linear epsilon negative (dielectric magnetic) medium is taken as m' medium. Results also depict that amplitude of the reflection (transmission) coefficient decreases (increases) as incident angle increases for linear epsilon negative medium. Moreover, amplitude of both the coefficients decrease (increases) by increasing ϵ_i^b for linear epsilon negative (dielectric magnetic) medium and the peaks of the coefficients also shift towards right by increasing the value of ϵ_i^b. On the other hand, it is also noted that amplitude of the coefficients increases by increasing both the permittivities (ϵ_i^b and ϵ_r^b) and incident angle for linear dielectric magnetic medium. On the other hand, for mu near zero medium (as m'), higher amplitude of the coefficients is noted when $\theta_i \to 30°$. Results also depict that amplitude of the coefficients is enhanced by taking for epsilon near zero medium.

Studying the impact of the noninteger dimension on the coefficients, it is noted that amplitude of the reflection coefficient decreases by increasing the noninteger dimension for $-3 < \epsilon_i^b < -0.4$ and $2.4 < \epsilon_i^b < 3$, but, increases for $-0.4 < \epsilon_i^b < 0.4$ and $2 < \epsilon_i^b < 2.4$. On the other hand, amplitude of the

transmission coefficient decreases by increasing the value of the noninteger dimension parameter for $-3 < \epsilon_i^b < 3$. Results also depict that amplitude of the reflection coefficient decreases by increasing the noninteger dimension for $-3 < \epsilon_r^b < -0.01$ and $\epsilon_r^b > 1.4$ and increases for $-0.01 < \epsilon_r^b < 1.4$. It is also noted that amplitude of the transmission coefficient decreases for $-3 < \epsilon_r^b < -0.01$ and $0.4 < \epsilon_r^b < 3$ whereas, increases for $-0.01 < \epsilon_i^b < 0.4$. Furthermore, it is studied that amplitude of the reflection coefficient decreases by increasing the value of the noninteger dimension for $-1 < \mu_r^b < -0.1$ and $\mu_r^b > 0.5$ but, increases for $0.1 < \mu_r^b < 0.5$.

3.2 P-polarization excitation

3.2.1 Description of the geometry and mathematical formulation
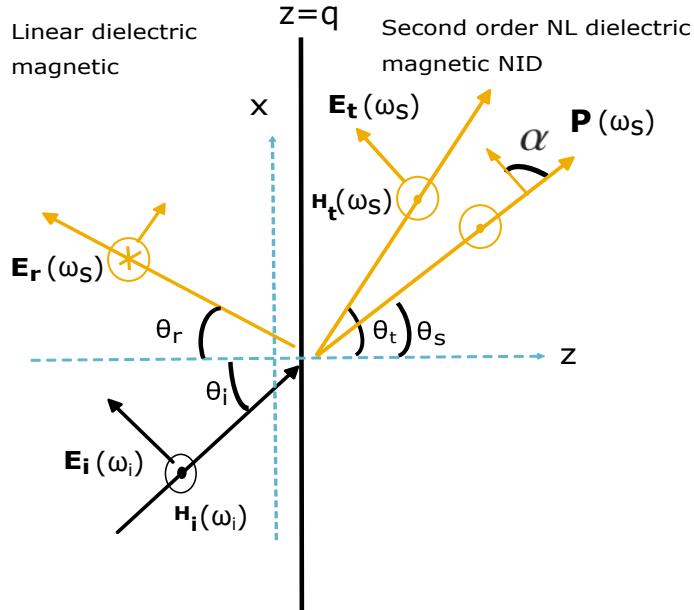

Figure 3.8: Linear dielectric magnetic and second order nonlinear dielectric magnetic NID planar interface excited by P-polarized plane wave.

Consider a planar interface placed at $z = q$ and excited by a P-polarized plan wave as depicted in Fig.3.8. Description of the geometry is given in Sec.3.1.2. Electric and magnetic fields associated with the incident plane wave

are $\mathbf{E_i} = (E_{ix}, 0, E_{iz})^T$ and $\mathbf{H_i} = (0, H_{iy}, 0)^T$, respectively. Furthermore induced NL polarization is $\mathbf{P}$, where in the following discussion $\hat{p}$ is used to represent a unit vector in the plane of Fig.3.8 and α is used to represent the angle formed between induced NL polarization and the wave vector: i.e: $\mathbf{P}$ and $\mathbf{k_t^b}$, as depicted in Fig.3.8. Reflected and transmitted fields are obtained by using the similar procedure as discussed in Sec.3.1.2. Equating the tangential components of the fields across the interface, following boundary conditions are achieved,

$$B_\parallel^R \cos\theta_r = B_\parallel^T \cos\theta_t A_1 + \left(\frac{P\omega_s^2 \mu_o \sin\alpha \cos\theta_s}{k_s^2 - k_t^{b2}} + \frac{P\omega_s^2 \mu_o \cos\alpha \sin\theta_s}{k_t^{b2}} \right) A_2$$

$$-\frac{B_\parallel^R e^{-jk_r^b q \cos\theta_r}}{\eta_r^b} = \frac{B_\parallel^T B_1}{\eta_t^b} + \left(\frac{P\omega_s^2 \mu_o \sin\alpha \cos\theta_s}{k_s^2 - k_t^{b2}} + \frac{P\omega_s^2 \mu_o \cos\alpha \sin\theta_s}{k_t^{b2}} \right) \left(\frac{B2}{\eta_s} \right)$$

$$(3.5)$$

Analytical solution of Eq.(3.5), provides the P-polarized unknown coefficients written below as,

$$B_\parallel^R = \frac{k_t^{b2} \eta_r^b \eta_s \left(k_s^2 - k_t^{b2} \right) \left(A_2 B_1 \eta_s - A_1 B_2 \delta_{tt} \right) \left(B_1 \delta_{rr} + A_1 \delta_t^e \right)}{\delta_{cc}^t \eta_t^b \left(A_2 \eta_s^e + B_2 \delta_{rr} \right)^2 \left(k_t^{b2} \sin(\alpha - \theta_s) + k_s^2 \cos\alpha \sin\theta_s \right)}$$

$$(3.6)$$

$$B_\parallel^T = \frac{k_t^{b2} \eta_s \left(k_t^{b2} - k_s^2 \right) \left(B_1 \delta_{rr} + A_1 \delta_t^e \right)}{\delta_{cc}^t \left(A_2 \eta_s^e + B_2 \delta_{rr} \right) \left(k_t^{b2} \sin(\alpha - \theta_s) + k_s^2 \cos\alpha \sin\theta_s \right)}$$

In Eq.(3.5)–Eq.(3.6), $B_\parallel^R$ and $B_\parallel^T$ are the unknown reflection and transmission coefficient, respectively. Furthermore, notations used to write these equations in compact form are given in appendix.

3.2.2   Results and discussion

Unknown P-polarized reflection and transmission coefficients derived in the previous section are discussed here as a function of different parameters. In Fig.3.9–Fig.3.11, impact of the non-linearity on the behavior of the coefficients is given. In Fig.3.9, coefficients are studied as a function of ϵ_i^b by taking specific values of ϵ_r^b (Fig.3.9), μ_r^c (Fig.3.9b), θ_i (Fig.3.9c) and α (Fig.3.9d). In Fig.3.9a, it is noted that amplitude of the reflection (transmission) coefficient decreases (increases) by increasing the value of ϵ_r^b. Furthermore, it is also noted that amplitude of the coefficients is greater for EN medium compared to the dielectric magnetic medium. On the other hand, it is also noted that behavior of the reflection (transmission) coefficient changes at $\epsilon_i^b = 0.2(0.4)$. In Fig.3.9b, it is noted that amplitude of the coefficients decreases by increasing the value of μ_r^b. It is also noted that amplitude of the reflection coefficient increases for EN and dielectric magnetic both mediums by increasing the incident angle. On the other hand, amplitude of the transmission coefficient decreases by taking higher values of the incident angle for $-1.7 < \epsilon_i^b < 0.3$ (Fig.3.9c). In Fig.3.9b, it is studied that amplitude of both the coefficients increases as $\alpha \to 90°$. Results depict that higher amplitude of the coefficients is achieved by using EN medium compared to dielectric magnetic medium. From the comparison of all subplots given in Fig.3.9, it is noted that higher amplitude of the reflection coefficient is achieved by using $\epsilon_i^b = -3$, $\epsilon_r^b = 1.9$, $\mu_r^b = 0.05$ and $\alpha = \theta_i = 60°$. In Fig.3.10, behavior of the coefficients is given as a function of ϵ_r^b for specific values of ϵ_i^b (Fig.3.10a), μ_r^b (Fig.3.10b), θ_i (Fig.3.10c) and α (Fig.3.10d). In Fig.3.10a, it is noted that amplitude of the coefficients increases by increasing ϵ_i^b for both EN and dielectric magnetic mediums. It is also noted that peaks of the reflection coefficient shift towards right by taking higher values of ϵ_i^b for dielectric magnetic medium. Whereas, amplitude of the coefficients decreases by increasing the value of μ_r^b, and no peaks shifting is noted (Fig.3.10b). In Fig.3.10c, it is noted that amplitude of the reflection (transmission) coefficient increases (decreases) by increasing the value of the incident angle for EN medium. It is interesting to note that higher amplitude of the transmission coefficient can be achieved by taking epsilon near zero medium for smaller value of $\theta_i (= 30°)$.

In Fig.3.10d, it is noted that amplitude of the coefficients increases as α is increased. It is also noted that for fixed value of α, amplitude of the reflection (transmission) coefficient decreases (increases) and $1 < \epsilon_r^b < 3$. Results also depict that higher amplitude of the coefficients is achieved for $\epsilon_r^b \to 0$ by taking $\epsilon_i^b = 0.8$, $\mu_r^b = 0.01$ and $\alpha = 60°$.

In Fig.3.11, coefficients are plotted as a function of α by taking specific values of ϵ_i^b (Fig.3.11a), ϵ_r^b (Fig.3.11b), μ_r^b (Fig.3.11c) and θ_i (Fig.3.11d). In Fig.3.11a, it is noted that amplitude of the coefficients increases by increasing the value of ϵ_i^b. It is noted that amplitude of the coefficients decreases by increasing the value of ϵ_r^b and μ_r^b (Fig.3.11b–Fig.3.11c), whereas increases by increasing the value of the incident angle (Fig.3.11d). Results also depict that for fixed value of ϵ_i^b, ϵ_r^b, μ_r^b or θ_i, amplitude of the coefficients increases as $\alpha \to 90°$.

Now, impact of the noninteger dimension of the medium m'', on the reflection and transmission coefficients is given in Fig.3.12–Fig.3.13. In Fig.3.12, coefficients are studied as a function of ϵ_i^b (Fig.3.12a), ϵ_r^b (Fig.3.12b) and α (Fig.3.12), for $D_2 \neq 2$. In all these subplots it is noted that amplitude of the coefficients decrease by increasing D_2. On the other hand, in Fig.3.13, coefficients are plotted as a function of dimension parameter by taking specific values of ϵ_i^b Fig.3.13a, ϵ_r^b (Fig.3.13b) and α (Fig.3.13c). Results also depict that amplitude of the coefficients, decreases as $D_2 \to 2$, for fixed values of the constitutive parameters.

(a)

(b)

(c)

Figure 3.9: (cont.)

(d)
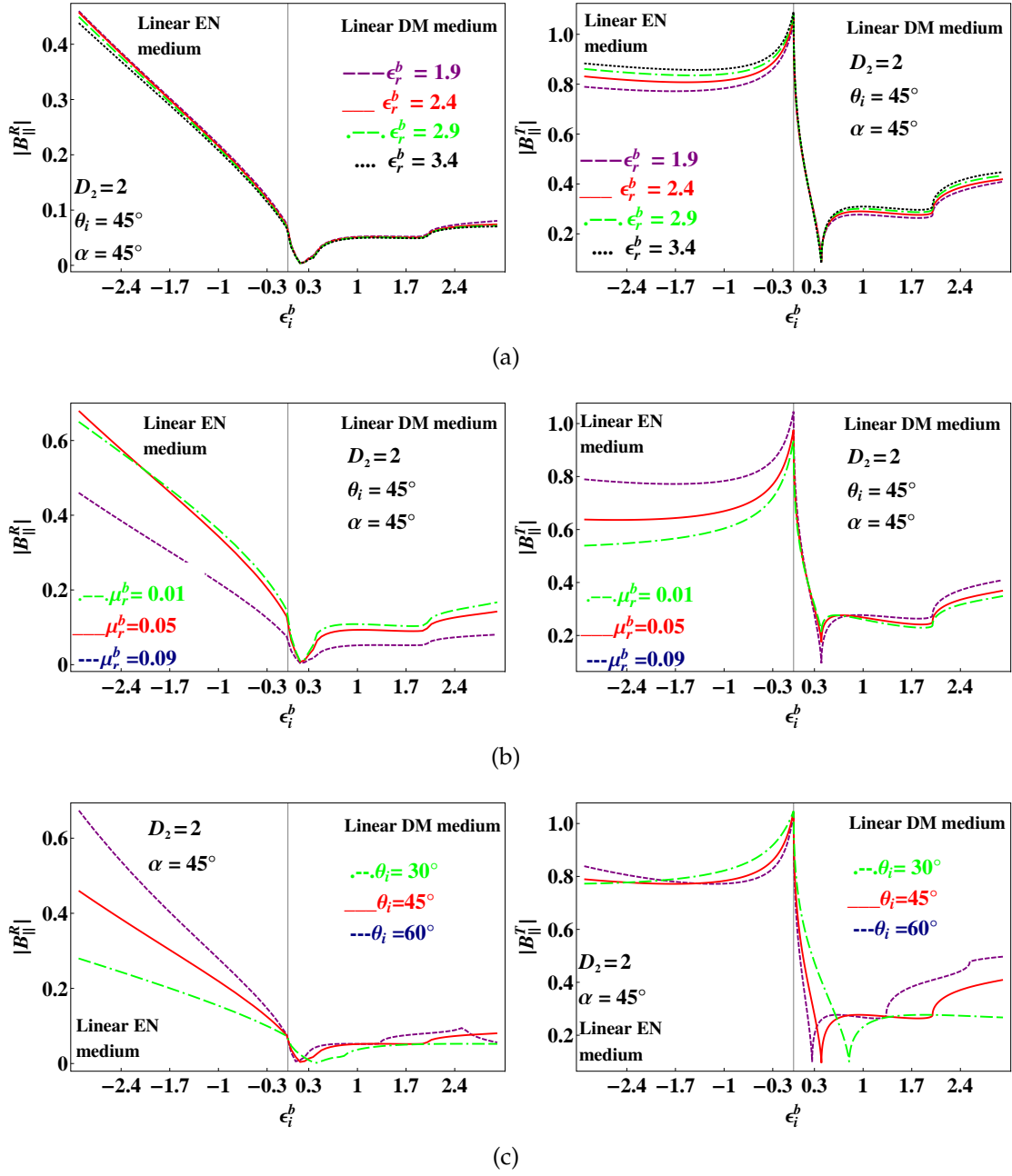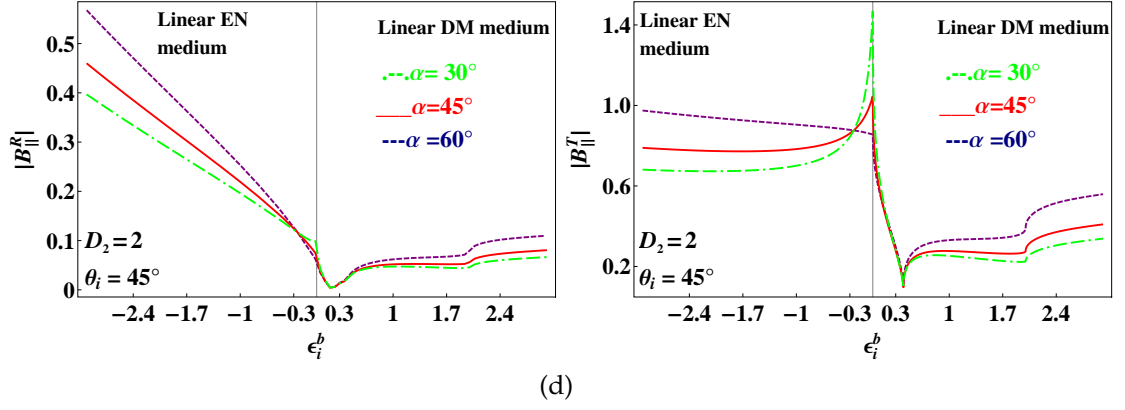
Figure 3.9: Behavior of $|B_\parallel^R|$ and $|B_\parallel^T|$ with respect ϵ_i^b for $D_2 = 2$.

(a)

(b)
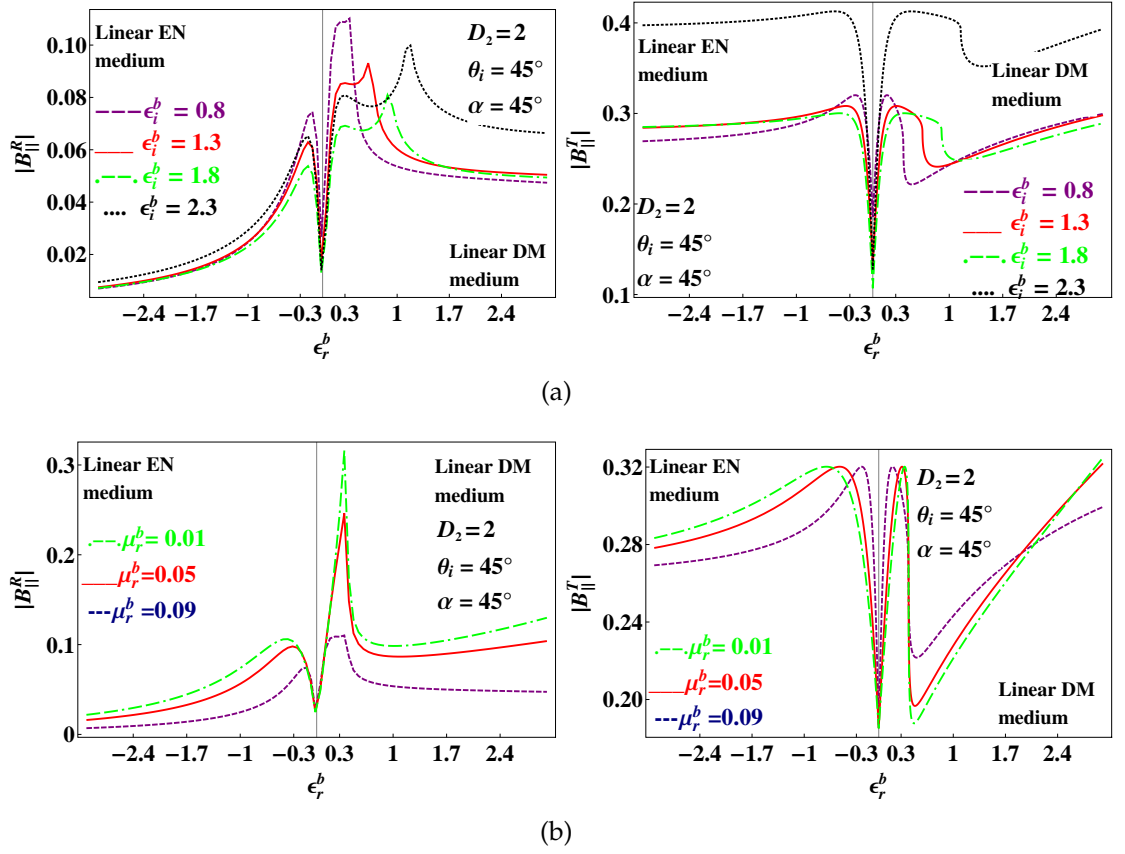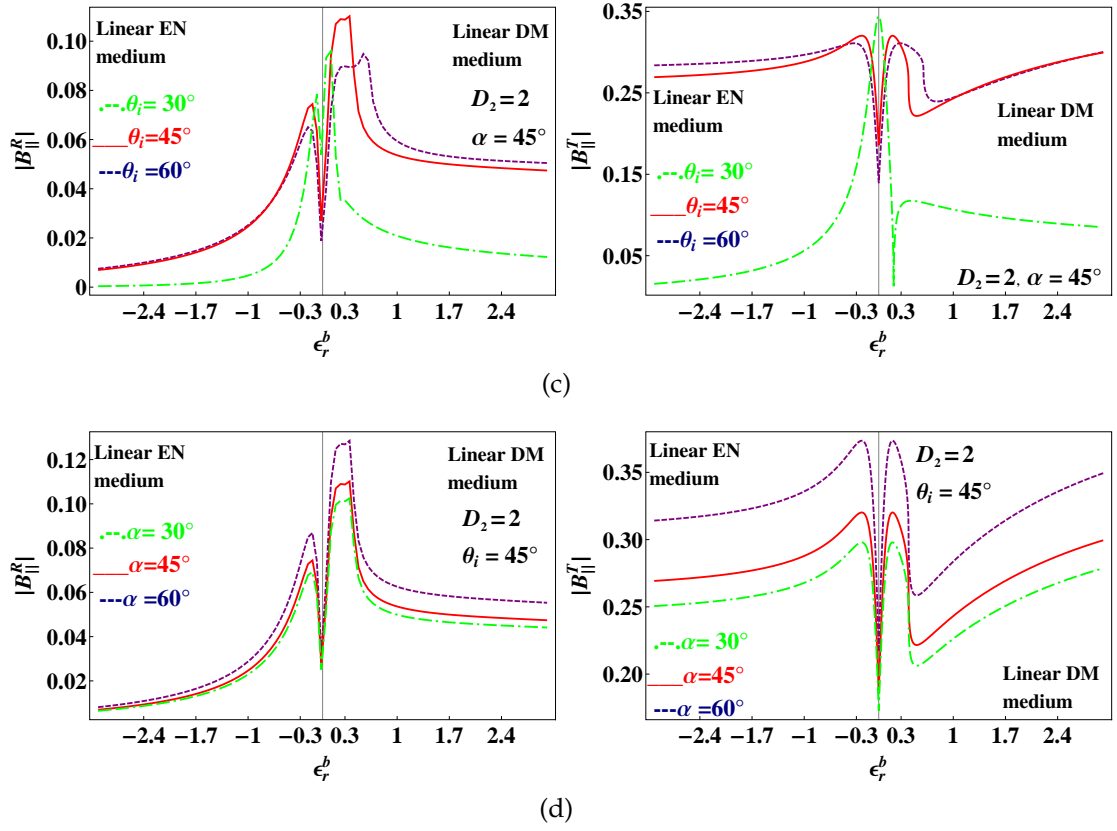
Figure 3.10: (cont.)

Figure 3.10: Behavior of $|B_\parallel^R|$ and $|B_\parallel^T|$ with respect ϵ_r^b for $D_2 = 2$.

(a)

(b)

(c)

Figure 3.11: (cont.)

(d)
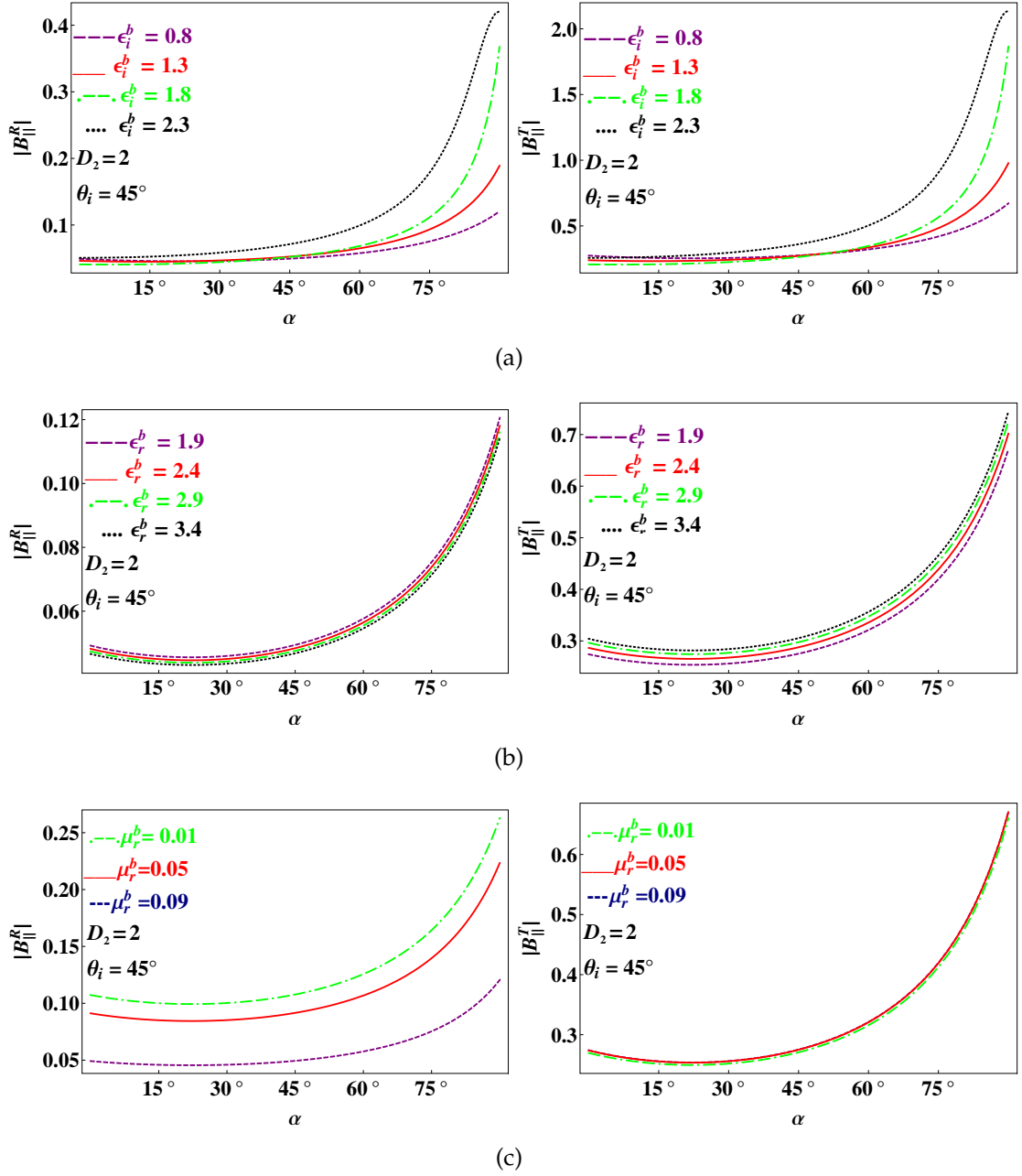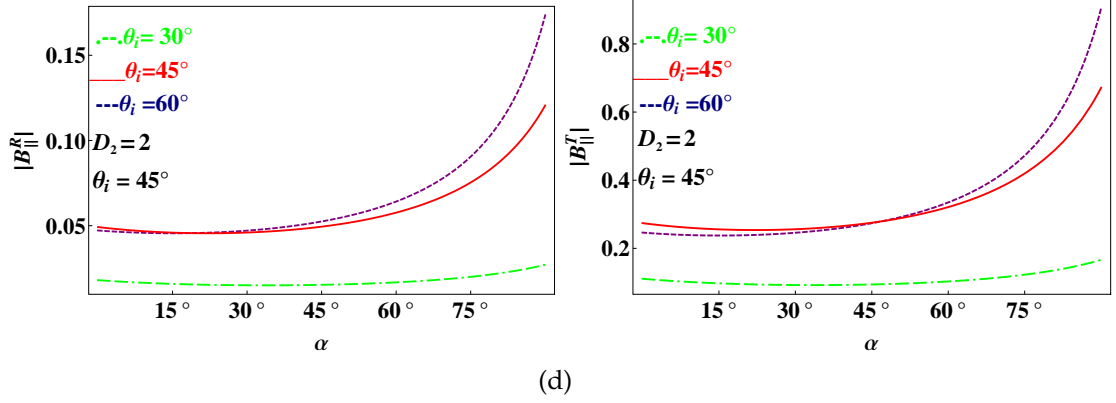
Figure 3.11: Behavior of $|B_{\parallel}^R|$ and $|B_{\parallel}^T|$ with respect α for $D_2 = 2$.

(a)

(b)

Figure 3.12: (cont.)

(c)
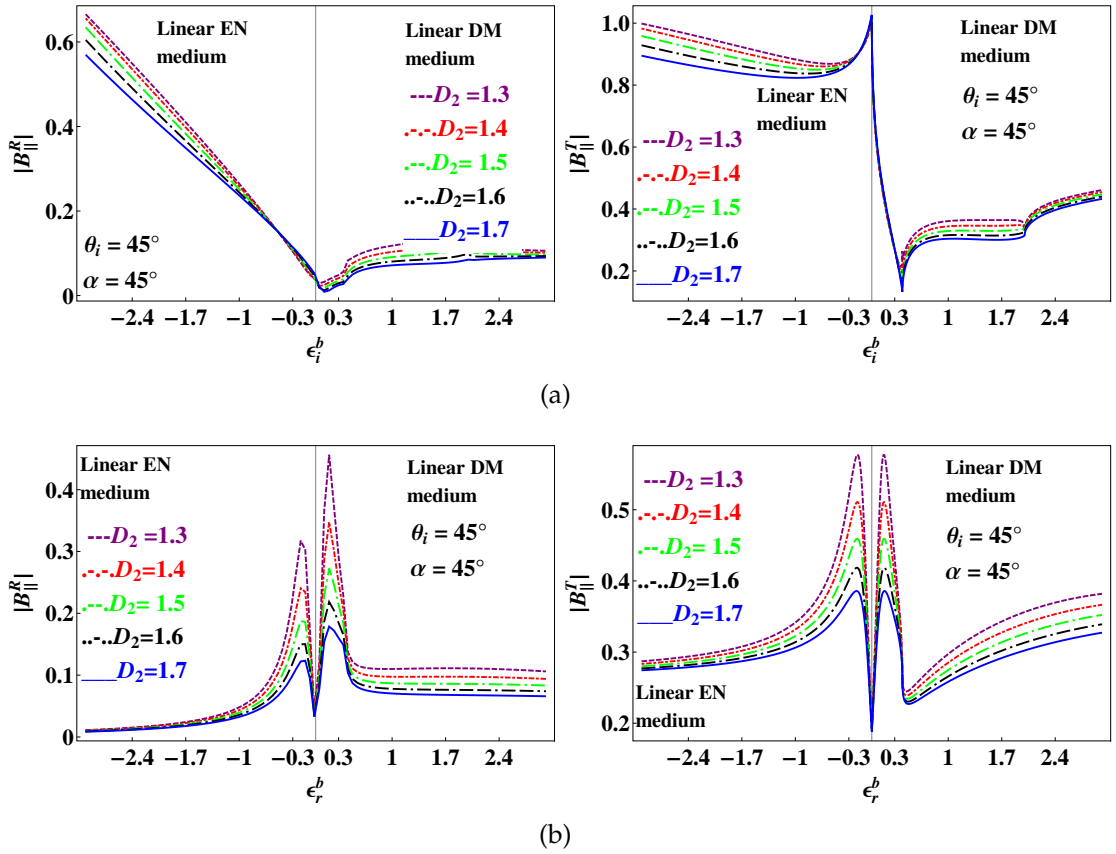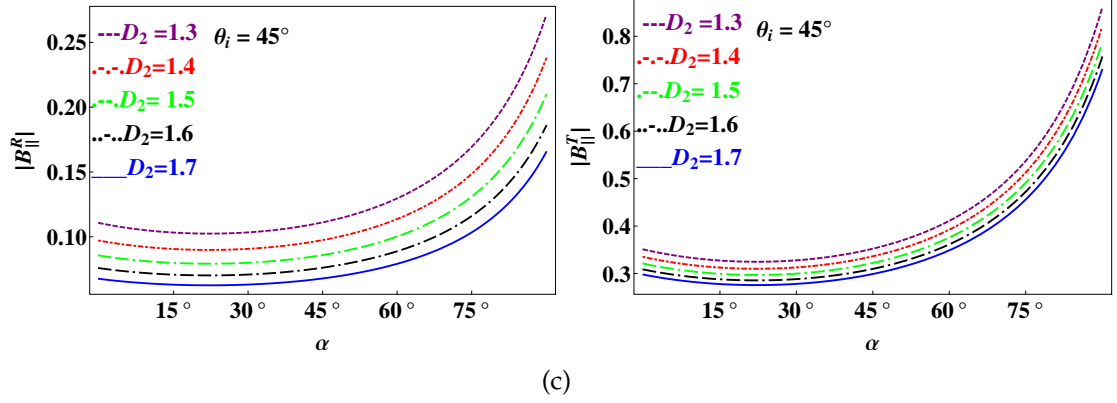
Figure 3.12: Behavior of $|B_\parallel^R|$ and $|B_\parallel^T|$ with respect (a) ϵ_i^b (b) ϵ_r^b and (c) α for the variations of the dimension parameter.

(a)

(b)

Figure 3.13: (cont.)

(c)
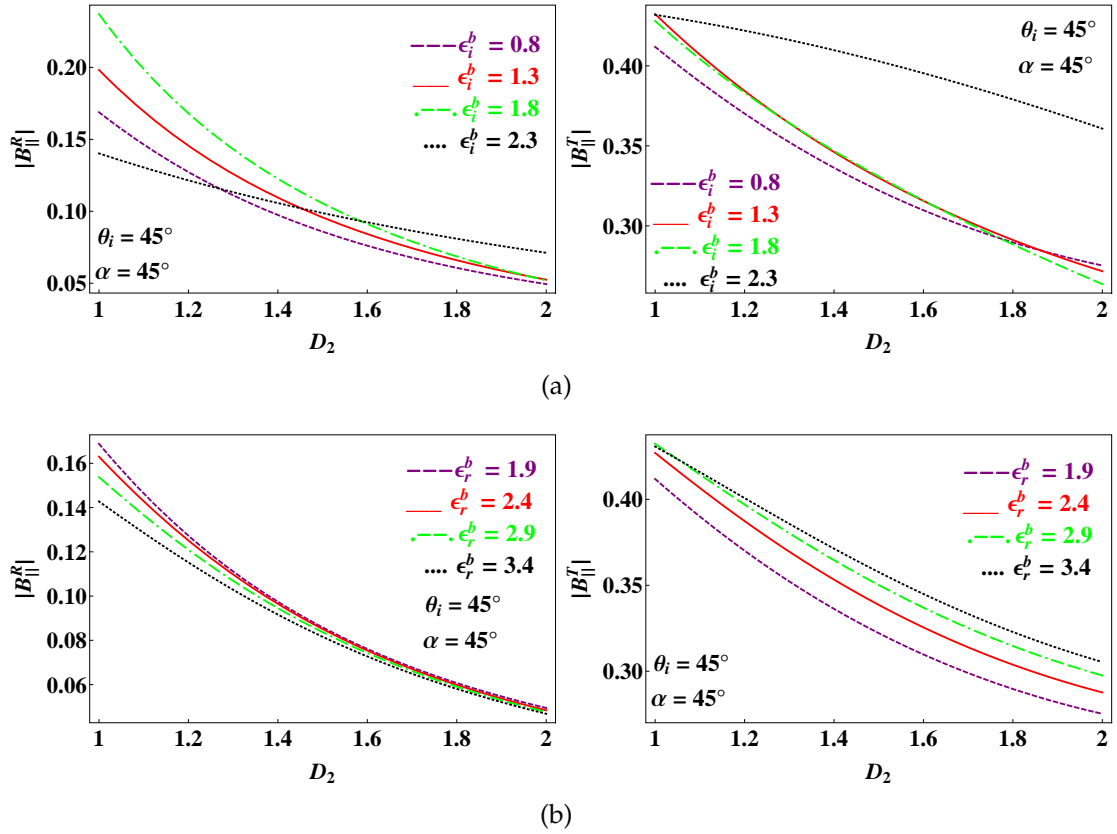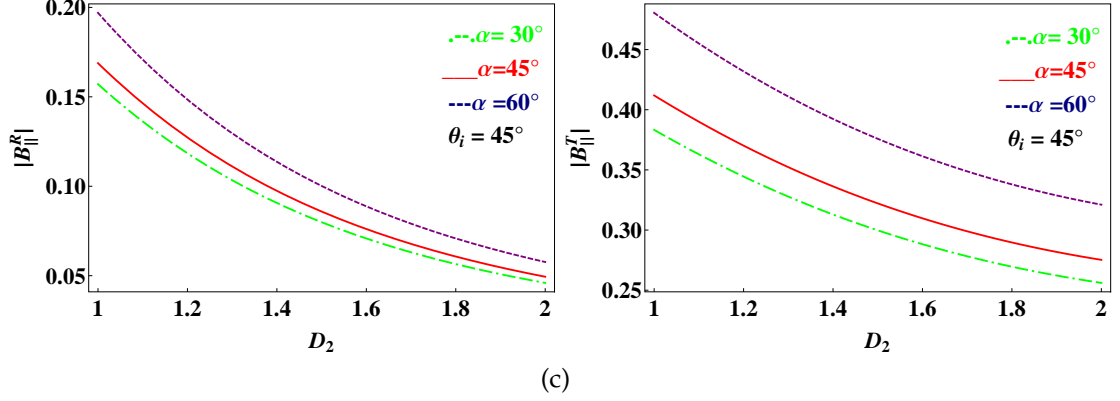
Figure 3.13: Behavior of $|B^R_{\parallel}|$ and $|B^T_{\parallel}|$ with respect to dimension parameter.
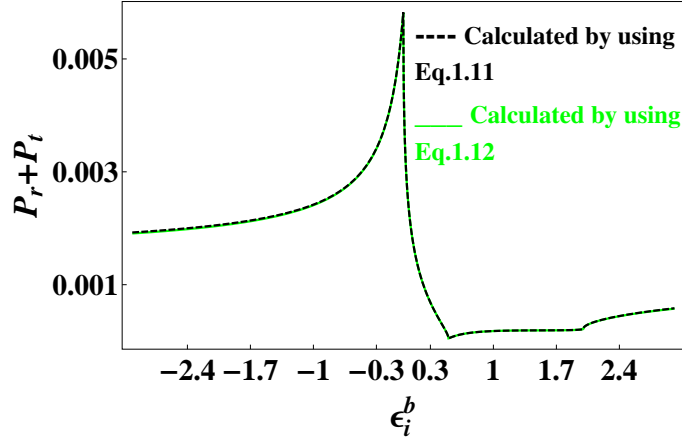
Figure 3.14: Sum of P-polarized reflected and transmitted powers for I^b .

3.2.3   Conclusion

Derivation and discussion of the second order P-polarized coefficients is given in this section for linear dielectric magnetic–second order nonlinear dielectric magnetic NID planar interface. Results depict that amplitude of the reflection (transmission) coefficient decreases (increases) by increasing the value of ϵ^b_r. Moreover, amplitude of both the coefficients decreases by increasing the value of nonlinear permeability. On the other hand, amplitude of the transmission coefficient decreases by taking higher values of θ_i for $-1.7 < \epsilon^b_i < 0.3$. It is also noted that amplitude of both the coefficients increases as $\alpha \rightarrow 90°$. Furthermore, higher amplitude of both the coefficients is noticed for epsilon

negative medium compared to the dielectric magnetic medium. Results also depict that higher amplitude of the reflection coefficient is achieved by using $\epsilon_i^b = -3$, $\epsilon_r^b = 1.9$, $\mu_r^b = 0.05$ and $\alpha = \theta_i = 60°$. Studying the impact of the noninteger dimension on the behavior of the coefficients, it is noted that amplitude of the coefficients decreases as $D_2 \to 2$ for fixed values of the constitutive parameters.

Chapter 4

Linear dielectric magnetic NID and nonlinear dielectric magnetic NID planar interface

In this chapter derivation and the discussion of the reflection and transmission coefficients is given when a S-polarized and P-polarized electromagnetic wave is used to excite the linear dielectric magnetic NID–second order nonlinear dielectric magnetic NID planar interface. Changes in the behavior of the coefficients is also reported when an epsilon negative or mu negative NID medium is taken instead of linear dielectric magnetic NID medium. In all these cases, contribution of the non-linearity and noninteger dimensions are studied separately. Moreover, specific ranges of the permittivities and permeability are also discussed for which higher amplitude of the coefficients can be observed. Results depict that higher amplitude of the reflection coefficient is achieved by using dielectric magnetic NID left half space compared to EN–NID medium. Results depict that dimensions of the NID mediums can be used to control the amplitude of the coefficients.
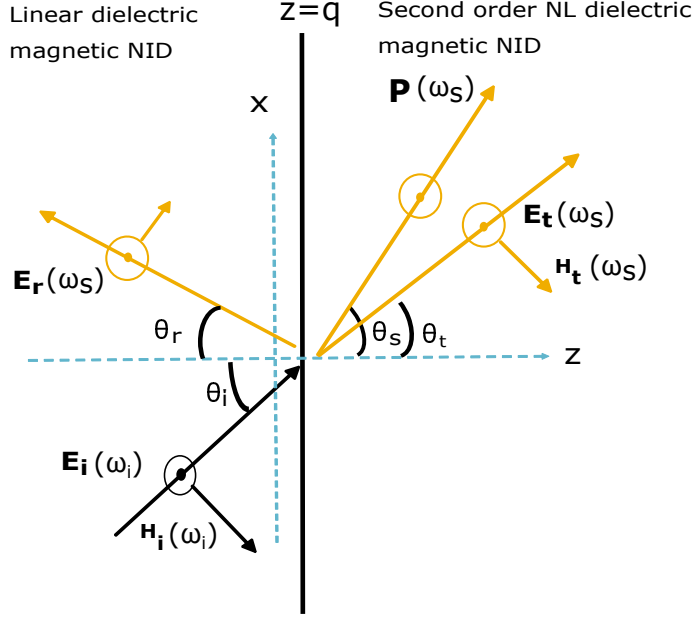
Figure 4.1: Linear dielectric magnetic NID and second order NL dielectric magnetic NID planar interface excited by S-polarized plane wave.

4.1   S-polarization excitation

4.1.1   Description of the geometry and mathematical formulation

Consider a planar interface placed at $z = q$ and is excited by a S-polarized wave of fundamental frequency ω_i, making an angle θ_i with the normal to the interface, as depicted in Fig.4.1. Left half plan which is symbolized as medium $m_\ominus$ is filled with linear dielectric magnetic NID medium and is characterized by the wave number $k_i^c = \frac{\omega_i}{c}\sqrt{\epsilon_i^c(\omega_i)}$, where, $\epsilon_i^c(\omega_i)$, (hereafter it is written as 'ϵ_i^{c}' for simplicity) is the fundamental permittivity of this medium. Right half space, contains second order NL dielectric magnetic NID medium (medium $m_\oplus$), which is characterized by the wave number $k_t^c = \frac{\omega_s}{c}\sqrt{\epsilon_t^c(\omega_s)}$ where, $\epsilon_t^c(\omega_s)$ (hereafter written as ϵ_t^c for simplicity) is the permittivity of $m_\oplus$ at second harmonic frrquency.

 Following the procedure of MSV in NID space, incident wave for NID medium

is expressed as,

$$\mathbf{E_i}(\omega_i) = \hat{\mathbf{y}}\Pi_i(\omega_i)exp\left(ik_ix\sin\theta_i\right)\left(k_iz\cos\theta_i\right)^{o_1}H_{o_1}^{(2)}\left(k_iz\cos\theta_i\right), \qquad (4.1)$$

In above equation, order of medium $m_\ominus$ and $m_\oplus$ are $o_1 = \left|\frac{3-D_1}{2}\right|$ and $o_2 = \left|\frac{3-D_2}{2}\right|$, respectively, whereas D_1 and D_2 are the respective dimensions of left and right half space mediums.

To obtain the transmitted wave, solution of the NL wave equation is obtained by using SVA approximation and MSV in NID space. Equating the tangential components of the waves across the interface, following boundary condition equations are obtained,

$$C_\perp^R A_r = C_\perp^T A_t + \frac{PA_s\omega_s^2\mu_o}{k_s^2 - k_t^{c2}}$$

$$\frac{C_\perp^R B_r \cos\theta_r}{\eta_r^c} = -\frac{C_\perp^T B_t \cos\theta_t}{\eta_t^c} - \frac{PB_s\cos\theta_s\omega_s^2\mu_o}{\eta_s(k_s^2 - k_t^{c2})} \qquad (4.2)$$

Analytical solution of Eq.(4.2) yields the following unknown coefficients,

$$C_\perp^R = -\frac{\eta_r^c\eta_s\left(k_s^2 - k_t^{c2}\right)\xi}{\eta_t^c\varpi\vartheta^2} \qquad (4.3)$$

$$C_\perp^T = -\frac{\eta_s\left(k_s^2 - k_t^{c2}\right)\left(A_tB_r\eta_t^c\cos\theta_r + A_rB_t\eta_r^c\cos\theta_t\right)}{\varpi\vartheta}, \qquad (4.4)$$

where $C_\perp^R$ and $C_\perp^T$ are the known reflection and transmission coefficients and the subscript is used to indicate the polarization of the incident electromagnetic wave, and

$$\xi = \left(A_tB_r\eta_t^c\cos\theta_r + A_rB_t\eta_r^c\cos\theta_t\right)\left(-A_tB_s\eta_t^c\cos\theta_s + A_sB_t\eta_s\cos\theta_t\right)$$

Different notations used to write the unknown coefficients in compact form are given in appendix.

4.1.2 Results and discussion

The S-polarized unknown coefficients which are derived in previous section are discussed here, as a function of ϵ_i^c, ϵ_r^c and μ_r^c. Analysis is also conducted by taking special cases of the original geometry: epsilon negative NID (EN–NID) or mu negative NID (MN–NID) as $m_\ominus$ mediums are considered in this regard. In the first part, analysis is conducted to study the impact of the non-linearity on the unknown coefficients by taking ordinary mediums, i.e; $D_1=D_2=2$ (Fig.4.2–Fig.4.4). Behavior of the unknown coefficients as a function of ϵ_i^c by taking specific values of ϵ_r^c (Fig.4.2a), μ_r^c (Fig.4.2b) and θ_i (Fig.4.2c) are given in Fig.4.2. It is noted that amplitude of the coefficients increases by increasing the values of the ϵ_r^c. Moreover, it is also noted that for specific value of ϵ_r^c, amplitude of both the coefficients increases for $\epsilon_i^c < 2$ and decreases for $\epsilon_i^c > 2$. It is also noted that amplitude of the coefficients increases by taking smaller values of μ_r^c and higher amplitude of both the coefficients are achieved by taking μ_r^c=0.01 and $1.7 < \epsilon_i^c < 2.4$ (Fig.4.2b). In Fig.4.2c, peaks of the coefficients are observed which shift towards right by increasing the value of the incident angle. It is also observed that amplitude of the reflection (transmission) coefficient decreases (increases) by increasing the incident angle. From the comparison of all subplots given in Fig.4.2, it is noted that amplitude of the coefficients for EN–NID $m_\ominus$ medium are negligible compared to dielectric magnetic NID $m_\ominus$ medium. Fig.4.3, depict the behavior of the reflection and transmission coefficients as a function of ϵ_r^c. It is observed that amplitude of the coefficients increases by increasing the value of ϵ_i^c (Fig.4.3a), except at ϵ_i^c=1.8, which provides higher amplitude of the reflection coefficient for $-2.3 < \epsilon_r^c < 0.65$ and $\epsilon_r^c > 1.15$. On the other hand, higher amplitude of the transmission coefficient is observed for $-3 < \epsilon_r^c < 0.85$ and $\epsilon_r^c > 1$. It is also noted that higher amplitude of the reflection coefficient can be achieved by taking negative values of ϵ_r^c compared to positive values. Results also depict that amplitude of the coefficients increases by taking smaller values of μ_r^c (Fig.4.3b) and higher values of the incident angle (Fig.4.3c). From the comparison of all these subplots, it is noted that higher amplitude of the reflection coefficient can be achieved by taking ϵ_r^c=-3, ϵ_i^c=2.3, μ_r^c=0.01 and θ_i=60°. On the other hand, higher amplitude of the transmission

coefficient can be achieved by taking ϵ_i^c=1.8, μ_r^c=0.01, θ_i=60° and by taking negative of ϵ_r.

In Fig.4.4, coefficients are plotted as a function of μ_r^c. It is noted that amplitude of the coefficients increases by increasing ϵ_i^c. It is noted that both coefficients behave differently at $\epsilon_i^c = 1.8(\approx \epsilon_r^c)$. It is also noted that amplitude of the reflection coefficient decreases by increasing the value of ϵ_r^c for $-1 < \mu_r^c < -0.45$ and increases for $\mu_r^c > 0.45$ (Fig.4.4b). It is noted that amplitude of the coefficients increases by increasing the value of the incident angle except at $-0.1 < \mu_r^c < 0.5$. From the comparison of all these subplots it is noted that higher amplitude of the coefficients can be achieved for mu near zero medium.
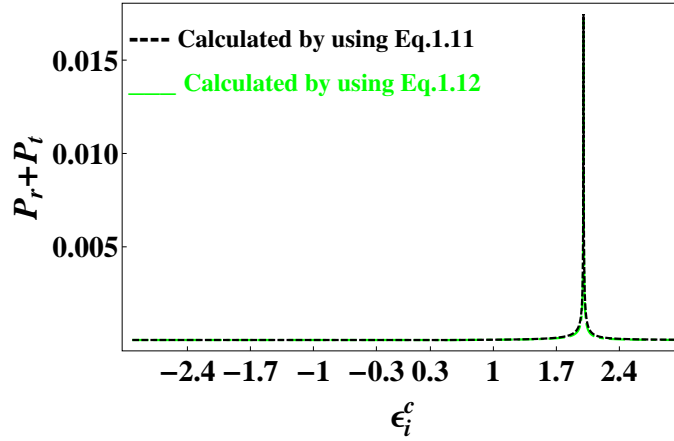
Figure 4.9: Sum of S-polarized reflected and transmitted powers for I^c .

Fig.4.5 and Fig.4.8, depict the contribution of the noninteger dimension of $M_\ominus$ and $M_\oplus$. Behavior of the coefficients are studied as a function of ϵ_i^c, ϵ_r^c and μ_r^c. It is noted that amplitude of the reflection coefficient increases by increasing D_1 for $-3 < \epsilon_i^c < 1.5$ whereas, decreases for $\epsilon_i^c > 1.5$ (Fig.4.5a). On the other hand, amplitude of the reflection coefficient also increases by increasing D_1 for $-3 < \epsilon_r^c < 0.25$ and $\epsilon_r^c > 1.2$. Whereas, amplitude of the transmission coefficient increases by increasing D_1 for $-3 < \epsilon_r^c < 0.1$ and $\epsilon_r^c > 1.8$ and decreases for $0.1 < \epsilon_r^c < 1.8$ (Fig.4.5b). It is also noted that amplitude of the reflection coefficient decreases by increasing D_1 for $-1 < \mu_r^c < -0.03$ and $\mu_r^c > 0.1$ but, increases for $-0.03 < \mu_r^c < 0.1$ (Fig.4.5c). From the comparison of all these subplots, it is noted that higher amplitude of the coefficients are achieved by

Figure 4.2: Behavior of $|C_\perp^R|$ and $|C_\perp^T|$ with respect to ϵ_i^c for $D_1 = D_2 = 2$.

Figure 4.3: Behavior of $|C_\perp^R|$ and $|C_\perp^T|$ with respect to ϵ_r^c for $D_1 = D_2 = 2$.

Figure 4.4: Behavior of $|C_\perp^R|$ and $|C_\perp^T|$ with respect to μ_r^c for $D_1 = D_2 = 2$.

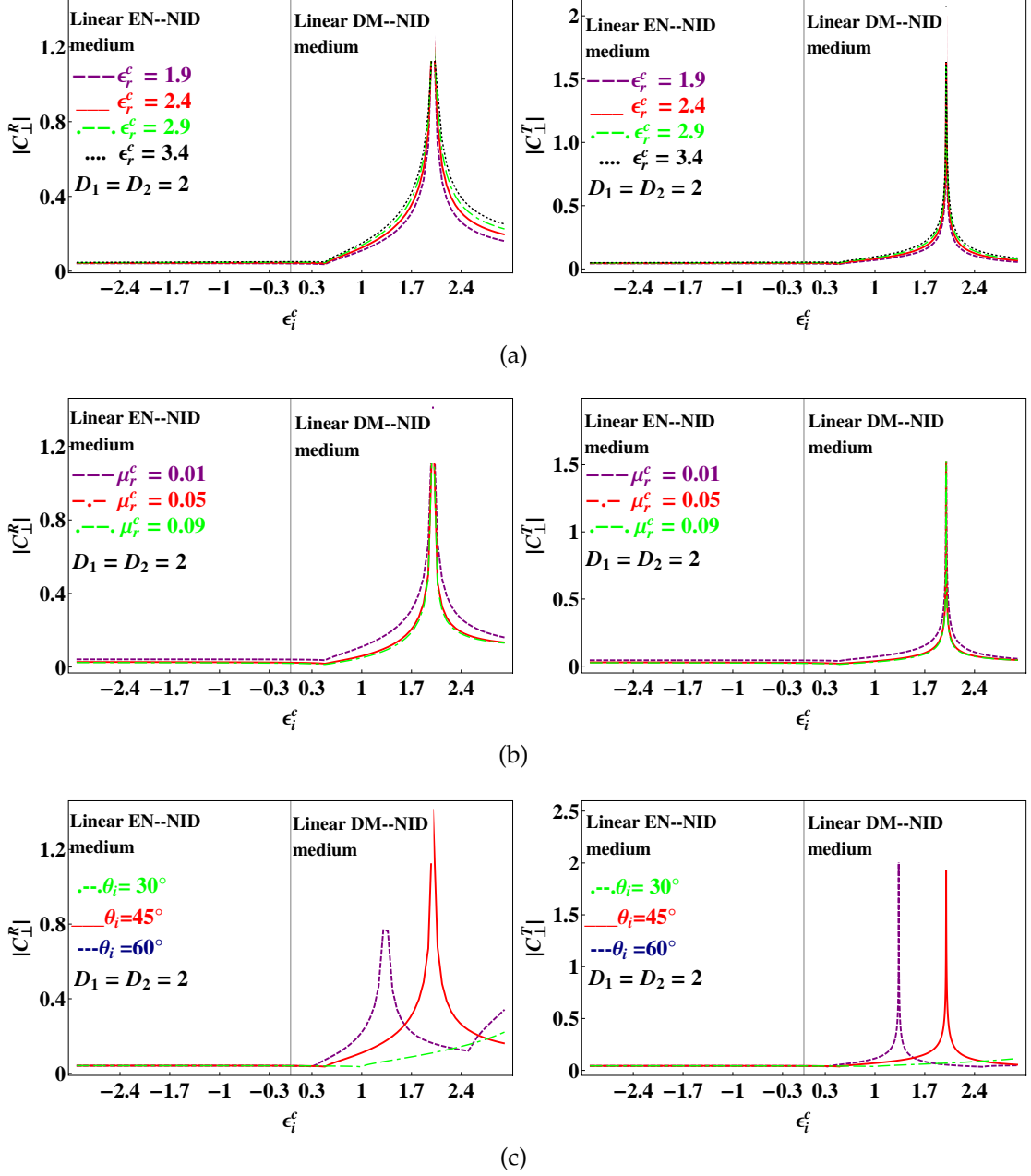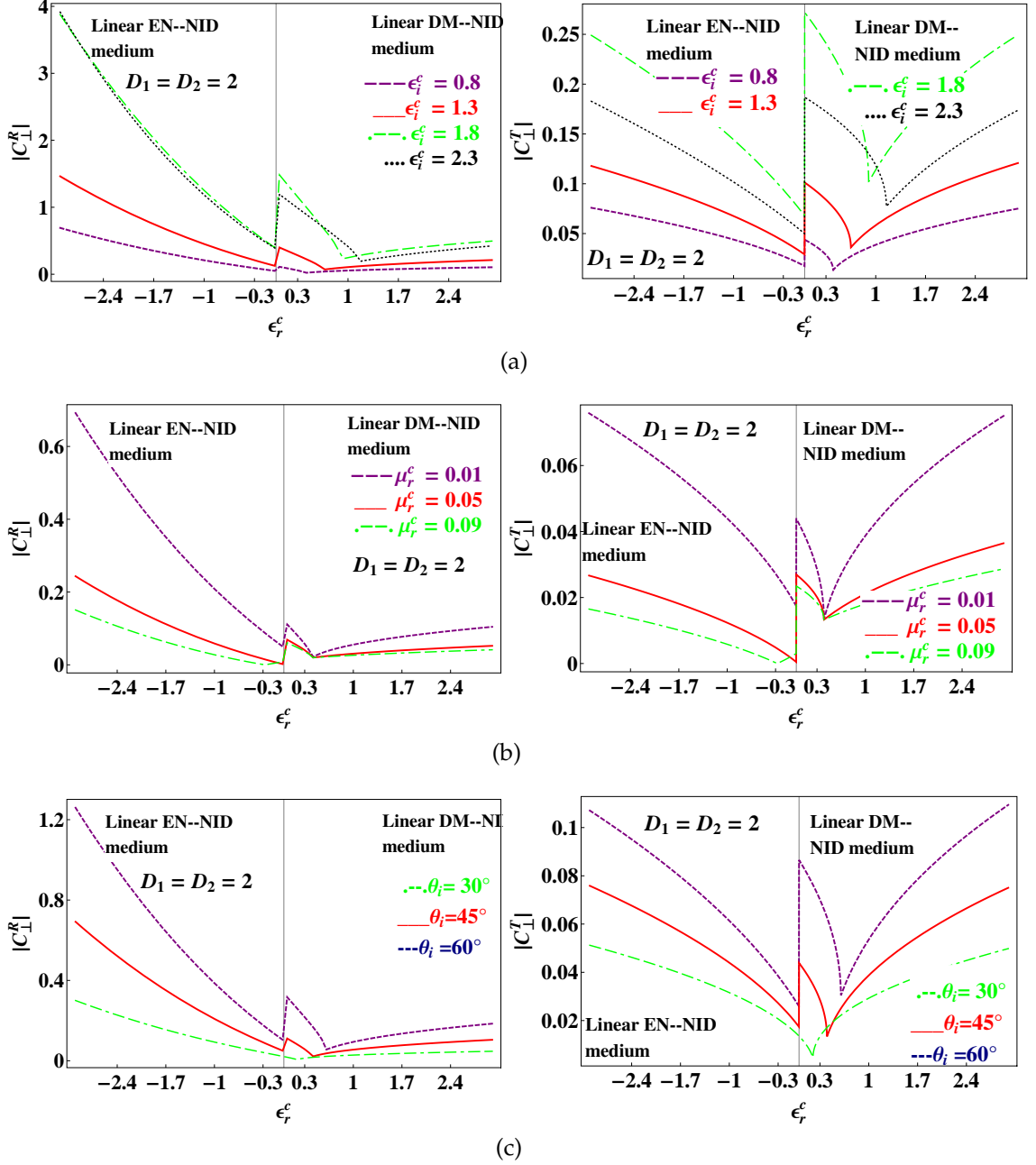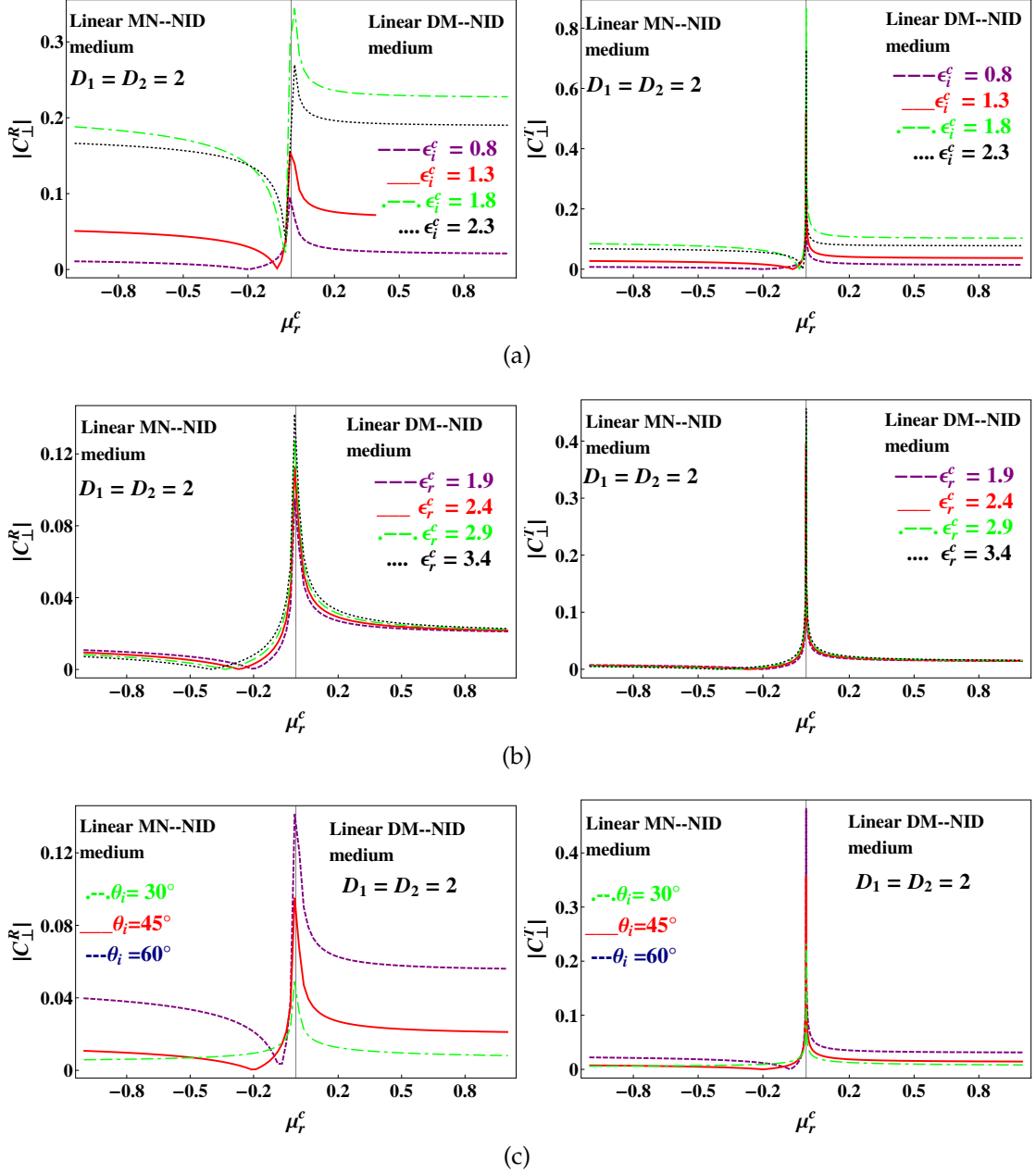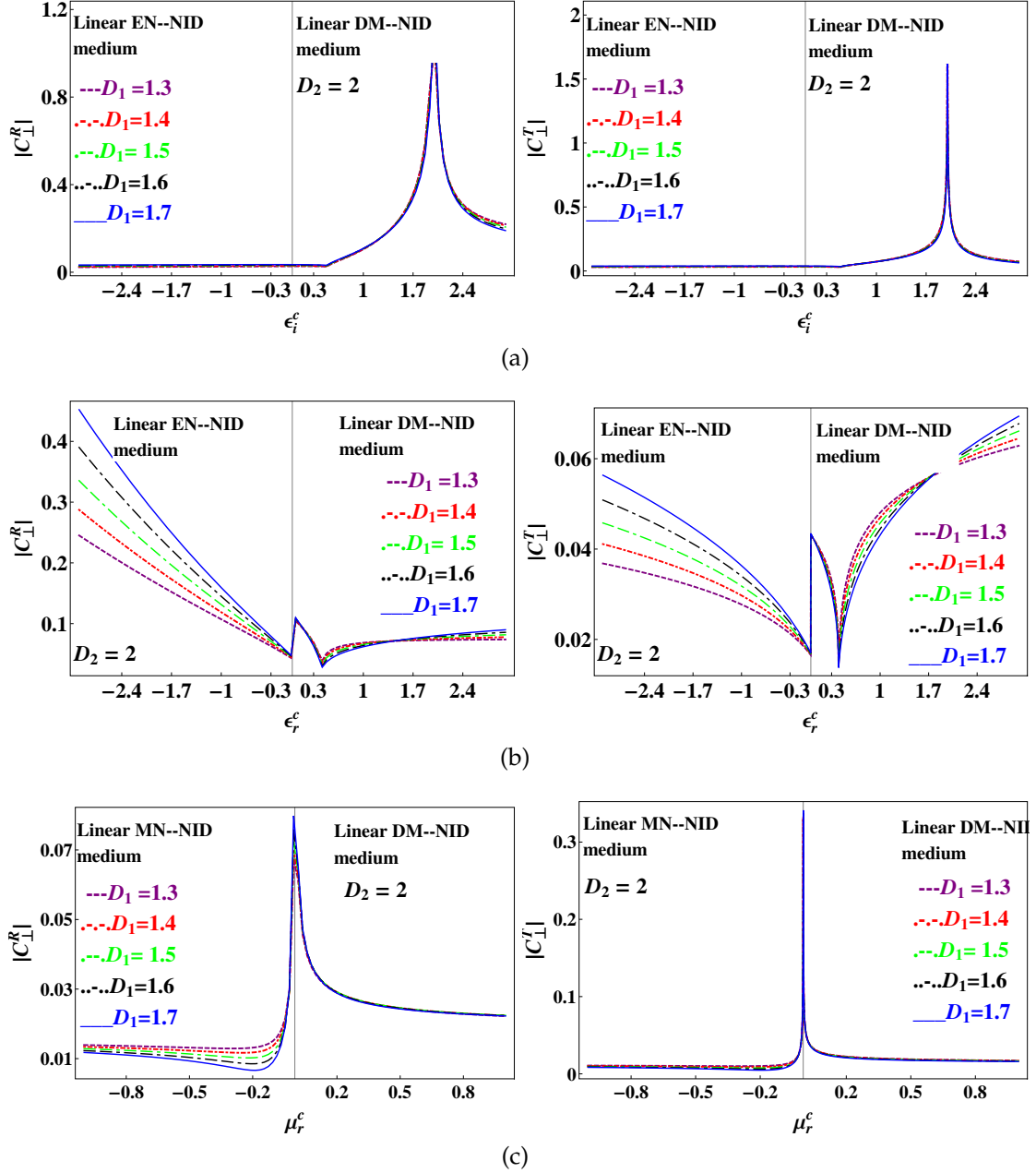Figure 4.5: Behavior of $|C_\perp^R|$ and $|C_\perp^T|$ with respect to (a) ϵ_i^c (b) ϵ_r^c (c) μ_r^c for $D_2 = 2, D_1 \neq 2$.
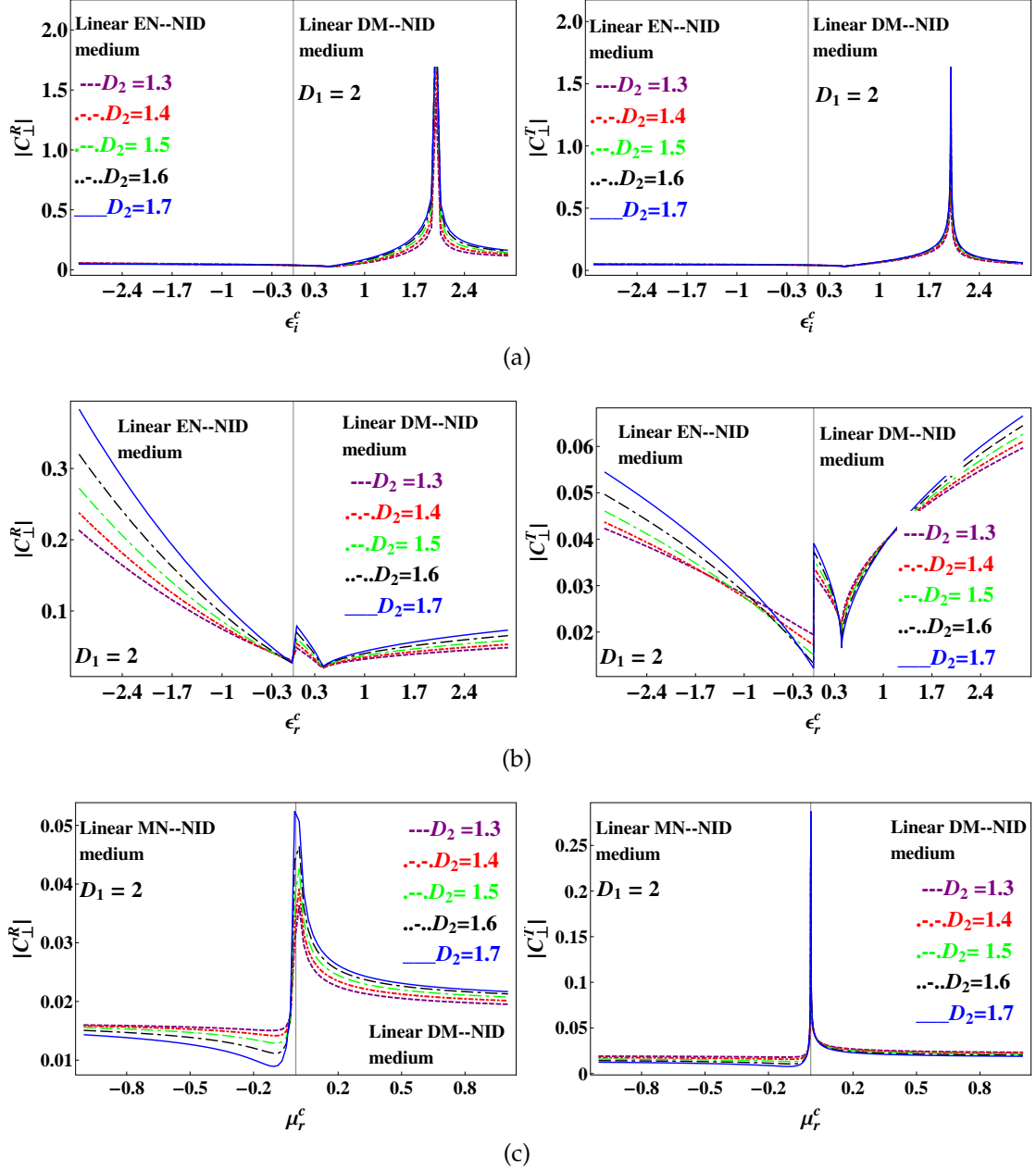
Figure 4.6: Behavior of $|C_\perp^R|$ and $|C_\perp^T|$ with respect to (a) ϵ_i^c (b) ϵ_r^c (c) μ_r^c for $D_1 = 2$, $D_2 \neq 2$.
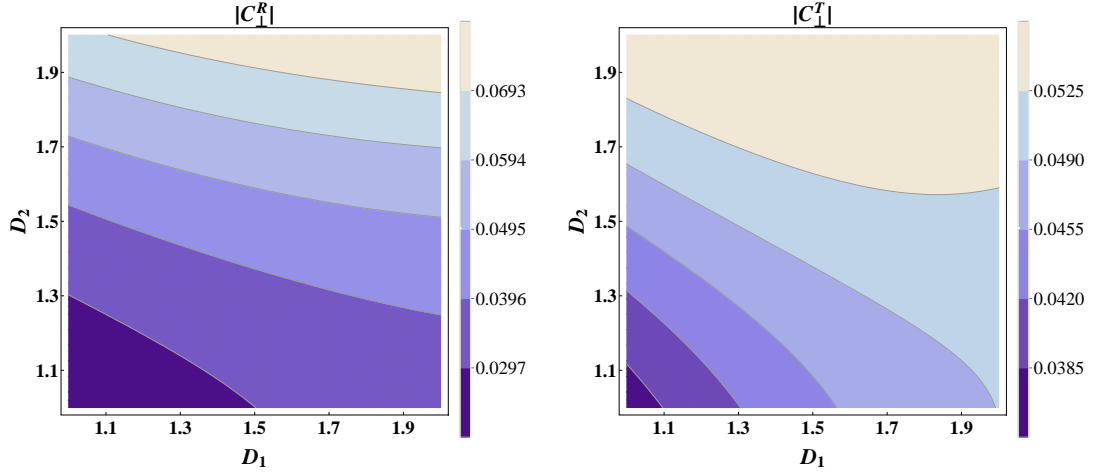
Figure 4.7: Contour plots of $|C_\perp^R|$ and $|C_\perp^T|$ with respect to D_1 and D_2 for $\epsilon_i^c = 0.8$, $\epsilon_r^c = 1.9$, $\mu_r^c = 0.01$, $\mu_i^c = 0.02$ and $\theta_i = 45°$.

taking higher values of the noninteger dimensions and $1.7 < \epsilon_i^c < 2.4$, $\epsilon_r^c = -3$ and mu near zero materials. Fig.4.6a, depict that amplitude of the coefficients increases by increasing the value of D_2. It is also noted that amplitude of the reflection coefficient increases by taking higher values of D_2. Whereas, transmission coefficient decreases by taking higher values of D_2 for $-0.7 < \epsilon_r^c < -0.05$ and $0.4 < \epsilon_r^c < 1$ (Fig.4.6b). On the other hand, Fig.4.6c, depict that amplitude of the reflection coefficient decreases (increases) by increasing the value of D_2 for $\mu_r^c < 0$ ($\mu_r^c > 0$). Fig.4.7, depict the contour plots of reflection and transmission coefficients by taking $\epsilon_i^c > 0$, $\epsilon_i^c > 0$ and $\mu_r^c > 0$. In Fig.4.8, contour plots of the coefficients are give for $\epsilon_i^c = -0.8$ (Fig.4.8a), $\epsilon_r^c = -1.9$ (Fig.4.8b) and $\mu_r^c = -0.01$ (Fig.4.8c). From the comparison of Fig.4.2–Fig.4.4 and Fig.4.5–Fig.4.8, it is noted that dimension of both the mediums are used as controlling factors for the amplitude of the coefficients by keeping the same shape.

4.1.3 Conclusion

Derivation and discussion of the S-polarized reflection and transmission coefficients are given in this section for linear dielectric magnetic NID–second order nonlinear dielectric magnetic NID planar interface. It is noted that amplitude of the coefficients increases (decreases) by increasing the values of ϵ_r^c (μ_r^c). Fur-
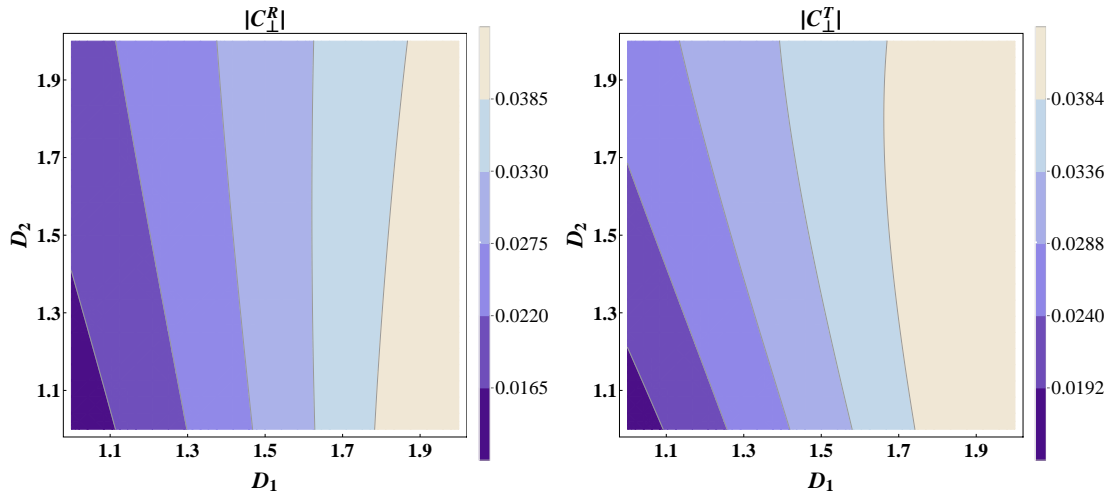
(a)
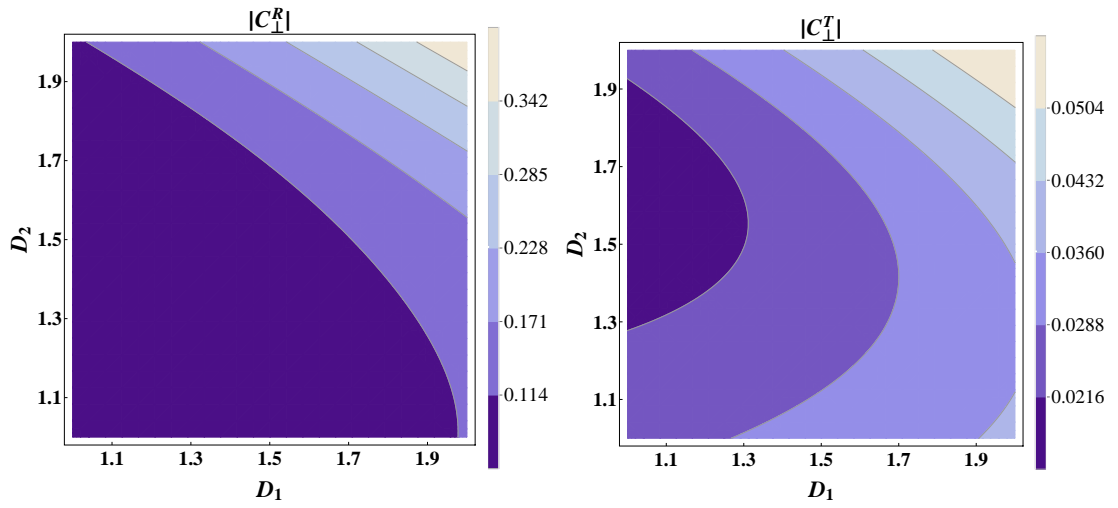
(b)

Figure 4.8: (cont.)
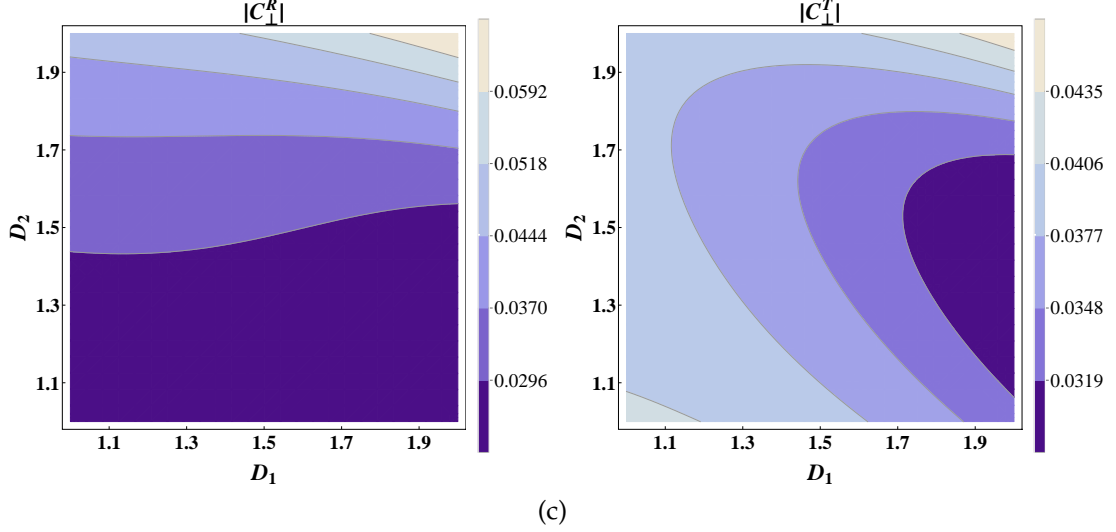
Figure 4.8: Contour plots of $|C_\perp^R|$ and $|C_\perp^T|$ with respect to D_1 and D_2 by taking $\mu_t^c = 0.02$ and $\theta_i = 45°$ for (a) $\epsilon_r^c = 1.9$, $\mu_r^c = 0.01$ and $\epsilon_i^c = -0.8$ (b) $\epsilon_i^c = 0.8$, $\mu_r^c = 0.01$ and $\epsilon_r^c = -1.9$ and (c) $\epsilon_i^c = 0.8$, $\epsilon_r^c = 1.9$ and $\mu_r^c = -0.01$.

thermore, peaks of the coefficients are also observed at specific values of linear permittivity, which shift towards right by increasing the incident angle. Results also depict that higher amplitude of both the coefficients are achieved by taking dielectric magnetic NID medium as left half space medium. It is studied that amplitude of the reflection coefficient increases by taking negative values of the ϵ_r. Moreover, amplitude of both the coefficients can be increased by using a material exhibiting $\epsilon_i^c \approx \epsilon_r^c$ for manufacturing a devices which is operating on a specific value of μ_r^c. In all cases: (a) $D_1 = D_2 = 2$, $D_1 \neq 2$ (b) $D_2 = 2$, $D_2 \neq 2$ (c) $D_1 = 2$, dimension of both the mediums are used as a controlling factor for the behavior of the coefficients by keeping the same shape.

4.2   P-polarization excitation

4.2.1   Description of the geometry and mathematical formulation

Consider a planar interface located at $z = q$ and excited by a P-polarized electromagnetic wave as depicted in Fig.4.10. Description of the geometry is given
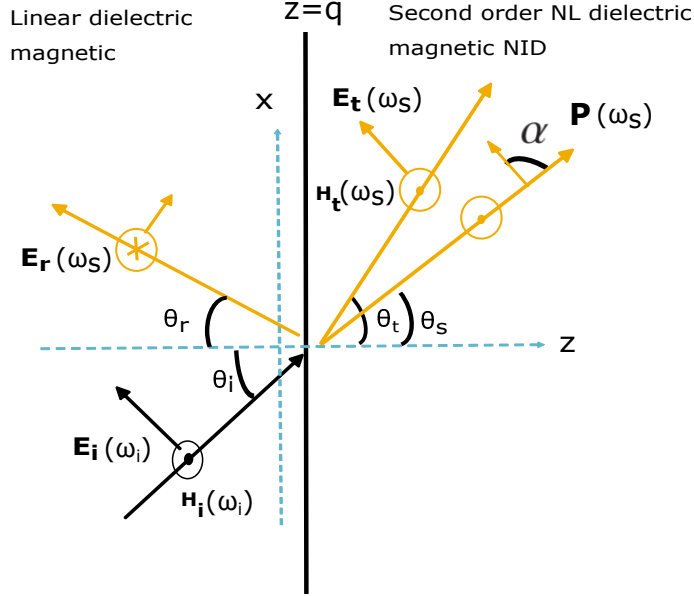
Figure 4.10: Linear NID magnetic and second order NL dielectric magnetic NID planar interface excited by P-polarized plane wave.

in Sec.4.1.1.

Using the procedure of MSV in NID space and SVA approximation for the solution of the NL wave equation (as discussed in Sec.4.1.1), P-polarized reflected and transmitted fields are obtained. Equating the tangential components of the fields across the interface following boundary condition are achieved,

$$C_{\parallel}^R A_r \cos \theta_r = C_{\parallel}^T A_t \cos \theta_t + \frac{P \omega_s^2 \mu_o A_s \cos \theta_s \sin \alpha}{k_s^2 - k_t^{c2}} + \frac{P \omega_s^2 \mu_o A_s \sin \theta_s \cos \alpha}{k_t^{c2}}$$

$$-\frac{C_{\parallel}^R B_r}{\eta_r^c} = \frac{C_{\parallel}^T B_t}{\eta_t^c} + \frac{P \omega_s^2 \mu_o B_s \sin \alpha}{\eta_s (k_s^2 - k_t^{c2})},$$

(4.5)

$C_{\parallel}^R$ and $C_{\parallel}^T$ are the unknown reflection and transmission coefficients, respectively and the subscripts are used to indicate the polarization of the incident electromagnetic wave. Analytical solution of Eq.(4.5), yields the unknown co-

efficients which are written below as,

$$
C_{\parallel}^R = \frac{k_t^{c2}\eta_r^c\eta_s\left(k_s^2 - k_t^{c2}\right)\left(\psi_1 + \psi_2\right)\left[k_t^{c2}\sin\alpha\left(\psi_3 - \psi_4\right) + \psi_5\left(k_s^2 - k_t^{c2}\right)\right]}{\delta_{cc}^t\eta_t^c\left[k_t^{c2}\psi_6 + A_s B_r \eta_s\left(k_t^{c2}\sin(\alpha - \theta_s) + k_s^2\cos\alpha\sin\theta_s\right)\right]^2}
$$

$$
C_{\parallel}^T = \frac{k_t^{c2}\eta_s\left(k_t^{c2} - k_s^2\right)\left(\psi_1 + \psi_2\right)}{\delta_{cc}^t\left[k_t^{c2}\psi_6 + A_s B_r \eta_s\left(k_t^{c2}\sin(\alpha - \theta_s) + k_s^2\cos\alpha\sin\theta_s\right)\right]}
$$

(4.6)

All definitions used to write the above equations in compact form are given in appendix.

4.2.2 Results and discussion

This section is devoted to the study of the behavior of the P-polarized reflection and transmission coefficients as a function of ϵ_i^c, ϵ_r^c, μ_r^c, θ_i and α. As stated in previous chapters, α is the angle formed between induced NL polarization and the wave vector, hence $\alpha = 0°$ and $\alpha = 90°$ depict that $\mathbf{P}||\mathbf{k_t^c}$ and $\mathbf{P} \perp \mathbf{k_t^c}$. Analysis presented in this section is divided into two parts. In the first part, behavior of the coefficients is studied by taking both ordinary half spaces, i.e; $D_1 = D_2 = 2$, to notice the impact of the non-linearity on the reflection and transmission coefficients. Plots given in Fig.4.11–Fig.4.13 depict this study. To study the impact of the noninteger dimensions on the reflection and transmission coefficients, second part of the analysis is further divided into two parts, i.e; (i) $D_1 = 2$ and $D_2 \neq 2$ (Fig.4.14) (ii) $D_2 = 2$ and $D_1 \neq 2$ (Fig.4.15).

In Fig.4.11, reflection and transmission coefficients are plotted as a function of ϵ_i^c by taking specific values of ϵ_r^c (Fig.4.11a), μ_r^c (Fig.4.11b), α (Fig.4.11c) and θ_i (Fig.4.11d). All these plots are obtained for epsilon negative–NID (EN–NID) and dielectric magnetic NID mediums. It is noted that amplitude of the reflection coefficient is greater for dielectric magnetic NID medium compared to EN–NID medium (Fig.4.11a). Furthermore, amplitude of the reflection coefficient decreases by increasing the value of ϵ_r^c for both mediums. On the other

hand, it is also noted that for epsilon near zero medium, reflection coefficient reaches to zero, i.e considered geometry composed of discussed material, behave as an absorber geometry. Similar behavior is observed when coefficients are studied for fixed value of ϵ_i^c and by taking specific values of μ_r^c (Fig.4.11b). It is noted that amplitude of both the coefficients increases by increasing the value of μ_r^c. In Fig.4.11c, coefficients are plotted by taking specific values of α. Significant changes are observed by changing values of alpha for dielectric magnetic NID medium and it is also noted that amplitude of the coefficients increases by taking higher values of α. Only amplitude of the transmission coefficient increases by decreasing α for epsilon near zero medium. On the other hand, in Fig.4.11d, coefficients are plotted by taking specific values of the incident angle. It is obvious to note that amplitude of the reflection (transmission) coefficient increases (decreases) by increasing the values of the incident angle. Furthermore it is also noted that for dielectric magnetic NID medium curves of the coefficients shift towards left by increasing the values of the incident angle.

In Fig.4.12, coefficients are plotted as a function of μ_r^c for mu negative–NID (MN–NID) and dielectric magnetic NID mediums. In Fig.4.12a (Fig.4.12b), it is noted that amplitude of the coefficients increasing (decreases) by increasing the values of ϵ_i^c (ϵ_r^c). On the other hand, it is also noted that amplitude of the reflection coefficient increases by decreasing the values of α for dielectric magnetic NID medium (Fig.4.12c). Whereas, amplitude of the coefficients increases by increasing the value of the incident angle for both MN–NID and dielectric magnetic NID mediums. Furthermore, in all these subplots it is also noted that amplitude of both the coefficients are negligible for mu near zero medium.

In Fig.4.13 coefficients are plotted as a function of α. Results presented in Fig.4.13a (Fig.4.13b), depict that amplitude of the coefficients increases (decreases) by increasing the values of ϵ_i^c(ϵ_r^c). It is also noted that amplitude of the coefficients increases by increasing the values of the incident angle (Fig.4.13d). Whereas, only amplitude of the reflection coefficient increases by increasing the value of μ_r^c. Moreover, amplitude of the transmission coefficient increases (decreases) by taking higher values of μ_r^c for $\alpha < 60°$ ($\alpha > 60°$): Fig.4.13c. Furthermore, in all these subplots it is also noted that amplitude of the coefficients

Figure 4.11: (cont.)

(d)
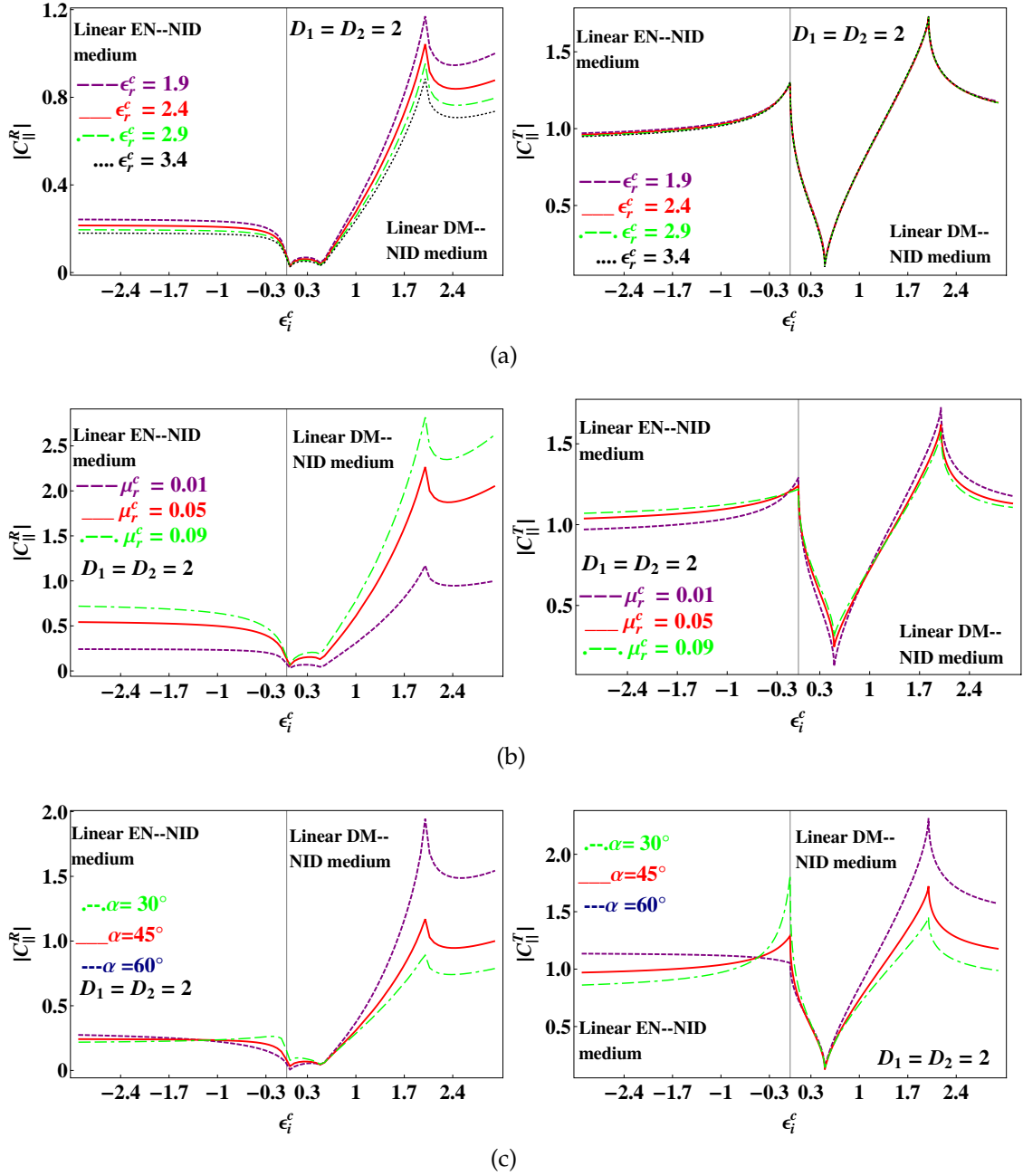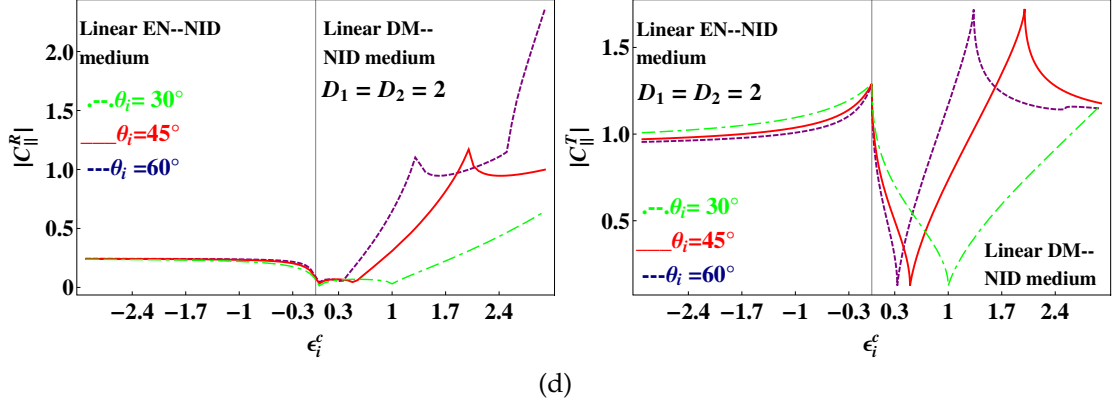
Figure 4.11: Behavior of $|C^R_\parallel|$ and $|C^T_\parallel|$ with respect to ϵ^c_i for $D_1 = D_2 = 2$.

increases as $\alpha \to 90°$, for fixed value of μ^c_r and θ_i and higher (smaller) values of $\epsilon^c_i(\epsilon^c_t)$.

Now, impact of the noninteger dimensions of both half spaces is reported (Fig.4.14–Fig.4.19). Plots given in Fig.4.14 are obtained to study the impact of the noninteger dimension of medium $M_\ominus$. It is noted that amplitude of the coefficients increases by taking higher dimension of medium $M_\ominus$, when plotted as a function of α and μ^c_r (Fig.4.14a, Fig.4.14d). On the other hand, amplitude of both the coefficients decreases by taking higher values of the noninterger dimensions of medium $M_\ominus$ when plotted as a function of ϵ^c_i and ϵ^c_r (Fig.4.14b, Fig.4.14c). Furthermore, it is also noted that behavior of both the coefficients changes for both epsilon and mu near zero mediums (Fig.4.14b–Fig.4.14d). In Fig.4.15, behavior of the coefficients are given which depict the impact of the noninteger dimension of medium $M_\oplus$, i.e; $D_1 = 2$ and $D_2 \neq 2$. From the comparison of all subplots in Fig.4.14–Fig.4.15 it is noted that dimensions of both the mediums play an important role in controlling the amplitude of the coefficients by keeping the same shape.

(a)

(b)

(c)

Figure 4.12: (cont.)

(d)
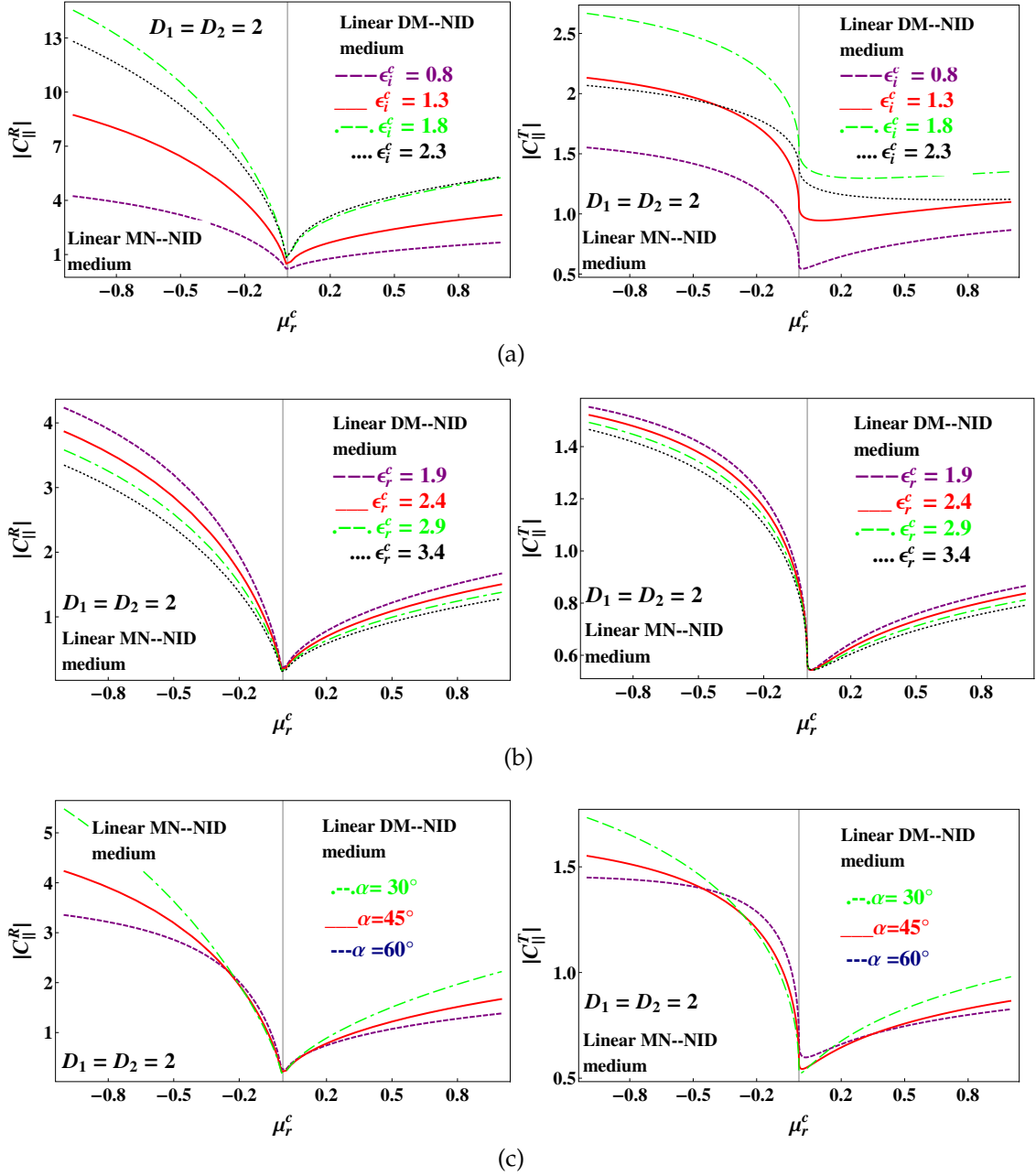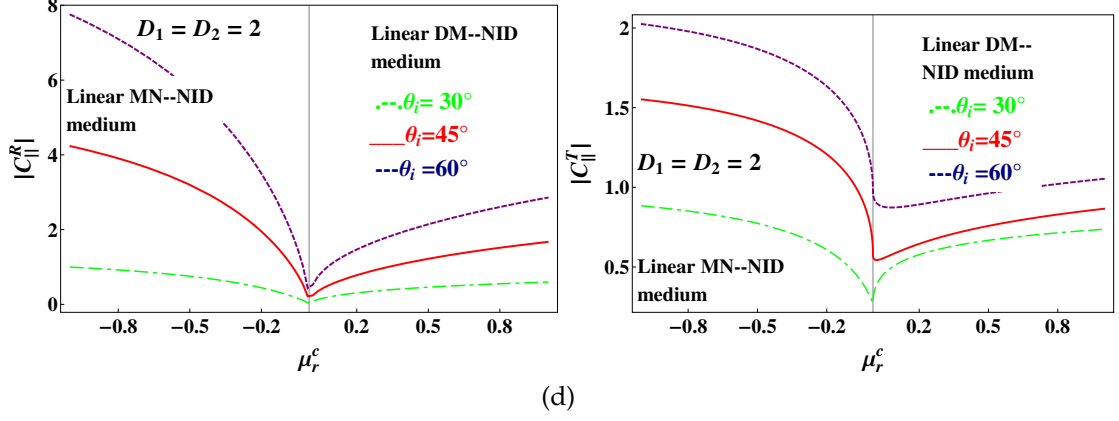
Figure 4.12: Behavior of $|C_\parallel^R|$ and $|C_\parallel^T|$ with respect to μ_r^c for $D_1 = D_2 = 2$.
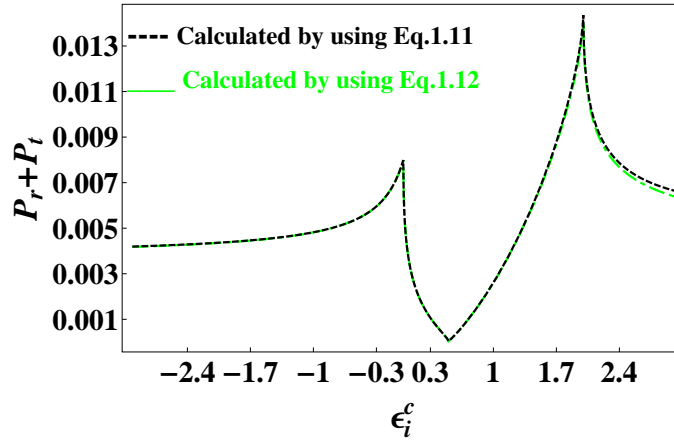
Figure 4.20: Sum of P-polarized reflected and transmitted powers for I^c .

4.2.3   Conclusion

Derivation and behavior of the second order P-polarized reflection and transmission coefficients is given in this section for linear dielectric magnetic NID–second order nonlinear dielectric magnetic NID planar interface. Higher amplitude of the reflection coefficient is noted for dielectric magnetic NID medium compared to epsilon negative medium. It is also noted that amplitude of the transmission coefficient increases by taking smaller value of α for epsilon or mu near zero mediums. Results also depict that amplitude of the reflection coefficient increases by increasing the nonlinear permeability for all values of

(a)

(b)

(c)

Figure 4.13: (cont.)

(d)
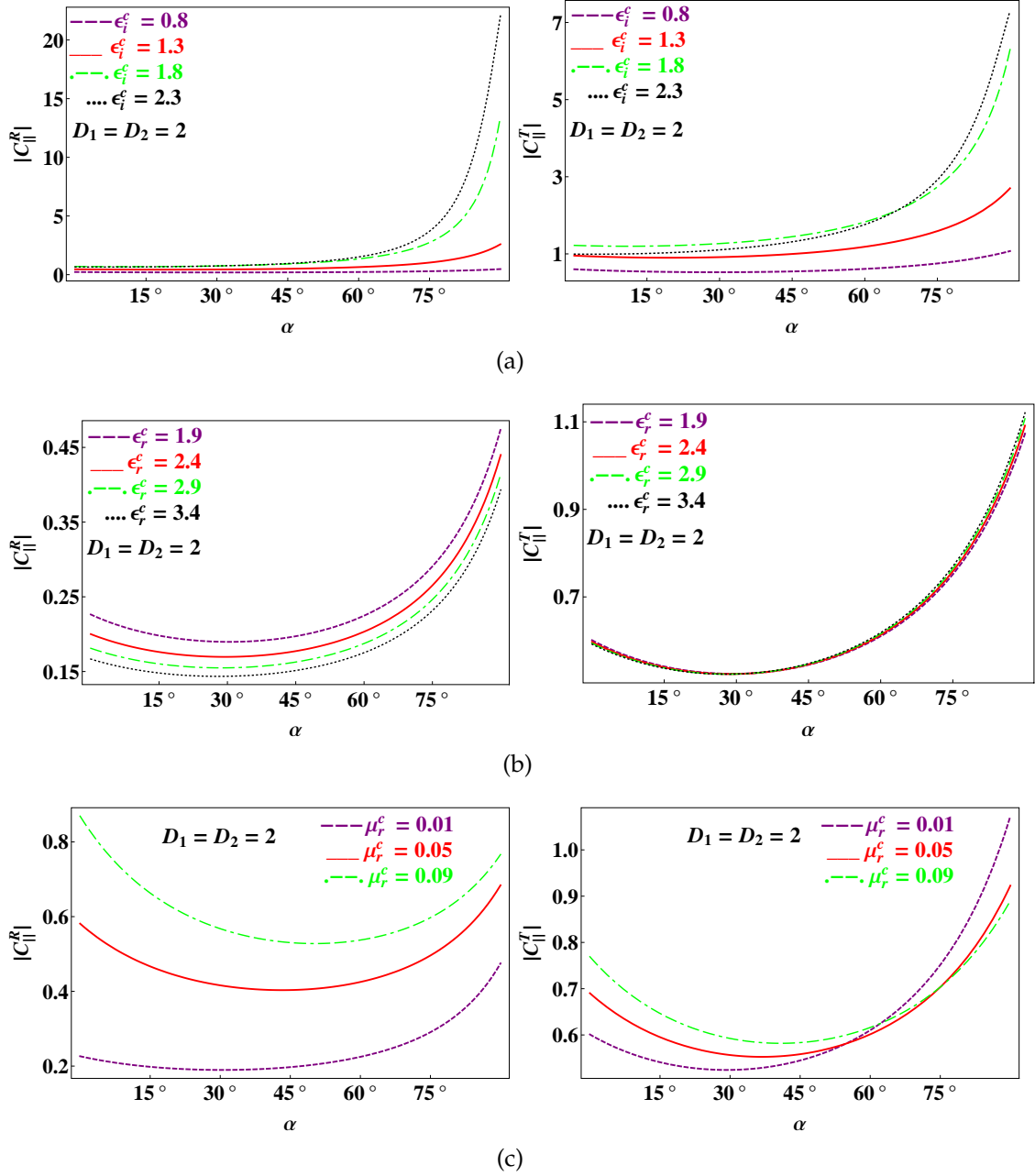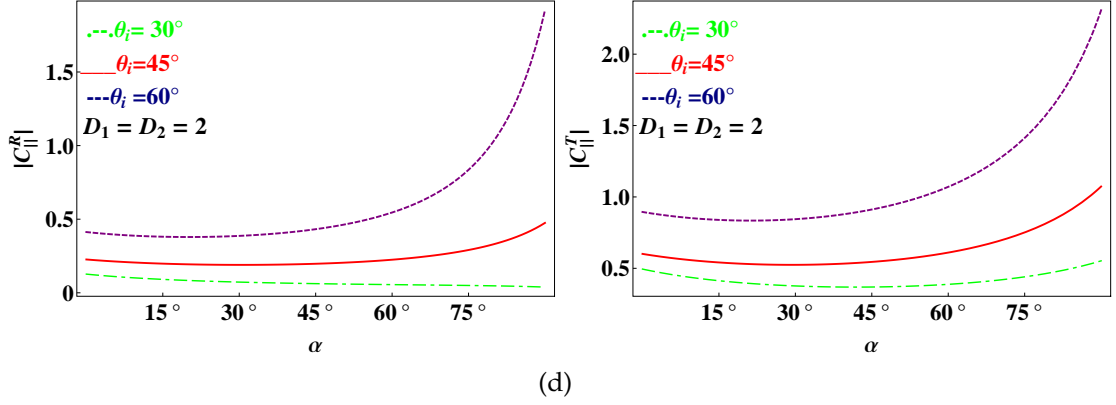
Figure 4.13: Behavior of $|C_\parallel^R|$ and $|C_\parallel^T|$ with respect to α for $D_1 = D_2 = 2$.

α. Whereas, amplitude of the transmission coefficient increases (decreases) for $\alpha < 60°$ ($\alpha > 60°$) by increasing μ_r^c. It is studied that amplitude of the coefficients increases (decreases) by taking higher dimension of NID mediums, when plotted as a function of α, μ_r^c (ϵ_i^c).
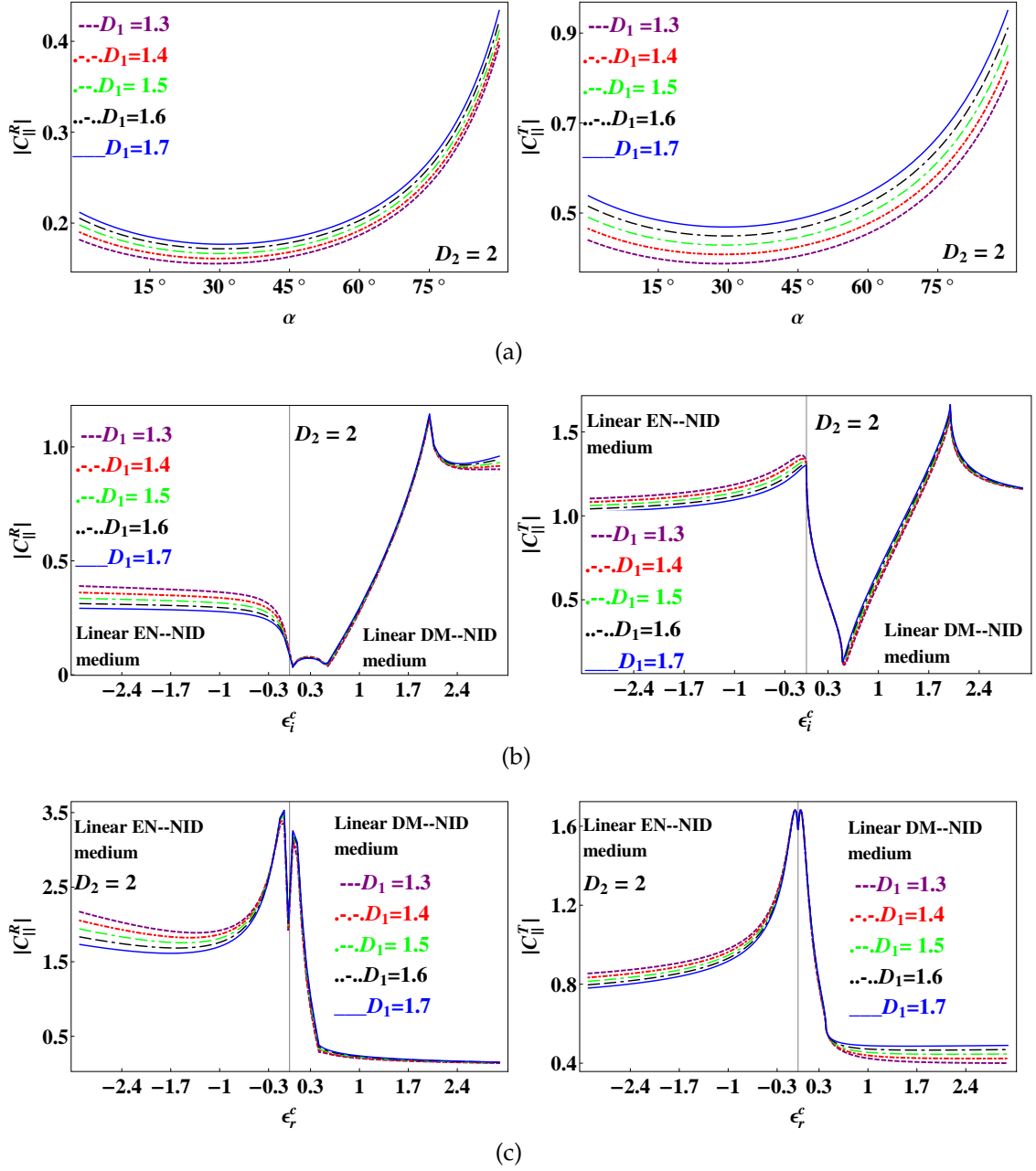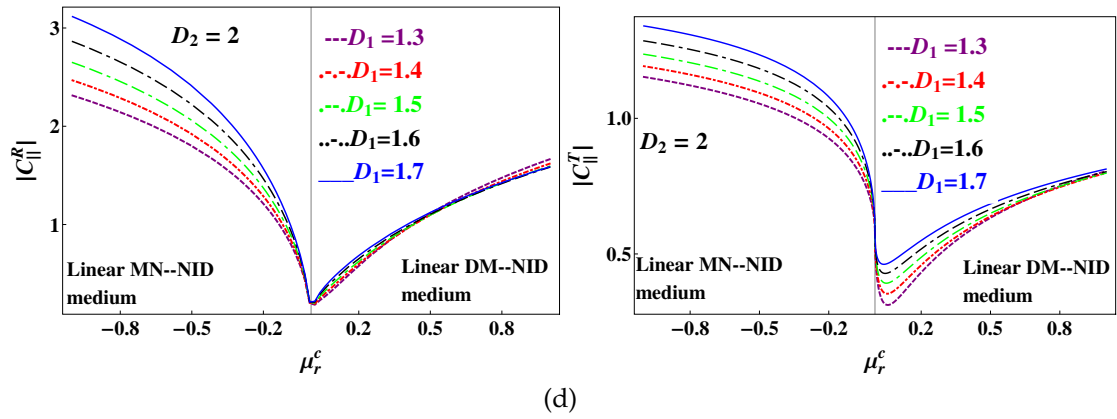
Figure 4.14: (cont.)

Figure 4.14: Behavior of $|C_{\parallel}^R|$ and $|C_{\parallel}^T|$ with respect to (a) α (b) ϵ_i^c (c) ϵ_r^c (d) μ_r^c for $D_2 = 2$ and $D_1 \neq 2$.

(a)

(b)

(c)

Figure 4.15: (cont.)

(d)
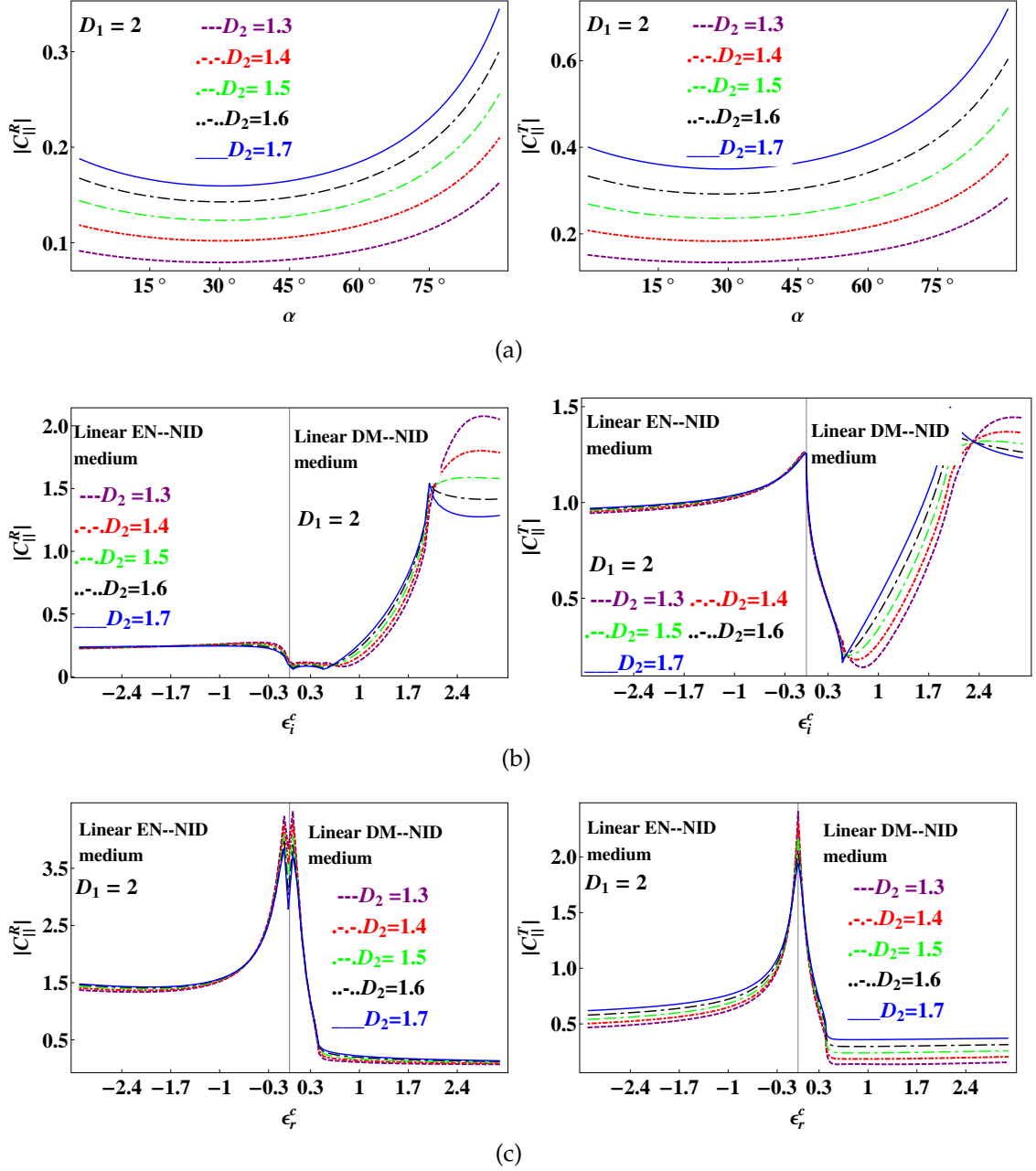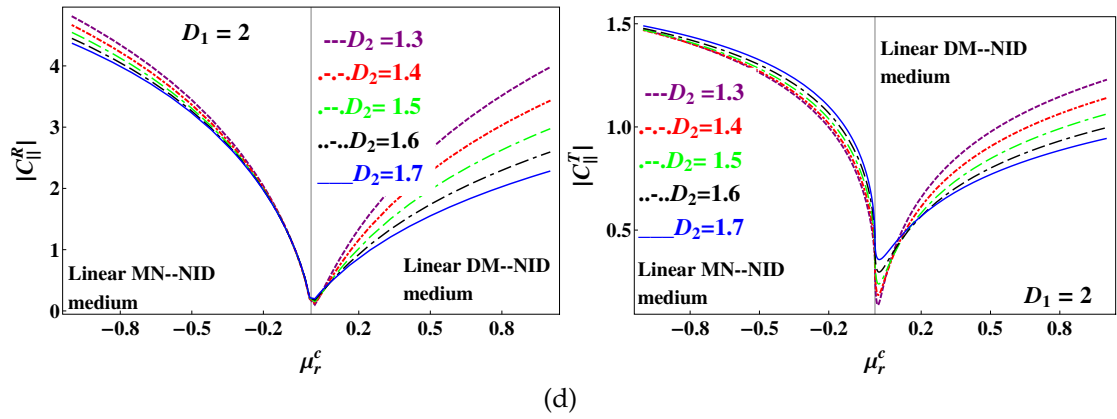
Figure 4.15: Behavior of $|C_\parallel^R|$ and $|C_\parallel^T|$ with respect to (a) α (b) ϵ_i^c (c) ϵ_r^c (d) μ_r^c for $D_1 = 2$ and $D_2 \neq 2$.
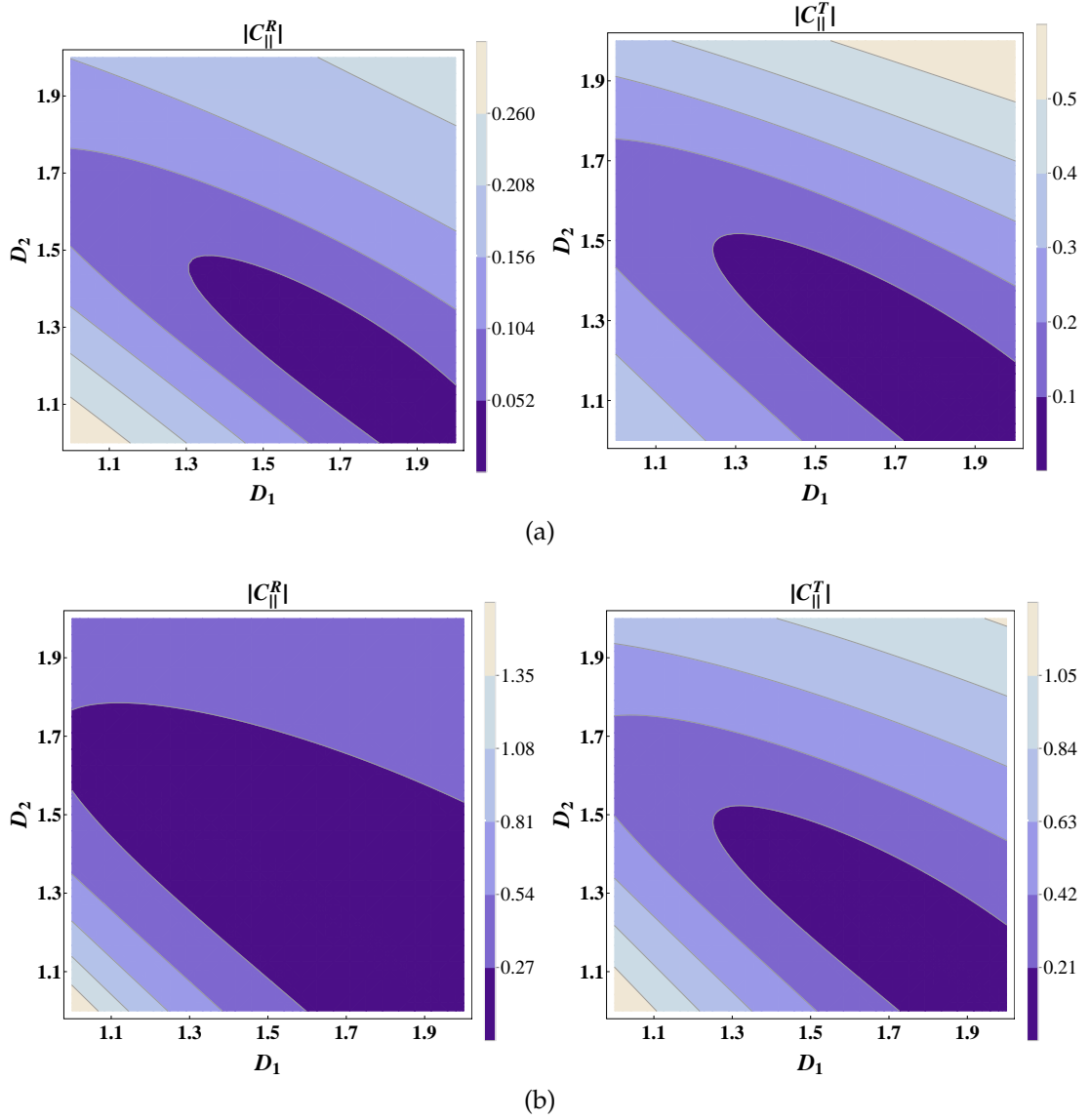
Figure 4.16: Contour plots of $|C^R_{\parallel}|$ and $|C^T_{\parallel}|$ with respect to D_1 and D_2 for (a) $\alpha = 0°$ and (b) $\alpha = 90°$ by taking $\mu_t = 0.02$, $\theta_i = 45°$, $\epsilon_r = 1.9$, $\mu_r = 0.01$ and $\epsilon_i = 0.8$.
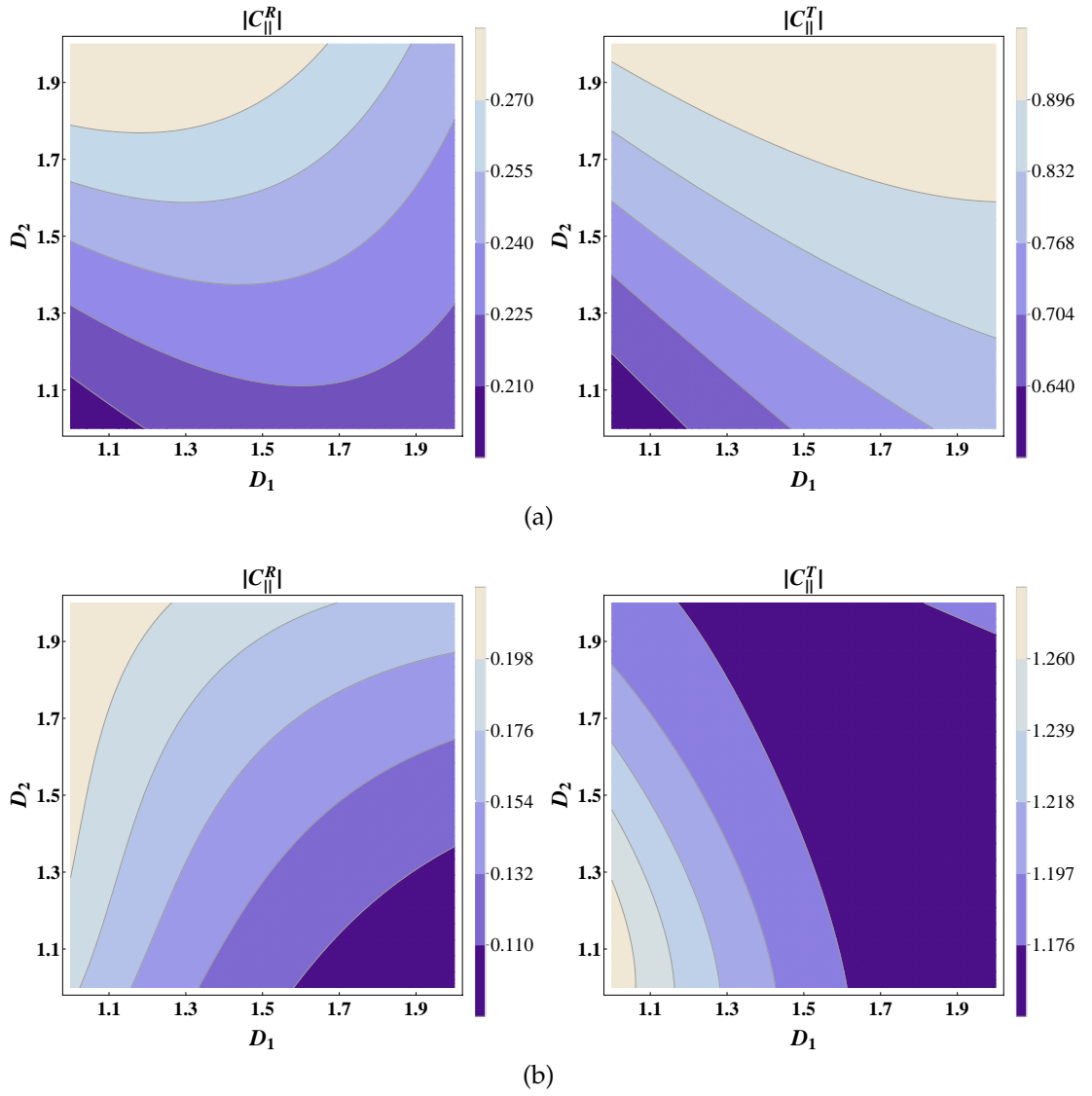
Figure 4.17: Contour plots of $|C_\parallel^R|$ and $|C_\parallel^T|$ with respect to D_1 and D_2 for (a) $\alpha = 0°$ and (b) $\alpha = 90°$ by taking $\mu_t = 0.02$, $\theta_i = 45°$, $\epsilon_r = 1.9$, $\mu_r = 0.01$ and $\epsilon_i = -0.8$.
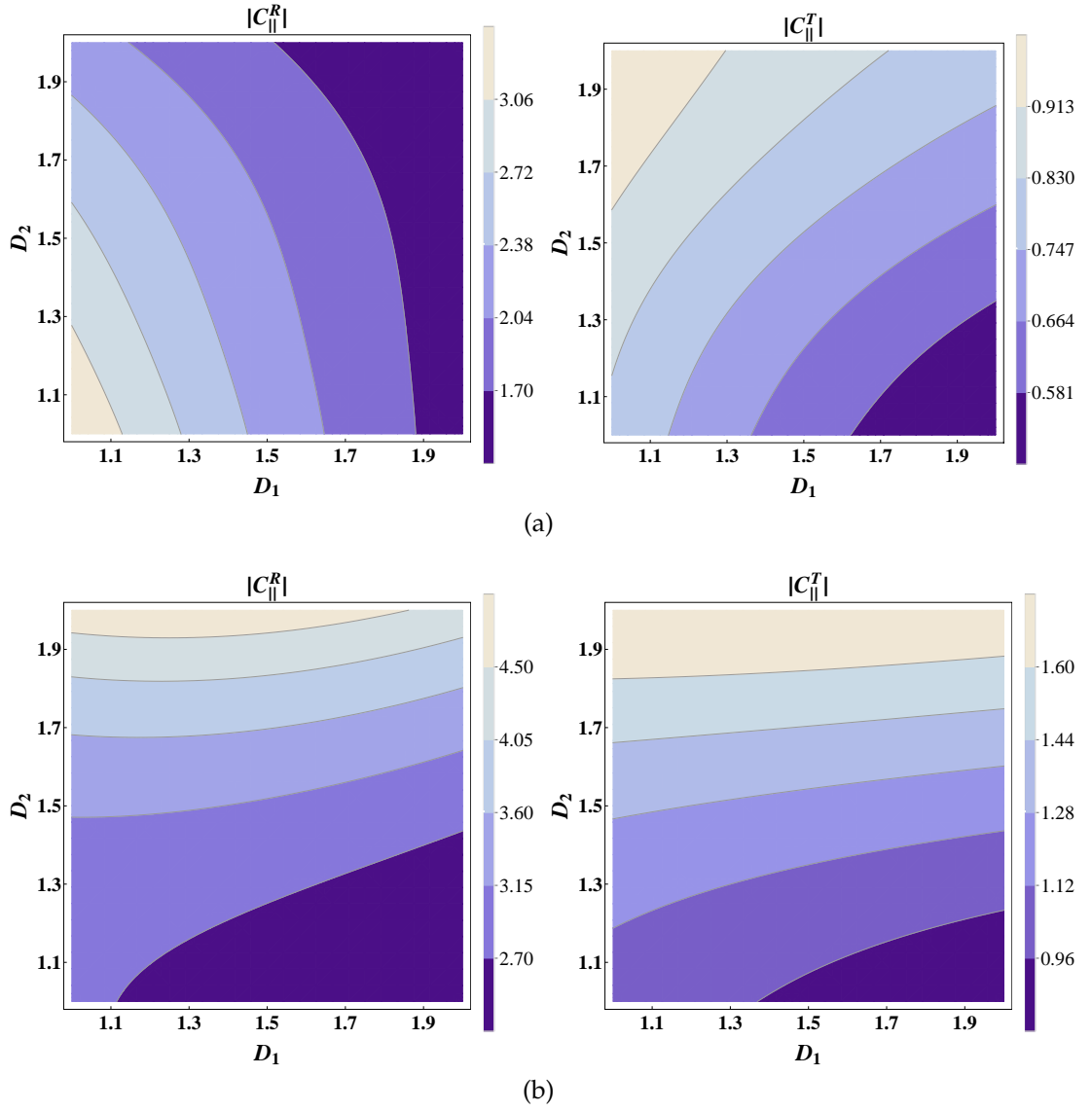
Figure 4.18: Contour plots of $|C_\parallel^R|$ and $|C_\parallel^T|$ with respect to D_1 and D_2 for (a) $\alpha = 0°$ and (b) $\alpha = 90°$ by taking $\mu_t = 0.02$, $\theta_i = 45°$, $\mu_r = 0.01$, $\epsilon_i = 0.8$ and $\epsilon_r = -1.9$.
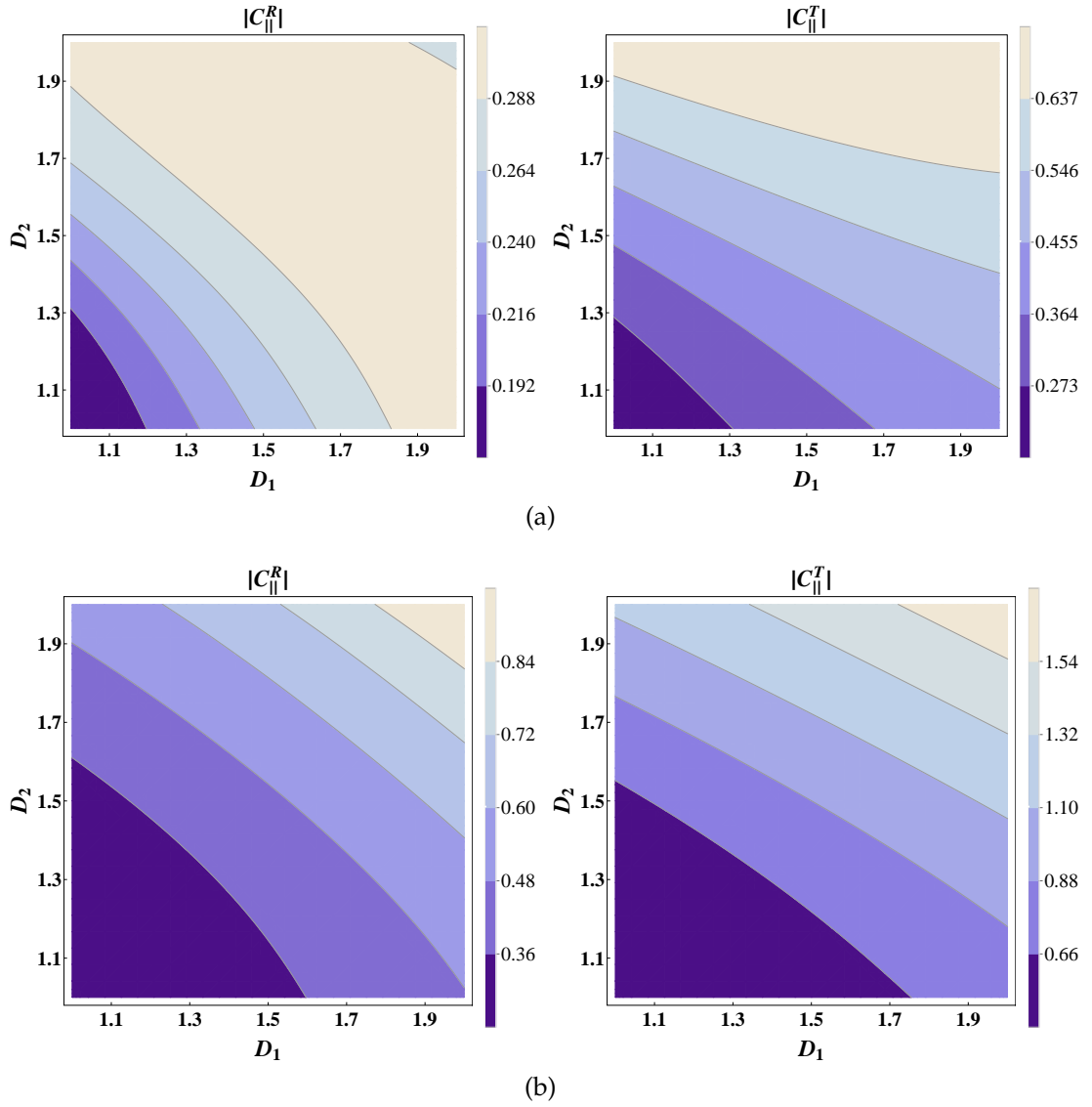
Figure 4.19: Contour plots of $\left|C_{\parallel}^R\right|$ and $\left|C_{\parallel}^T\right|$ with respect to D_1 and D_2 for (a) $\alpha = 0°$ and (b) $\alpha = 90°$ by taking $\mu_t = 0.02$, $\theta_i = 45°$, $\epsilon_r = 1.9$, $\epsilon_i = -0.8$ and $\mu_r = -0.01$.

Chapter 5

Conclusions and proposed applications

Detailed conclusions of the study presented in all the chapters are listed below,

* In this thesis, a study to note the impact of the presence of non-linearity and/or noninteger dimensions, on the reflection and transmission of a dielectric magnetic–dielectric magnetic (DM–DM) planar interface geometry is presented. Both S and P-polarization excitations are considered in this regard. All the nonlinear materials considered in this study are of second harmonic generation type, that is, mathematically permittivity of the nonlinear medium contains two terms, linear and nonlinear. Due to this reflected and transmitted coefficients has two terms first order and second order. It is important to note that nonlinear coefficients vanishes if nonlinear part of the permittivity is removed. Only behavior of the second order reflection and transmission characteristics is presented in this thesis. Moreover, nonlinear permeability (permeability observed at second harmonic frequency) is used throughout the analysis. By taking different noninteger values of the dimension of the noninteger dimensional (NID) medium, reflected and transmitted powers changes independently but the sum of both the powers remain the same. All planar geometries are named in such a way that first part of each name represents the excitation side. Behavior of the second order coefficients are presented as a function of permittivities, permeability and noninteger dimension pa-

rameter.

* First, the impact of presence of NID and non-linearity is noted by incorporating them into two different half spaces, i.e; nonlinear DM–linear DM noninteger dimensional interface. It is noticed that due to the presence of NID environment, the reflected power, compared to the transmitted power, can be significantly enhanced, for specific values of linear permittivity and positive values of nonlinear permeability.

* In the second consideration, contributions of the non-linearity and noninteger dimensions are incorporated into one half space, i.e; linear DM–nonlinear DM noninteger dimensional interface. In this scenario, remarkable enhancement in the transmitted power are observed (compared to reflected power), for specific values of the linear permittivity. Moreover, the values of linear permittivity are adjusted by tuning the incident angle and nonlinear permeability. Peaks of both the coefficients are also observed for only specific values of linear permittivity

* In the last consideration, impact of the presence of non-linearity and noninteger dimensions are noted by incorporating them simultaneously in both half spaces, i.e; linear DM noninteger dimensional–nonlinear DM noninteger dimensional interface. Significant enhancement in the S-polarized coefficients is noticed as linear permittivity approaches nonlinear permittivity. On the other hand, higher amplitude of the P-polarized reflection coefficient is noticed for DM noninteger dimensional medium compared to epsilon negative noninteger dimensional medium.

* It is concluded from the observations drawn from studying these scenarios that tuning of both noninteger dimension/dimensions and the non-linearity can be used for controlling the behavior of the coefficients.

5.1   Proposed applications

Some potential medical applications of the presented work are discussed now. In vertebrate tissues, collagen fiber protects the tendon from deformation [139]

and also stores the energy for the muscles. Among this fiber category, collagen-I (C-I), is the main component fond in bone structure, ovary, breast stoma, kidney, liver and lungs. Hence, abnormality in C-I fiber causes mid to sever issues related to these organs, like cancer [140–142]. Similarly, some pathogenic disorders like: sjorgren's syndrome, osteogenesis imperfecta and rheumatoid arthritis occur due to the abnormality in fibrillar collagen fiber. Experimental studies revel that SHG imaging/SHG microscopy for clinical applications is more powerful tool compared to classical histological methods [143] due to its sub-micron resolution capability on optical wavelengths. Further, SHG is also capable of providing 3-dimensional imaging of tissues, which provide more information compared to standard procedures [144–148]. Presented work can be used for the SHG imaging of the C-I and fibrillar collagen fiber. Further, presented work can also be used to study the cellular membrane interactions, e.g; protein, DNA, RNA etc [149]. Moreover, a layered interface can also be fabricated to enhance the sub-micron imaging for clinical applications.

Study of the NLO properties, especially SHG, is a difficult task for the noble metals (silver and gold) due to their higher extinction losses in the optical spectrum [150]. The metallic nano-structures also has thermal instabilities due to the conduction losses. This problem is resolved by using the nitride-based and conductive oxides materials, for example, Indium Tin Oxide (ITO), having higher melting point compared to the noble metals and chemical stability [151–153]. Moreover, ITO also has compatibility of fabrication standards to the silicon industry. The ENZ metallic/dielectric fractal metasurfaces deposited on ITO thin film sample, can be used to study the reported results.

References

[1] Boyd RW. Nonlinear optics academic press. *San Diego*, 155, 1992.

[2] Balanis CA. *Advanced engineering electromagnetics*. John Wiley & Sons, 2012.

[3] Fluck D and Günter P. Efficient second-harmonic generation by lens wave-guiding in $knbo_3$ crystals. *Optics Communications*, 147(4-6):305–308, 1998.

[4] Jensen OB Andersen PE Sumpf B Erbert G Hansen AK, Tawfieq M and Petersen PM. Concept for power scaling second harmonic generation using a cascade of nonlinear crystals. *Optics express*, 23(12):15921–15934, 2015.

[5] Ubachs W. Lecture notes, nonlinear optics. 2007.

[6] Bloembergen N and Pershan PS. Light waves at the boundary of nonlinear media. *Physical review*, 128(2):606, 1962.

[7] Peters CW Franken PA, Hill AE and Weinreich G. Generation of optical harmonics. *Physical Review Letters*, 7(4):118, 1961.

[8] Giorgetti C Tancogne DN and Véniard V. Ab initio description of second-harmonic generation from crystal surfaces. *Physical Review B*, 94(12):125301, 2016.

[9] Ward JF Bass M, Franken PA and Weinreich G. Optical rectification. *Physical Review Letters*, 9(11):446, 1962.

[10] New GHC and Ward JF. Optical third-harmonic generation in gases. *Physical Review Letters*, 19(10):556, 1967.

[11] She CY Karangelen NE Elton RC Reintjes J, Eckardt RC and Andrews RA. Generation of coherent radiation at 53.2 nm by fifth-harmonic conversion. *Physical Review Letters*, 37(23):1540, 1976.

[12] Williams DJ Prasad PN et al. *Introduction to nonlinear optical effects in molecules and polymers*, volume 1. Wiley New York, 1991.

[13] Zyss J and Ledoux I. Nonlinear optics in multipolar media: theory and experiments. *Chemical reviews*, 94(1):77–105, 1994.

[14] Leszczynski J Papadopoulos MG, Sadlej AJ et al. *Non-linear optical properties of matter*. Springer, 2006.

[15] Coe BJ. Switchable nonlinear optical metallochromophores with pyridinium electron acceptor groups. *Accounts of Chemical Research*, 39(6):383–393, 2006.

[16] Lim SJ You TS Zou G, Jo H and Ok KM. Rb3vo (o2) 2co3: a four-in-one carbonatoperoxovanadate exhibiting an extremely strong second-harmonic generation response. *Angewandte Chemie International Edition*, 57(28):8619–8622, 2018.

[17] Asadpour SH and Soleimani HR. Transmission and reflection properties of incident pulse in a dielectric slab doped with quantum dot. *Superlattices and Microstructures*, 62:217–224, 2013.

[18] Asadpour SH and Soleimani HR. Transmission and reflection properties of propagated pulse through defect slab based biexciton coherence. *Optics Communications*, 333:226–231, 2014.

[19] Sarsen Ak Valagiannopoulos C and Alù A. Angular memory of photonic metasurfaces. *IEEE Transactions on Antennas and Propagation*, 69(11):7720–7728, 2021.

[20] Valagiannopoulos C. Multistability in coupled nonlinear metasurfaces. *IEEE Transactions on Antennas and Propagation*, 2022.

[21] Paniagua DR Kalashnikov DA Ha ST Maß TWW Kuznetsov AI Anthur AP, Zhang H and Krivitsky L. Continuous wave second harmonic generation enabled by quasi-bound-states in the continuum on gallium phosphide metasurfaces. *Nano Letters*, 20(12):8745–8751, 2020.

[22] Boltasseva A Kildishev AV and Shalaev VM. Planar photonics with metasurfaces. *Science*, 339(6125):1232009, 2013.

[23] Shadrivov IV Lapine M and Kivshar YS. Colloquium: nonlinear metamaterials. *Reviews of Modern Physics*, 86(3):1093, 2014.

[24] Aieta F Khorasaninejad M Genevet P, Capasso F and Devlin R. Recent advances in planar optics: from plasmonic to dielectric metasurfaces. *Optica*, 4(1):139–152, 2017.

[25] Tymchenko M Krasnok A and Alù A. Nonlinear metasurfaces: a paradigm shift in nonlinear optics. *Materials Today*, 21(1):8–21, 2018.

[26] Pertsch T Staude I and Kivshar YS. All-dielectric resonant meta-optics lightens up. *Acs Photonics*, 6(4):802–814, 2019.

[27] Hopkins B Miroshnichenko AE Shcherbakov MR Camacho MR Fedyanin AA Neshev DN Rahmani M, Shorokhov AS and Kivshar YS. Nonlinear symmetry breaking in symmetric oligomers. *ACS Photonics*, 4(3):454–461, 2017.

[28] Saravi S Keeler GA Yang Y Reno J Peake GM Setzpfandt F Staude I Pertsch T Liu S, Sinclair MB et al. Resonantly enhanced second-harmonic generation using iii–v semiconductor all-dielectric metasurfaces. *Nano letters*, 16(9):5426–5432, 2016.

[29] Sinclair MB Keeler GA Peake GM Vabishchevich PP, Liu S and Brener I. Enhanced second-harmonic generation using broken symmetry iii–v semiconductor fano metasurfaces. *Acs Photonics*, 5(5):1685–1690, 2018.

[30] Miroshnichenko AE Lysevych M Volkovskaya I Smirnova DA Camacho MR Zangeneh KK Karouta F Kaushal V Sautter JD, Xu L et al. Tailoring second-harmonic emission from (111)-gaas nanoantennas. *Nano letters*, 19(6):3905–3911, 2019.

[31] Li Y Rakovich A Cortés E Maier SA Cambiasso J, Grinblat G. Bridging the gap between dielectric nanophotonics and the visible regime with effectively lossless gallium phosphide antennas. *Nano letters*, 17(2):1219–1225, 2017.

[32] Chen W Chen J Wu W Liu W Chen Y Cai W Ren M Ma J, Xie F and Xu J. Nonlinear lithium niobate metasurfaces for second harmonic generation. *Laser & Photonics Reviews*, 15(5):2000521, 2021.

[33] Fejer MM. Nonlinear optical frequency conversion. *Physics today*, 47(5):25–33, 1994.

[34] Lu CY Weinfurter H Zeilinger A Pan JW, Chen ZB and Żukowski M. Multiphoton entanglement and interferometry. *Reviews of Modern Physics*, 84(2):777, 2012.

[35] Petrich W. Mid-infrared and raman spectroscopy for medical diagnostics. *Applied Spectroscopy Reviews*, 36(2-3):181–237, 2001.

[36] Kang M He X Halas NJ Nordlander P Zhang S Shi J, Li Y and Xu H. Efficient second harmonic generation in a hybrid plasmonic waveguide by mode interactions. *Nano Letters*, 19(6):3838–3845, 2019.

[37] Vyunishev AM and Arkhipkin VG. Quasi-phase-matched second-harmonic generation in nonlinear crystals with harmonic modulation of nonlinearity. *Laser Physics*, 30(4):045401, 2020.

[38] Zhang S Li G and Zentgraf T. Nonlinear photonic metasurfaces. *Nature Reviews Materials*, 2(5):1–14, 2017.

[39] Tymchenko M Krasnok A and Alù A. Nonlinear metasurfaces: a paradigm shift in nonlinear optics. *Materials Today*, 21(1):8–21, 2018.

[40] Johnson AS Cojocaru C Akozbek N Coppens ZJ Perez SD Wall S Rodriguez SL, Scalora M and Trull J. Study of second and third harmonic generation from an indium tin oxide nanolayer: Influence of nonlocal effects and hot electrons. *Apl Photonics*, 5(1):010801, 2020.

[41] Taguchi D Lim E and Iwamoto M. Study of rectifying property of ito/pi/tips-pentacene/au diodes by electric field induced optical second harmonic generation. *Organic Electronics*, 14(7):1903–1908, 2013.

[42] Arie A and Voloch N. Periodic, quasi-periodic, and random quadratic nonlinear photonic crystals. *Laser & Photonics Reviews*, 4(3):355–373, 2010.

[43] Qayyum A and Abbas M. Study of reflection/transmission behavior of a planar nonlinear dielectric–nid interface. *Results in Optics*, 5:100119, 2021.

[44] Qayyum A and Abbas M. Study of reflection and transmission coefficients of a linear dielectric–nonlinear nid planar interface. *Physica B: Condensed Matter*, 644:414217, 2022.

[45] Qayyum A and Abbas M. Impact of non-linearity and non-integer dimension on the reflection and transmission coefficients. *Journal of Electromagnetic Waves and Applications*, pages 1–12, 2022.

[46] Qayyum A and Abbas M. Quasi phase matched second order reflection and transmission coefficients. *Physica B: Condensed Matter*, 650:414506, 2023.

[47] Mara Galli, Vincent Wanie, Diogo Pereira Lopes, Erik P Månsson, Andrea Trabattoni, Lorenzo Colaizzi, Krishna Saraswathula, Andrea Cartella, Fabio Frassetto, Poletto L, et al. Generation of deep ultraviolet sub-2-fs pulses. *Optics letters*, 44(6):1308–1311, 2019.

[48] Zawischa I Killi A Stolzenburg C, Schüle W and Sutter D. 700w intracavity-frequency doubled yb: Yag thin-disk laser at 100 khz repe-

tition rate. In *Solid State Lasers XIX: Technology and Devices*, volume 7578, pages 75–83. SPIE, 2010.

[49] Shen YR. Principles of nonlinear optics. 1984.

[50] Wang B. Second harmonic generation in disordered nonlinear crystals: application to ultra-short laser pulse characterization. 2017.

[51] Nisenoff M Maker PD, Terhune RW and Savage CM. Effects of dispersion and focusing on the production of optical harmonics. *Physical review letters*, 8(1):21, 1962.

[52] Fejer MM. Nonlinear optical frequency conversion. *Physics today*, 47(5):25–33, 1994.

[53] Kinsey N and Khurgin J. Nonlinear epsilon-near-zero materials explained: opinion. *Optical Materials Express*, 9(7):2793–2796, 2019.

[54] Kinsler P. Refractive index and wave vector in passive or active media. *Physical Review A*, 79(2):023839, 2009.

[55] Wang S Wang J Shen C Ding J Li W Huang P Wang D, Li T and Lu C. Characteristics of nonlinear optical absorption and refraction for kdp and dkdp crystals. *Optical Materials Express*, 7(2):533–541, 2017.

[56] Ramesh BR Sukumar M and Ramamurthi K. Linear and third-order nonlinear optical properties of likb4o7 single crystals. *Applied Physics B*, 121(3):369–373, 2015.

[57] HervéL and Mihalache D. Models of few optical cycle solitons beyond the slowly varying envelope approximation. *Physics Reports*, 523(2):61–126, 2013.

[58] Sapaev IB Sapaev UK Amanov R Ruziev ZJ, Sapaev B and Nazaraliev D. On theory of approximation methods in the study of second harmonic generation of ultrashort laser pulses in periodic crystals. In *AIP Conference Proceedings*, volume 2432, page 020008. AIP Publishing LLC, 2022.

[59] Shen YR. Principles of nonlinear optics. 1984.

[60] Lembrikov B. *Nonlinear Optics: Novel Results in Theory and Applications*. BoD–Books on Demand, 2019.

[61] Aurélien C Lin G and Chembo YK. Nonlinear photonics with high-q whispering-gallery-mode resonators. *Advances in Optics and Photonics*, 9(4):828–890, 2017.

[62] Myers LE and Bosenberg WR. Periodically poled lithium niobate and quasi-phase-matched optical parametric oscillators. *IEEE Journal of Quantum Electronics*, 33(10):1663–1672, 1997.

[63] Alam SU Biffi G Grudinin AB Ross GW Traynor NJ, Lefort L and Hanna DC. Strong self-phase modulation in periodically poled lithium niobate under subpicosecond pump pulses. 1998.

[64] Huo F He W Liu J, Ouyang C and Cao A. Progress in the enhancement of electro-optic coefficients and orientation stability for organic second-order nonlinear optical materials. *Dyes and Pigments*, 181:108509, 2020.

[65] De LVA. Aspects of wave propagation in a nonlinear medium: Birefringence and the second-order magnetoelectric coefficients. *Physical Review A*, 105(2):023530, 2022.

[66] Brouers F and Al-Musawi TJ. Brouers-sotolongo fractal kinetics versus fractional derivative kinetics: a new strategy to analyze the pollutants sorption kinetics in porous materials. *Journal of hazardous materials*, 350:162–168, 2018.

[67] He JH. Fractal calculus and its geometrical explanation. *Results in Physics*, 10:272–276, 2018.

[68] Degiorgio V. Mandelbrot, bb the fractal geometry of nature. *Scientia RS*, 78(119), 1984.

[69] Hirschfeld WVC Klein K, Maier T and Spatz JP. Marker-free phenotyping of tumor cells by fractal analysis of reflection interference contrast microscopy images. *Nano letters*, 13(11):5474–5479, 2013.

[70] Gaikwad RM Woodworth CD Dokukin ME, Guz NV and Sokolov I. Cell surface as a fractal: normal and cancerous cervical cells demonstrate different fractal behavior of surface adhesion maps at the nanoscale. *Physical review letters*, 107(2):028101, 2011.

[71] Li X Jamhiri B Jalal FE, Xu Y and Iqbal M. Fractal approach in expansive clay-based materials with special focus on compacted gmz bentonite in nuclear waste disposal: A systematic review. *Environmental Science and Pollution Research*, 28(32):43287–43314, 2021.

[72] He Y. *Real-world solutions for improving estimates of land-atmosphere exchanges in heterogeneous landscapes*. Bangor University (United Kingdom), 2016.

[73] Lutz JH Lathrop JI and Summers SM. Strict self-assembly of discrete sierpinski triangles. *Theoretical Computer Science*, 410(4-5):384–405, 2009.

[74] Feder J. Fractals. new york, london: Plenum press. 1988.

[75] Sun X and Jaggard DL. Wave interactions with generalized cantor bar fractal multilayers. *Journal of applied physics*, 70(5):2500–2507, 1991.

[76] Tarasov VE. Acoustic waves in fractal media: Non-integer dimensional spaces approach. *Wave Motion*, 63:18–22, 2016.

[77] Rouhipour H Ahmadi A, Neyshabouri MR and Asadi H. Fractal dimension of soil aggregates as an index of soil erodibility. *Journal of Hydrology*, 400(3-4):305–311, 2011.

[78] Petreska I Sandev T and Lenzi EK. Harmonic and anharmonic quantum-mechanical oscillators in noninteger dimensions. *Physics Letters A*, 378(3):109–116, 2014.

[79] Maraghechi P and Elezzabi AY. Enhanced thz radiation emission from plasmonic complementary sierpinski fractal emitters. *Optics express*, 18(26):27336–27345, 2010.

[80] Werner DH and Ganguly S. An overview of fractal antenna engineering research. *IEEE Antennas and propagation Magazine*, 45(1):38–57, 2003.

[81] Hou B Chan CT Wen W, Zhou L and Sheng P. Resonant transmission of microwaves through subwavelength fractal slits in a metallic plate. *Physical Review B*, 72(15):153406, 2005.

[82] Beltram F Walther C Jérôme F Beere HE Ritchie DA Mahler L, Tredicucci A and Wiersma DS. Quasi-periodic distributed feedback laser. *Nature Photonics*, 4(3):165–169, 2010.

[83] Allain C and Cloitre M. Optical diffraction on fractals. *Physical Review B*, 33(5):3566, 1986.

[84] Nicola DS. Reflection and transmission of cantor fractal layers. *Optics communications*, 111(1-2):11–17, 1994.

[85] Jaggard DL and Sun X. Reflection from fractal multilayers. *Optics letters*, 15(24):1428–1430, 1990.

[86] Cui TJ and Liang CH. Inverse scattering method for arbitrary fractal cantor bar multilayers. *Journal of Physics D: Applied Physics*, 26(11):1843, 1993.

[87] José T. Experimental methods for studying fractal aggregates. In *On growth and form*, pages 145–162. Springer, 1986.

[88] Jaggard DL and Sun X. Fractal surface scattering: a generalized rayleigh solution. *Journal of Applied Physics*, 68(11):5456–5462, 1990.

[89] Nicola DS. Reflection and transmission of cantor fractal layers. *Optics communications*, 111(1-2):11–17, 1994.

[90] Tarasov VE. Continuous medium model for fractal media. *Physics Letters A*, 336(2-3):167–174, 2005.

[91] Mughal MJ Zubair M and Naqvi QA. *Electromagnetic fields and waves in fractional dimensional space*. Springer Science & Business Media, 2012.

[92] Tarasov VE. Electromagnetic waves in non-integer dimensional spaces and fractals. *Chaos, Solitons & Fractals*, 81:38–42, 2015.

[93] Stillinger FH. Axiomatic basis for spaces with noninteger dimension. *Journal of Mathematical Physics*, 18(6):1224–1234, 1977.

[94] Palmer C and Stavrinou PN. Equations of motion in a non-integer-dimensional space. *Journal of Physics A: Mathematical and General*, 37(27):6987, 2004.

[95] Golmankhaneh AK Baleanu D and Golmankhaneh AK. On electromagnetic field in fractional space. *Nonlinear Analysis: Real World Applications*, 11(1):288–292, 2010.

[96] Tarasov VE. *Fractional dynamics: applications of fractional calculus to dynamics of particles, fields and media*. Springer Science & Business Media, 2011.

[97] Mughal MJ Zubair M and Naqvi QA. *Electromagnetic fields and waves in fractional dimensional space*. Springer Science & Business Media, 2012.

[98] M Zubair, MJ Mughal, and QA Naqvi. An exact solution of the spherical wave equation in d-dimensional fractional space. *Journal of Electromagnetic Waves and Applications*, 25(10):1481–1491, 2011.

[99] Rizvi AA Abbas M and Naqvi QA. Two dimensional green's function for non-integer dimensional dielectric half space geometry. *Optik*, 127(20):8530–8535, 2016.

[100] Fiaz MA Abbas M, Rizvi AA and Naqvi QA. Scattering of electromagnetic plane wave from a low contrast circular cylinder buried in non-

integer dimensional half space. *Journal of Electromagnetic Waves and Applications*, 31(3):263–283, 2017.

[101] Jaggard DL. On fractal electrodynamics. In *Recent advances in electromagnetic theory*, pages 183–224. Springer, 1990.

[102] Kim Y and Jaggard DL. The fractal random array. *Proceedings of the IEEE*, 74(9):1278–1280, 1986.

[103] Jaggard DL and Spielman T. Triadic cantor target diffraction. *Microwave and optical technology letters*, 5(9):460–466, 1992.

[104] Goutelard C. Fractal theory of large arrays of lacunar antennas. In *Electromagn. Wave Propagat. Panel Symp.(AGARD-CP-528)*, volume 35, pages 1–35, 1992.

[105] Puente C. Fractal design of multiband antenna arrays. *Elec. Eng. Dept. Univ. Illinois, Urbana-Champaign, ECE*, 477, 1994.

[106] Marichev OI Samko SG, Kilbas AA et al. *Fractional integrals and derivatives*, volume 1. Gordon and breach science publishers, Yverdon Yverdon-les-Bains, Switzerland, 1993.

[107] Tarasov VE. Fractional fokker–planck equation for fractal media. *Chaos: An Interdisciplinary Journal of Nonlinear Science*, 15(2):023102, 2005.

[108] Engheia N. On the role of fractional calculus in electromagnetic theory. *IEEE Antennas and Propagation Magazine*, 39(4):35–46, 1997.

[109] Engheta N. Fractional curl operator in electromagnetics. *Microwave and Optical Technology Letters*, 17(2):86–91, 1998.

[110] Tarasov VE and Zaslavsky GM. Fractional ginzburg–landau equation for fractal media. *Physica A: Statistical Mechanics and its Applications*, 354:249–261, 2005.

[111] Tarasov VE. Possible experimental test of continuous medium model for fractal media. *Physics Letters A*, 341(5-6):467–472, 2005.

[112] Rizvi AA Abbas M and Naqvi QA. Fractional dual fields to the maxwell equations for a line source buried in dielectric half space. *Optik*, 129:225–230, 2017.

[113] Kauranen M and Zayats AV. Nonlinear plasmonics. *Nature photonics*, 6(11):737–748, 2012.

[114] Feth N Klein MW, Wegener M and Linden S. Experiments on second-and third-harmonic generation from magnetic metamaterials. *Optics Express*, 15(8):5238–5247, 2007.

[115] Wegener M Klein MW, Enkrich C and Linden S. Second-harmonic generation from magnetic metamaterials. *Science*, 313(5786):502–504, 2006.

[116] Baselli M Großmann S Biagioni P Locatelli A Angelis C Cerullo G Osellame R Hecht B Celebrano M, Wu X et al. Mode matching in multiresonant plasmonic nanoantennas for enhanced second harmonic generation. *Nature nanotechnology*, 10(5):412–417, 2015.

[117] Lovera A Thyagarajan K, Rivier S and Martin OJF. Enhanced second-harmonic generation from double resonant plasmonic antennae. *Optics express*, 20(12):12860–12865, 2012.

[118] Rahmani M Sidiropoulos TPH Hong M Oulton RF Aouani H, Navarro CM and Maier SA. Multiresonant broadband optical antennas as efficient tunable nanosources of second harmonic light. *Nano letters*, 12(9):4997–5002, 2012.

[119] Ayala OC Zhang Y, Grady NK and Halas NJ. Three-dimensional nanostructures as highly efficient generators of second harmonic light. *Nano letters*, 11(12):5519–5523, 2011.

[120] Barnes PRF O'regan B Walsh A Eames C, Frost JM and Islam MS. Ionic transport in hybrid lead iodide perovskite solar cells. *Nature communications*, 6(1):1–8, 2015.

[121] Argyropoulos C Chen Pai Y Lu F Demmerle F Boehm G Amann M Alu A Lee J, Tymchenko M and Belkin MA. Giant nonlinear response from plasmonic metasurfaces coupled to intersubband transitions. *Nature*, 511(7507):65–69, 2014.

[122] Moreno F Albella P, Alcaraz O and Maier SA. Electric and magnetic field enhancement with ultralow heat radiation dielectric nanoantennas: considerations for surface-enhanced spectroscopies. *Acs Photonics*, 1(6):524–529, 2014.

[123] Cortés E Rahmani M Roschuk T Grinblat G Oulton RF Bragas AV Caldarola M, Albella P and Maier SA. Non-plasmonic nanoantennas for surface enhanced spectroscopies with ultra-low heat conversion. *Nature communications*, 6(1):1–8, 2015.

[124] Yu YF Markovich D Paniagua D Gonzaga L Samusev A Kivshar Y Luk'yanchuk B Bakker RM, Permyakov D and Kuznetsov AI. Magnetic and electric hotspots with silicon nanodimers. *Nano Letters*, 15(3):2137–2142, 2015.

[125] Hopkins B Shorokhov AS Staude I Melik G Decker M Ezhov AA Miroshnichenko A Brener I Shcherbakov MR, Neshev DN et al. Enhanced third-harmonic generation in silicon nanoparticles driven by magnetic response. *Nano letters*, 14(11):6488–6492, 2014.

[126] Stepanenko O Leo G Carletti L, Locatelli A and Angelis C. Enhanced second-harmonic generation from magnetic resonance in algaas nanoantennas. *Optics express*, 23(20):26544–26550, 2015.

[127] Neshev DN Hopkins B Staude I Melik GV Ezhov AA Miroshnichenko AE Brener I Fedyanin AA Shcherbakov MR, Shorokhov AS et al. Nonlinear interference and tailorable third-harmonic generation from dielectric oligomers. *Acs Photonics*, 2(5):578–582, 2015.

[128] Shorokhov AS Chong KE Choi D Staude I Miroshnichenko AE Neshev DN Fedyanin AA Shcherbakov MR, Vabishchevich PP and Kivshar YS.

Ultrafast all-optical switching with magnetic resonances in nonlinear dielectric nanostructures. *Nano letters*, 15(10):6985–6990, 2015.

[129] Falkner M Dominguez J Neshev DN Brener I Pertsch T Decker M, Staude I and Kivshar YS. High-efficiency dielectric huygens' surfaces. *Advanced Optical Materials*, 3(6):813–820, 2015.

[130] Decker M Fofang NT Liu S Gonzales E Dominguez J Luk T Neshev DN Brener I Staude I, Miroshnichenko AE et al. Tailoring directional scattering through magnetic and electric resonances in subwavelength silicon nanodisks. *ACS nano*, 7(9):7824–7832, 2013.

[131] Paniagua D Fu Y Luk'yanchuk B Yu YF, Zhu AY and Kuznetsov AI. High-transmission dielectric metasurface with 2π phase control at visible wavelengths. *Laser & Photonics Reviews*, 9(4):412–418, 2015.

[132] Tsukernik A Pandey A Nikolskiy K Litchinitser NM Shalaev MI, Sun J. High-efficiency all-dielectric metasurfaces for ultracompact beam manipulation in transmission mode. *Nano letters*, 15(9):6261–6266, 2015.

[133] James A Dominguez J Liu S Campione S Subramania GS Luk TS Decker M Neshev DN Chong K, Staude I et al. Polarization-independent silicon metadevices for efficient optical wavefront control. *Nano letters*, 15(8):5369–5374, 2015.

[134] Hasman E Lin D, Fan P and Brongersma ML. Dielectric gradient metasurface optical elements. *science*, 345(6194):298–302, 2014.

[135] Anderson Z Kravchenko II Briggs DP Moitra P, Yang Y and Valentine J. Realization of an all-dielectric zero-index optical metamaterial. *Nature Photonics*, 7(10):791–795, 2013.

[136] Staude I James AR Dominguez J Liu S Subramania GS Decker M Neshev DN Brener I Chong KE, Wang L et al. Efficient polarization-insensitive complex wavefront control using huygens' metasurfaces based on dielectric resonant meta-atoms. *Acs Photonics*, 3(4):514–519, 2016.

[137] Stepanenko O Leo G Carletti L, Locatelli A and Angelis C. Enhanced second-harmonic generation from magnetic resonance in algaas nanoantennas. *Optics express*, 23(20):26544–26550, 2015.

[138] Liscidini M and Andreani LC. Second-harmonic generation in doubly resonant microcavities with periodic dielectric mirrors. *Physical Review E*, 73(1):016613, 2006.

[139] Nakamura A Tsukiji S Ujihara Y Sugita S, Suzumura T and Nakamura M. Second harmonic generation light quantifies the ratio of type iii to total (i+ iii) collagen in a bundle of collagen fiber. *Scientific reports*, 11(1):1–11, 2021.

[140] Pointer KB Liu Y Lieberthal TJ Kao WJ Kuo JS Loeffler AG Ouellette JN, Drifka CR and Eliceiri KW. Navigating the collagen jungle: the biomedical potential of fiber organization in cancer. *Bioengineering*, 8(2):17, 2021.

[141] Simon H Hinton D Goldsmith RH Patankar M Alkmin S, Brodziski R and Campagnola PJ. Role of collagen fiber morphology on ovarian cancer cell migration using image-based models of the extracellular matrix. *Cancers*, 12(6):1390, 2020.

[142] Tzardi M Tsafa E Fotakis C Athanassakis I Tsafas V, Gavgiotaki E and Filippidis G. Polarization-dependent second-harmonic generation for collagen-based differentiation of breast cancer samples. *Journal of Biophotonics*, 13(10):e202000180, 2020.

[143] Campagnola PJ and Dong CY. Second harmonic generation microscopy: principles and applications to disease diagnosis. *Laser & Photonics Reviews*, 5(1):13–26, 2011.

[144] Ro Y Krouglov S Akens MK Wilson BC Golaraei A, Mirsanaye K and Barzda V. Collagen chirality and three-dimensional orientation studied with polarimetric second-harmonic generation microscopy. *Journal of biophotonics*, 12(1):e201800241, 2019.

[145] Wu W Hill RL Smid M Martens JWM Turner BM Desa DE, Strawderman RL and Brown EB. Intratumoral heterogeneity of second-harmonic generation scattering from tumor collagen and its effects on metastatic risk prediction. *BMC cancer*, 20(1):1–14, 2020.

[146] Holzapfel GA Sadeghinia MJ, Skallerud B and Prot V. Biomechanics of mitral valve leaflets: Second harmonic generation microscopy, biaxial mechanical tests and tissue modeling. *Acta biomaterialia*, 141:244–254, 2022.

[147] Brown RM Brown IV Edward B Hill RL Turner BM Brown III Edward B Desa DE, Wu W. Second-harmonic generation imaging reveals changes in breast tumor collagen induced by neoadjuvant chemotherapy. *Cancers*, 14(4):857, 2022.

[148] Martínez Y Bueno JM and Ávila FJ. Collagen organization, polarization sensitivity and image quality in human corneas using second harmonic generation microscopy. In *Photonics*, volume 9, page 672. MDPI, 2022.

[149] Sly KL Tran RJ and Conboy JC. Applications of surface second harmonic generation in biological sensing. *Annual Review of Analytical Chemistry*, 10:387–414, 2017.

[150] Shalaev VM Naik GV and Boltasseva A. Alternative plasmonic materials: beyond gold and silver. *Advanced Materials*, 25(24):3264–3294, 2013.

[151] Kim J Naik GV and Boltasseva A. Oxides and nitrides as alternative plasmonic materials in the optical range. *Optical materials express*, 1(6):1090–1099, 2011.

[152] Boltasseva A and Atwater HA. Low-loss plasmonic metamaterials. *Science*, 331(6015):290–291, 2011.

[153] Naik GV Emani NK Shalaev VM West PR, Ishii S and Boltasseva A. Searching for better plasmonic materials. *Laser & photonics reviews*, 4(6):795–808, 2010.

There surely came over man a period of time when he was a thing not worth mentioning.

(Al-Insan : 1)

Turnitin Originality Report

STUDY OF OPTICAL PROPERTIES OF NONINTEGER DIMENSIONAL NONLINEAR MEDIUM   by Adil Qayyum Bhatti .

From PhD (PhD DRSML)

- Processed on 31-Mar-2023 10:53 PKT
- ID: 2051790038
- Word Count: 25965

Similarity Index
7%
Similarity by Source

Internet Sources:
   5%
Publications:
   5%
Student Papers:
   3%

Focal Person (Turnitin)
Quaid-i-Azam University
Islamabad

sources:

1 1% match (Internet from 05-Dec-2018)
http://www.speedwayracing.co.nz/wp-content/uploads/2012/06/2012%20SNZ%20Rulebook%20-%20SpeedwayRacing.co.nz.pdf

2 1% match (Internet from 09-Sep-2014)
http://www.passcape.com/download/misc/hybrid_all.ini

3 < 1% match (Sheng Zeng, Shaoping Wang, Bing Sun, Qibing Liu. "Propagation Characteristics of Blasting Stress Waves in Layered and Jointed Rock Caverns", Geotechnical and Geological Engineering, 2017)
Sheng Zeng, Shaoping Wang, Bing Sun, Qibing Liu. "Propagation Characteristics of Blasting Stress Waves in Layered and Jointed Rock Caverns", Geotechnical and Geological Engineering, 2017

4 < 1% match (Internet from 02-May-2020)
http://atomoptics-nas.uoregon.edu/~dsteck/teaching/quantum-optics/quantum-optics-notes.pdf

5 < 1% match (Internet from 26-Dec-2021)
https://dokumen.pub/nonlinear-optics-4th-ed-9780128110027-9780128110034-0128110031.html

6 < 1% match (Internet from 09-Sep-2017)
https://semspub.epa.gov/work/10/100008385.pdf

7 < 1% match (student papers from 25-Mar-2016)
Submitted to Higher Education Commission Pakistan on 2016-03-25